12-1972

An investigation of the variables affecting steam condensation on the outside of a horizontal tube bundle

David Martin Eissenberg

To the Graduate Council:

I am submitting herewith a dissertation written by David Martin Eissenberg entitled "An investigation of the variables affecting steam condensation on the outside of a horizontal tube bundle." I have examined the final electronic copy of this dissertation for form and content and recommend that it be accepted in partial fulfillment of the requirements for the degree of Doctor of Philosophy, with a major in Chemical Engineering.

, Major Professor

We have read this dissertation and recommend its acceptance:

Accepted for the Council:

Carolyn R. Hodges

Vice Provost and Dean of the Graduate School

(Original signatures are on file with official student records.)

13

November 1972

To the Graduate Council:

I am submitting herewith a dissertation written by David Martin Eissenberg, entitled "An Investigation of the Variables Affecting Steam Condensation on the Outside of a Horizontal Tube Bundle." I recommend that it be accepted in partial fulfillment of the requirements for the degree of Doctor of Philosophy, with a major in Chemical Engineering.

[illegible]

Major Professor

We have read this dissertation and recommend its acceptance:

Julian Elliott

John W. Prados

Oran L. Culberson

L. G. Alexander

Accepted for the Council:

Hilton A. Smith

Vice Chancellor for Graduate Studies and Research

AN INVESTIGATION OF THE VARIABLES AFFECTING STEAM CONDENSATION ON THE OUTSIDE OF A HORIZONTAL TUBE BUNDLE

A Dissertation

Presented to

the Graduate Council of

The University of Tennessee

In Partial Fulfillment

of the Requirements for the Degree

Doctor of Philosophy

---

by

David Martin Eissenberg

December 1972

ACKNOWLEDGMENTS

This investigation was part of the Nuclear Desalination Program carried out at the Oak Ridge National Laboratory operated by the Union Carbide Corporation for the U. S. Atomic Energy Commission. The investigation was supported in part by the U. S. Department of the Interior, Office of Saline Water under an interagency agreement. The author is grateful for the continuing support and guidance of R. P. Hammond and I. Spiewak in initiating and executing the investigation.

The loop detailed design, construction, and shakedown operation was carried out with the assistance of P. P. Holz, whose careful attention to details was in a large measure responsible for the attainment of the objectives within the planned time and budget. Assisting in loop operation at various times were J. L. Winters, J. M. Baker and P. H. Harley with J. P. Hurst as technician. The MIT School of Chemical Engineering Practice carried out a problem which has been incorporated into the present results.

Assistance in data reduction programming was provided by L. Jung. The program was converted from BASIC to FORTRAN by H. M. Noritake and J. A. Hafford.

The figures were prepared by F. M. Burkhalter, and the typing was done by J. O. Brown, both of whom provided skillful assistance and helpful suggestions.

Finally, the forbearance shown by Ethel, Joel, Judith, Sara, Mike and Tom, in cheerfully allowing their husband and father the time needed to complete the preparation of this manuscript, is without doubt the principal factor in its final completion.

ABSTRACT

The accurate prediction of the thermal performance of large multitube steam condensers for application to the distillation desalination of seawater depends on the availability of correlations for calculating each of the film heat transfer coefficients for individual tubes located within the condenser as a function of local conditions. Although correlations are available, there have been few experimental verifications of their accuracy or even of their validity in the specific application to desalination, particularly with respect to the two film coefficients associated with the condensation process, the condensate film heat transfer coefficient and the non-condensable gas film heat transfer coefficient.

A horizontal multitube steam condenser was built and operated in the present work in order to investigate the individual and combined effects of steam temperature, steam velocity, condensate rain, and non-condensable gas fraction on the thermal performance of a vertical array of five tubes located within the condenser over the range of interest of each of the variables of importance to the distillation desalination process.

The results were analyzed by comparison with existing and improved correlations. The effect of condensate rain on the condensate film heat transfer coefficient was found to be consistent with previous investigations. A new side drainage model described the observed results and provided the basis for improved prediction methods. The effect of steam velocity was found to be similar in the horizontal direction to that observed by previous investigators in the vertical direction. The effect could be accounted for as being due to the lateral transport of the condensate by the steam out of the region of active condenser tubes, and thus unlikely to occur in large tube bundles. The effect of temperature on the condensate film heat transfer coefficient was found to be consistent with the theoretical prediction of the Nusselt equation.

The combined effect of gas concentration, steam velocity, condensing rate and condensing temperature on the non-condensable gas film heat transfer coefficient was correlated using the Colburn mass transfer j factor and a modified j factor, with the latter being preferred because it led to a considerable decrease in the data scatter about the correlating line. A cavity flow model for describing the process of condensation in the presence of gas in a tube bundle was described and the results analyzed in terms of it.

Design equations for predicting the film coefficients were presented, with values based on the present work incorporated. Recommendations for additional work to generalize the present results are included.

TABLE OF CONTENTS

LIST OF TABLES

LIST OF FIGURES

LIST OF SYMBOLS

a	Exponent on the Prandtl number in Equation (39)
A	Coefficient in Equation (14)
A_B	Outside area of tubes in a condenser tube bundle
A_i	Inside area of a condenser tube
A_s	Flow area between tubes, shown in Figure 18
A_T	Outside area of a condenser tube
C_i	Coefficient in Equation (12)
C_p	Heat capacity
d_i	Inside diameter of a condenser tube
d_o	Outside diameter of a condenser tube
D	Binary diffusion coefficient
F_d	Fraction of side drainage as defined by Equation (31)
F_m	Mole fraction of non-condensable gas
g	Gravitational acceleration
g_R	Reynolds flux
G	Mass velocity based on minimum flow area
G_m	Molar velocity of bulk steam or steam-nitrogen mixture past a tube (G/M_b)
G_s	Mass velocity of steam based on superficial flow area
h_o	Film heat transfer coefficient for sensible heat transfer on the outside of a tube
h_c	Condensate film heat transfer coefficient
h_{cn}	Condensate film heat transfer coefficient for the nth tube from the top of a vertical column of horizontal tubes

$\bar{h}_{cn}$	Mean condensate film heat transfer coefficient for a vertical column of n horizontal tubes
$\bar{h}_{e5}$	Mean effective shell side film heat transfer coefficient for a vertical column of five tubes as defined by Equation (72)
h_g	Non-condensable gas film heat transfer coefficient
$\bar{h}_g$	Bundle mean non-condensable gas film heat transfer coefficient
h_i	Convective film heat transfer coefficient for liquid flowing inside a tube
$\bar{h}_i$	Bundle mean convective film heat transfer coefficient
h_N	Condensate film heat transfer coefficient for a single horizontal tube calculated from Equation (13)
h_w	Tube wall heat transfer coefficient
H	Steam velocity head
IR	Inundation ratio, ratio of condensate collected in the center drain trough to condensate produced in the active tube bundle
j_H	Sensible heat transfer j factor defined by Equation (38)
j_M	Colburn mass transfer j factor defined by Equation (39)
j_{MS}	Spalding mass transfer j factor defined by Equation (64)
k	Thermal conductivity
k_f	Mean thermal conductivity of condensate film
k_g	Mass transfer coefficient defined by Equation (36)
k_m	Molar transfer coefficient, k_g/M_s
Le	Lewis number, (Pr/Sc)
LMTD	Log mean driving force for a tube bundle defined by Equation (2)
m	Exponent on the tube number in Equation (26)
M_b	Mean molecular weight of the bulk steam-nitrogen mixture flowing past a condenser tube

M_c Mean molecular weight of the steam-nitrogen mixture at the condensate film surface

M_g Average molecular weight as defined by Equation (60)

M_s Molecular weight of steam

n The height of a tube bundle or the location of a tube within a tube bundle, both measured by counting tubes from the top in a vertical line

N_s Molar velocity of steam to the condensate surface through a stagnant steam-gas film

Nu Nusselt number for sensible heat transfer inside a tube ($h_i d_i/k$)

Nu_I Dimensional group defined by Equation (80)

Nu_{II} Dimensional group defined by Equation (81)

Nu_N Nusselt number for condensation outside a tube ($h_N d_o/k$)

p Exponent in Equation (14)

$\bar{p}_g$ Log mean partial pressure of nitrogen defined by Equation (42)

p_{gb} Partial pressure of nitrogen in the bulk steam-nitrogen mixture flowing past a condenser tube

p_{gc} Partial pressure of nitrogen in the steam-nitrogen mixture of the condensate film surface

p_{sb} Partial pressure of steam in the bulk steam-nitrogen mixture flowing past a condenser tube

p_{sc} Partial pressure of steam in the steam-nitrogen mixture at the condensate film surface

p_T Total pressure of steam-nitrogen mixture

Pr Prandtl number ($C_p \mu/k$)

Pr_L Prandtl number of cooling water inside tube

Q_B Condenser bundle heat duty

Q_T Condenser tube heat duty

Re_L Reynolds number of cooling water inside tube $(\frac{d_i V_\rho}{\mu_L})$

Re_s Reynolds number based on superficial $(\frac{d_o G_s}{\mu})$ velocity of vapor flowing across tube bundle

Re_v Reynolds number based on vapor velocity passing through minimum flow area for flow normal to tube bundles $(d_o G/\mu)$

R_c Thermal resistance due to the condensate film

R_f Thermal resistance due to solids fouling inside and outside surfaces of tube

$\overline{R}_f$ Mean fouling thermal resistance for a tube bundle

R_g Thermal resistance due to the non-condensable gas film

R_i Thermal resistance due to the convective film

R_w Thermal resistance of tube wall defined by Equation (11)

$\overline{R}_w$ Mean wall thermal resistance for a tube bundle

S Distance between tube centers for equilateral triangular arrays of tubes

Sc Schmidt number $(\mu/\rho D)$

T_b Saturation temperature of steam or steam-nitrogen mixture flowing past a tube

T_c Saturation temperature of steam at its partial pressure at the condensate film surface

ΔT_c Temperature difference across condensate film

ΔT_g Temperature difference between condensate film surface and bulk steam-nitrogen flowing past a condenser tube

T_i	Temperature of cooling water entering a tube
T_{iB}	Mean temperature of cooling water entering tubes in a tube bundle
T_{iv}	Temperature of cooling water entering barometric condenser
ΔT_L	Mean temperature difference across convective film inside a tube
ΔT_{lm}	Log mean temperature difference for a condenser tube defined by Equation (5)
T_o	Temperature of cooling water leaving a tube
T_{oB}	Mean temperature of cooling water leaving tubes in a tube bundle
T_{ov}	Temperature of cooling water leaving barometric condenser
T_{si}	Temperature of steam or steam-gas mixture entering a tube bundle
U	Overall heat transfer coefficient for a condenser tube defined by Equation (4)
$\overline{U}_B$	Mean overall heat transfer coefficient for a tube bundle defined by Equation (1)
U_n	Overall heat transfer coefficient for the nth tube from the top in a tube bundle
$\overline{U}_n$	Mean overall heat transfer coefficient for a tube bundle n tubes high
V	Linear velocity of cooling water flowing inside tube
W	Condenser tube cooling water mass flow rate
W_b	Barometric condenser cooling water mass flow rate
W_s	Condensate mass flow rate for a single tube

W_{sv} Steam vent mass flow rate

W_{corr} Bypass steam mass flow rate

X_{gb} Mole fraction nitrogen in the bulk steam-nitrogen mixture flowing past a condenser tube

X_{gc} Mole fraction nitrogen in the steam-nitrogen mixture at the condensate film surface

X_{sb} Mole fraction steam in the bulk steam-nitrogen mixture flowing past a condenser tube

X_{sc} Mole fraction steam in the steam-nitrogen mixture at the condensate film surface

Greek Symbols

δ Thickness of the sensible heat transfer and of the mass transfer stagnant film on the tube outside

Γ Mass film velocity of condensate

μ Viscosity of steam

μ_f Viscosity of condensate film at condensing temperature

μ_L Viscosity of cooling water at mean bulk temperature inside tube

μ_w Viscosity of cooling water at the mean inside tube wall temperature

ρ Density of bulk steam or steam-nitrogen mixture

ρ_f Density of condensate film at condensing temperature

ρ_L Density of cooling water at bulk mean temperature

λ Latent heat of evaporation of water

CHAPTER I

INTRODUCTION

Steam surface condensers constitute the major component of seawater distillation plants of the multistage flash (MSF) evaporator type, the most common in use. A typical MSF flowsheet is shown in Figure 1. The steam condensers in that process consist of single tube-pass horizontally oriented multitube bundles, which are arranged within the flashing stage compartments as shown in Figure 2. The tubes are cooled by brine passing successively through the stage condensers from the low temperature to high temperature stages countercurrent to the flow of flashing brine and condensate in the trays beneath. In passing through a given stage, the brine in the tubes is heated about 5°F by condensation of the flashed vapor, with the mean temperature difference between tube side brine and condensing steam (expressed as LMTD) of about 10°F. Multistage flash evaporators contain between 20 and 40 such flashing stages arranged in one or more close-coupled series trains, operating between the ambient seawater temperature and a maximum temperature in the range 180-250°F. (The upper limit is dictated by the scale control method used.) Tube diameters used in the condensers are 5/8 - 1 in. OD, with seawater-resistant copper alloys such as aluminum brass or cupronickel being used for the tubing material. The tube bundles contain approximately 1000 tubes per million gallons per day total plant capacity.

The temperature range of flash evaporators covers both pressure and vacuum steam conditions. The stages operating under vacuum are susceptible to inleakage of air through flanged joints and leaking welds which

ORNL–DWG 72–12444

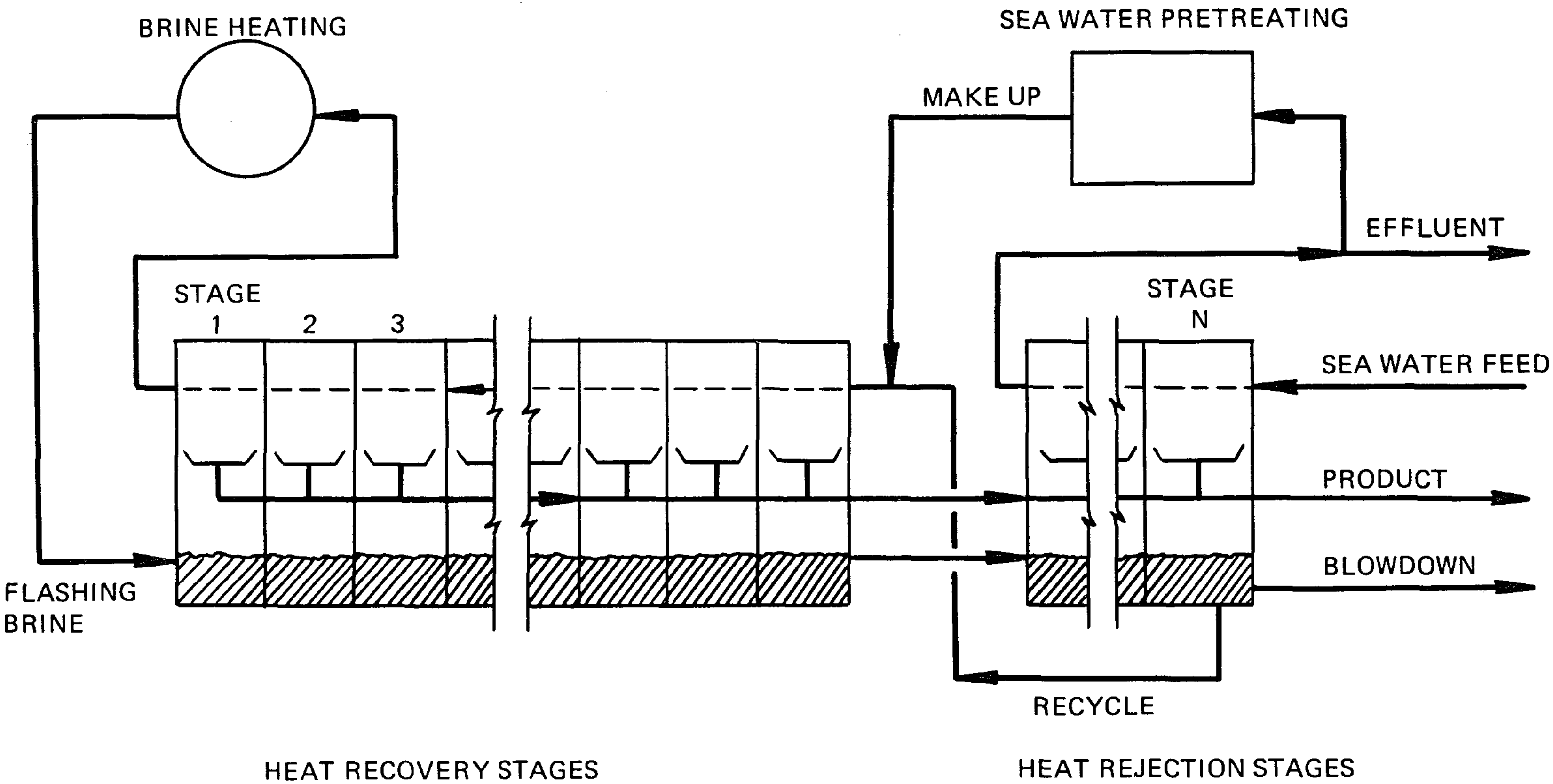

FIGURE 1

MULTISTAGE FLASH EVAPORATOR FLOWSHEET

ORNL–DWG 72–12445

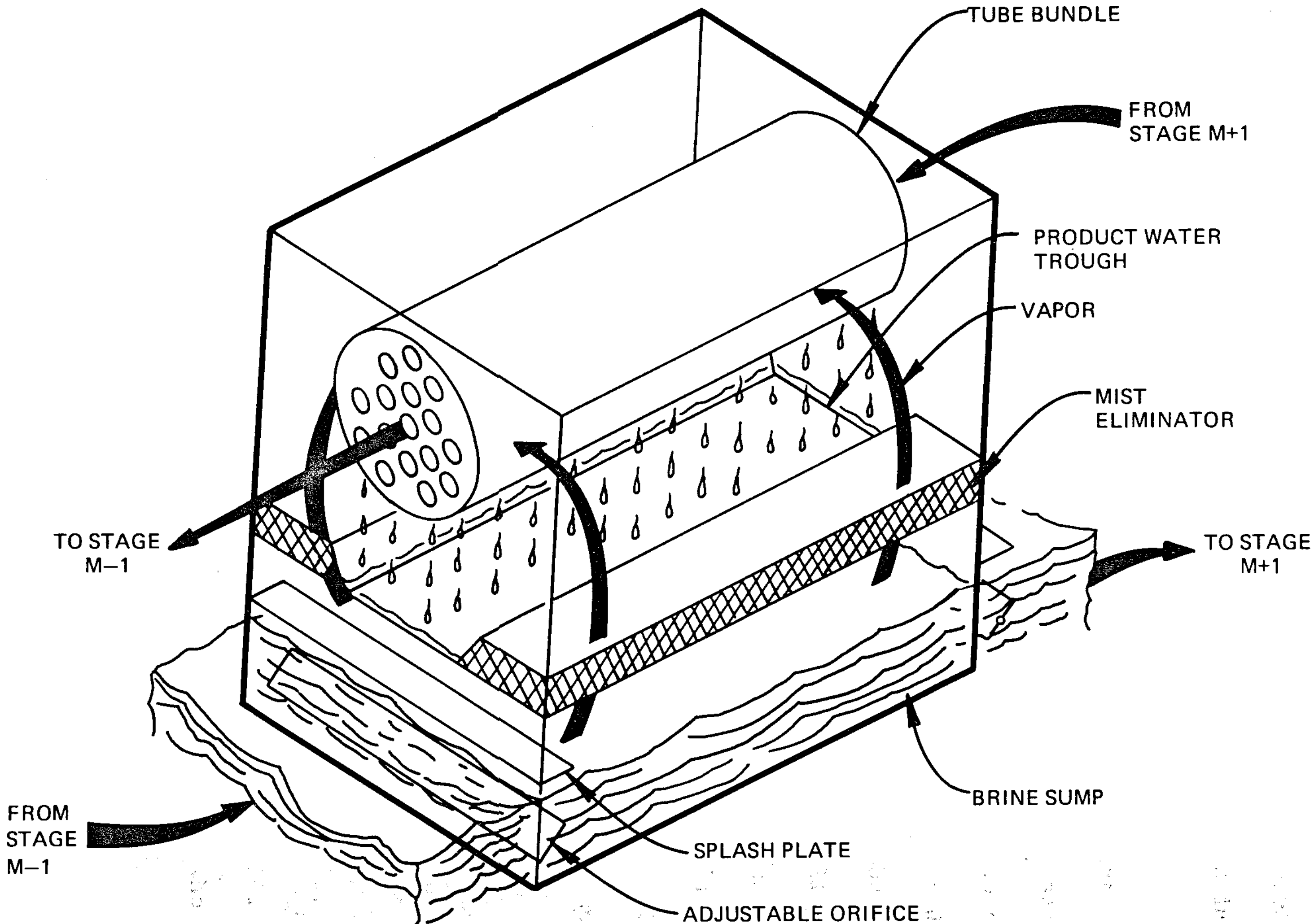

FIGURE 2

SCHEMATIC DRAWING OF A TYPICAL FLASH EVAPORATOR STAGE can flow along with the vapor into the shell side of the condenser bundle. The higher temperature (above atmospheric stages)are less subject to containing non-condensing gas, although the highest temperature stage will contain small amounts of carbon dioxide which remains in the brine after deaeration.

The design of stage condenser tube bundles (as with any heat exchanger) consists of the selection of a suitable bundle cross sectional shape which conforms to the stage dimensions and which appears to provide good steam flow patterns, and the calculation, usually by trial and error, of the required heat transfer area based on the assumed bundle shape and such constraints as brine velocity, tube diameter, wall thickness, and length. Because the stage condensers are all single pass and linked together in series, both with respect to the brine flow in the tubes and the flashing brine and condensate streams on the shell side, the calculation of their heat transfer areas is part of a more complex computation of the entire process flowsheet.

Condenser Heat Transfer Performance

The definition of the heat transfer performance of the stage condensers is that conventionally used in the process industries and described in many texts. This involves the concept of a bundle mean overall heat transfer coefficient ($\overline{U}_B$) which is related to the heat duty of the condenser (Q_B) by the equation:

$$Q_B = \overline{U}_B \cdot A_B \cdot \mathrm{LMTD} \tag{1}$$

where the temperature driving force (LMTD) is based on overall bundle parameters:

$$\mathrm{LMTD} = \frac{T_{oB} - T_{iB}}{\ln \dfrac{T_{si} - T_{iB}}{T_{si} - T_{oB}}} \tag{2}$$

The condenser heat duty is the sum of the heat duties of each of the tubes:

$$Q_B = \sum_T Q_T \tag{3}$$

where:

$$Q_T = U \cdot A_T \cdot \Delta T_{lm} \tag{4}$$

and the temperature driving force is based on the local parameters:

$$\Delta T_{lm} = \frac{T_o - T_i}{\ln \dfrac{T_b - T_i}{T_b - T_o}} \tag{5}$$

By convention, each tube overall heat transfer coefficient is considered to be composed of series film resistances. For the case of condensation on the outside of the tube with some non-condensable gas present and sensible heat transfer inside the tube, the resistances commonly included are:

$$\frac{1}{U} = \frac{d_o}{d_i h_i} + R_w + \frac{1}{h_{cn}} + \frac{1}{h_g} + R_f \tag{6}$$

as shown schematically in Figure 3. The wall resistance (R_w) and by convention, the fouling resistance (R_f), will be constant within a given bundle, whereas the remaining three resistances, being located within fluid streams, will vary depending on the properties of the fluid streams.

The central problem of predicting condenser performance is correctly estimating $\overline{U}_B$. This can be done in several ways, depending primarily on the desired accuracy and the intended application. The procedure described in standard heat transfer texts[1,2] and used in the chemical process industry for the design of small condensers is based on bundle average film resistances. Although the film resistances pertain conceptually to a single tube, as an approximation they are applied to the bundle as a whole. According to this method, the bundle overall heat transfer coefficient is the sum of the five bundle averaged resistances:

$$\frac{1}{\overline{U}_B} = \frac{d_o}{d_i \overline{h}_i} + \overline{R}_w + \frac{1}{\overline{h}_c} + \frac{1}{\overline{h}_g} + \overline{R}_f \qquad (7)$$

which are evaluated separately and then combined.

This procedure, although commonly used, has several defects which contribute to its generally limited accuracy. The major defect arises from the fact that three of the resistances vary from tube to tube, while the remaining two are constant. If the variations are sufficiently large, and if the resistances which vary are of the same order of magnitude as the constant resistances, the process of summing the mean values of each resistance leads to a different result than summing the resistances for each tube and adding the resulting heat loads. In practice, this can

ORNL–DWG 72–12446

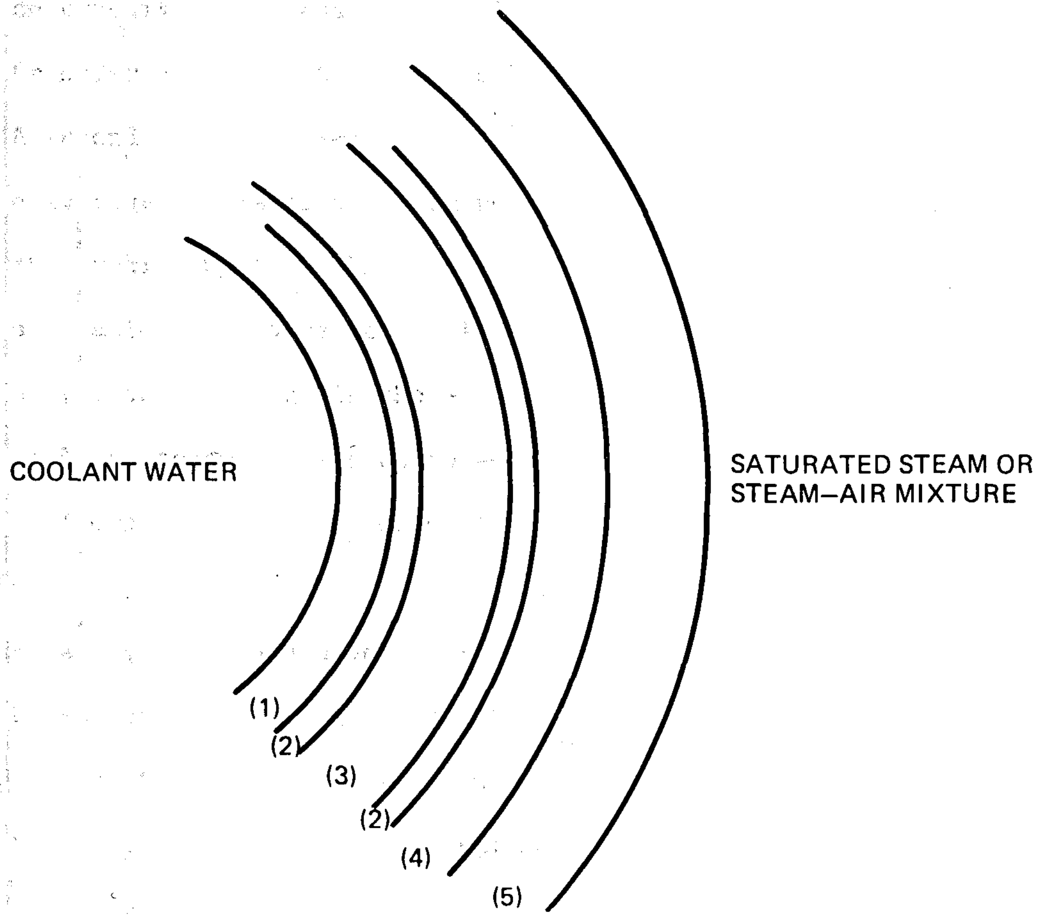

RESISTANCE	SYMBOL
(1) CONVECTIVE FILM	R_i OR $\frac{d_o}{d_i h_i}$
(2) SOLIDS FOULING	R_f
(3) TUBE WALL	R_w
(4) CONDENSATE FILM	R_c OR $\frac{1}{h_c}$
(5) NON CONDENSING GAS FILM	R_g OR $\frac{1}{h_g}$

FIGURE 3

HEAT TRANSFER RESISTANCES FOR CONDENSATION ON THE OUTSIDE OF A TUBE AND SENSIBLE HEAT TRANSFER ON THE INSIDE lead to significant error in large condensers. The error is always on the conservative side; that is, it leads to a low value of the overall heat transfer coefficient for the bundle.

A second source of error are the methods required to estimate the bundle average values of the film resistances. The commonly cited equation for predicting $\overline{h}_{cn}$ is known to be conservative. On the other hand the calculation procedure for estimating $\overline{h}_g$ is so complicated that it is generally ignored except in the extreme cases where the inlet stream contains a large concentration of non-condensable gas, as for example in dehumidifiers. Omitting $\overline{h}_g$ when it should be included leads to underdesign.

Finally, a third source of error arises in part from the fact that the above approximations are known to the designer. The fouling resistance, rather than being chosen on the basis of accounting for the thermal resistance of layers of solids fouling, is generally chosen from a compilation such as the TEMA Tables,[3] which is known to be very conservative.[4] As a result, the method based on bundle averaged film coefficients virtually insures that condensers will be overdesigned. Because of their small size, however, and small contribution to the usual chemical product cost, overdesigned condensers in the process chemical industry are not considered to be a problem.

In the case of the stage condensers used in desalination plants, the tube bundles are much larger than used in the process chemical industry. In addition, there is a strong incentive to obtain accurate rather than conservative designs, since the installed cost of the desalting plant condensers constitutes a large fraction of the total plant cost. A similar situation prevails in the case of steam turbine surface condensers used in stationary power plants.

As a result computer design programs have been evolved for both desalting plant and power plant condensers from which more accurate estimates of $\overline{U}_B$ can be obtained. These programs involve the separate calculation of overall heat transfer coefficients for small groups of tubes within the bundle rather than for the bundle as a whole. By dividing the bundle into homogeneous groups, overall heat transfer coefficients for the groups can be obtained from group average values of the film coefficients with much less error than for the bundle as a whole. The heat loads of the groups can then be summed and substituted into Equation (1) to obtain $\overline{U}_B$. In addition, as a result of the greater accuracy, selection of a fouling factor can also be made more realistically, on the basis of the expected solids fouling, rather than from the conventional TEMA tabulation. In order for these more detailed calculations to realize that objective, however, it is necessary for each of the correlations used for evaluating the various film resistances to be capable of predicting the expected heat transfer with as great or greater accuracy than possible with the more approximate method. To establish this would require experimental verification in multitube condensers such that each of the relevant parameters is varied systematically over as much of the range of interest as possible. Such a verification has not previously been carried out. This is the objective of the present program.

CHAPTER II

BACKGROUND

In Chapter I, it was noted that one can calculate the heat transfer performance of a condenser by dividing it into groups of tubes and calculating group-average overall heat transfer coefficients from group-average values of the film resistances. In following this procedure, the film resistances are evaluated based on local values of the parameters which affect each film. These parameters include the temperatures of steam and cooling water, the water velocity in the tube, the steam velocity past the tube outside, the non-condensable gas concentration, and the condensate rain rate. Of these, the parameters which vary with position in the bundle are the latter three.

The steam mass velocity variation with location in a condenser bundle is a consequence of the interaction between the steady decrease of steam mass flow along the flow path as condensation occurs, and the change in the open cross sectional area along that path due to the overall bundle shape. Its magnitude is also affected by the bundle vent rate and by the bundle friction factor-Reynolds number relationship. Thus, although the steam mass flow rate itself always will decrease monotonically along the flow path due to condensation on each tube, the steam mass velocity can be made to increase if the percentage change in flow area exceeds the change in mass flow rate. It is possible also to design a tapered tube bundle which has a steam mass velocity which is constant throughout the entire bundle.

In a similar fashion, the non-condensable gas fraction will also change with location in a condenser, increasing along the steam flow path from front face to vent as a result of the loss of steam with no associated loss in gas. The change is not necessarily linear, but depends on the condensation rate at each position on the flow path and on the vent rate.

Finally, the condensate rain rate, or mass flow rate of condensate raining onto a given tube, is a function of the number of tubes above it and thus also depends on the bundle cross section geometry, although according to a different set of criteria.

In dividing the bundle into groups for the computer calculation of heat transfer, the size and arrangement of the groups and the sophistication of the calculation are dictated by the overall bundle geometry and by the methodology of the computer programs. ORCON, a program developed at ORNL,[5] calculates the overall heat transfer coefficient, steam pressure, steam mass velocity, non-condensable gas fraction, and condensate rain rate for tube groups in sequence moving from the entrance face to the vent. An iteration procedure is used to match the total vent rate and pressure drop with those required by the flowsheet. An inherent assumption in the detailed design calculation of ORCON is that the various film resistances applicable for a group are that of a representative tube, that is, one exposed to the same conditions as the average of the tubes in the group. Thus, in preparing the computer program, the correlations used are for individual tubes located within large bundles.

In the following sections, the methodology and correlations for predicting the applicable individual tube heat transfer coefficients for tubes within tube bundles are reviewed, with reference to areas where the present experiments are directed. Where pertinent, theoretical and semi-theoretical derivations are presented, including those developed in the course of the present experimental work. No attempt has been made to provide a comprehensive review of the literature of condensation heat transfer. Most of the references, dealing both with theoretical and experimental aspects of the subject, pertain to simpler geometries or flow conditions, and are not relevant to the current work.

Individual Tube Heat Transfer Coefficients

In calculating the overall heat transfer coefficient for steam condensing on the outside of single horizontal tubes in which cooling water flows in turbulent forced convection, five series thermal resistances were defined,

$$\frac{1}{U} = \frac{d_o}{d_i h_i} + R_w + \frac{1}{h_{cn}} + \frac{1}{h_g} + R_f \qquad (6)$$

These film resistances divide the total temperature difference (ΔT_{lm}) into film temperature differences. Three of these resistances are located within flowing streams and are expressed conventionally as film coefficients based on the area where the films are located.

Individual film heat transfer equations can be written for each film analogous to Equation (4).

$$Q_T/A_i = h_i \ \Delta T_i \qquad (8)$$

$$Q_T/A_T = h_c \ \Delta T_c \qquad (9)$$

$$Q_T/A_T = h_g \ \Delta T_g \tag{10}$$

The wall resistance is obtained from the thermal conductivity and thickness of the tube wall:

$$R_w = \frac{d_o \ \ln d_1/d_L}{2k} \tag{11}$$

and the fouling resistance from a suitable evaluation of the expected fouling tendencies of the steam and cooling water.

In the present work only the two film coefficients on the tube outside (h_c and h_g) were investigated. The correlation equation assumed for predicting h_i was the conventional Sieder-Tate type:

$$\frac{h_i d_i}{k} = C_i \ (Re_L)^{0.8} \ (Pr_L)^{0.33} \ \left(\frac{\mu_w}{\mu_L}\right)^{0.14} \tag{12}$$

with C_i obtained experimentally for the tubes used in the condenser using the Wilson plot method.

Condensate Film Heat Transfer Coefficient

The basic correlating equation for the heat transfer coefficient for condensation on the outside of a single horizontal smooth tube is the well known theoretical equation of Nusselt,[6] commonly written in either of two equivalent forms, one based on the film ΔT:

$$h_N = 0.725 \left\{ \frac{k_f^{\ 3} \ \rho_f^{\ 2} \ g\lambda}{\mu_f \ d_o \ \Delta T_c} \right\}^{1/4} \tag{13a}$$

and the other on the tube condensation rate:

$$h_N = 0.76 \left\{ \frac{k_f^{\,3} \rho_f^{\,2} g}{\mu_f \Gamma} \right\}^{1/3} \qquad (13b)$$

The derivation of this equation, given in many reference books, requires the following assumptions:[1]

1. The heat delivered by the vapor is latent heat only.

2. The flow of the condensate film along the surface is laminar with the heat of condensation transferred through the film by conduction.

3. The thickness of the film at any point is a function of the condensation rate at that point and the net amount of condensate passing the point.

4. The velocity gradient across the film is a function of the relation between the wall frictional shearing force and the weight of the film. There is no shearing force acting on the vapor side of the condensate film.

5. The condensation rate at every point is proportional to the quantity of heat transferred, which is in turn related to the thickness of the film and of the temperature difference between the vapor and the surface.

6. The condensate film is so thin that the temperature gradient through it is linear.

7. The physical properties of the condensate are taken at the mean film temperature.

8. The surface is smooth and clean.

9. The temperature at the surface of the solid is constant.

10. The curvature of the film is neglected.

All of these assumptions are reasonably met in the case of laminar film condensation of slow moving steam on the outside of a single horizontal smooth tube.

It is of interest to note that one can derive a more general form of the Nusselt equation by dimensional analysis without the need for the Nusselt assumptions. By considering that the variables which affect the heat transfer coefficient are the set: k_f, μ_f, g, Γ, ρ_f, the Buckingham Pi method leads to the following relationship:

$$h_c = A \left\{ \frac{k_f^3 \rho_f^2 g}{\mu_f^2} \right\}^{1/3} \left(\frac{\Gamma}{\mu_f}\right)^p \tag{14}$$

where the first term in parenthesis on the right hand side is sometimes referred to as the Condensation Group, and the second term is seen to be proportional to a film Reynolds number.

A prediction method using these groups was developed by Dukler[7] based on boundary layer theory for application to vertically oriented condensing surfaces. He prepared parametric plots of the ratio of the Condensation Group to the condensate film heat transfer coefficient plotted against the film Reynolds number, with the condensate Prandtl number and a vapor shear term as parameters. His theoretical predictions for the case of zero vapor shear, Prandtl numbers betweel 0.1 and 5, and Reynolds numbers less than 100 asympotically approached the Nusselt equation (laminar flow) predicted line drawn for the case of vertical surfaces. That is, the exponent on the Reynolds number approached -1/3, and the constant approached the Nusselt predicted value. There was no sharp laminar-turbulent transition in Dukler's results.

It is noted that a single horizontal tube with steam condensing at 212°F on its outside will have a film Reynolds number (at its midpoint) of 2-5, depending on the values of U and the ΔT_{lm}. Even the bottom tube of a 10 tube high array will have a Reynolds number less than 100, thus lending theoretical support to the use of the Nusselt equation for predicting the performance of at least the top tube of a horizontal condenser tube bundle.

Experiments by many investigators have confirmed the validity of the single tube Nusselt equation for the case of Freon,[8,9] and organics[2] as well as steam,[1] and over a range of temperatures and condensing rates. Agreement is generally within ten percent. Where values differ significantly, either non-condensable gas or dropwise condensation has been suspected, either by the author or by later investigators. Thus, it is concluded that for the case of a single horizontal tube (the top tube in a bundle), no additional work is needed to improve the existing correlation.

Condensate Rain Effect

When condenser tubes are arrayed horizontally in bundles, in addition to the condensate continually formed on each tube, there is a rain of condensate onto each tube from above, with the thickness of the total condensate layer on the lower tubes reflecting the added flow. Although the single tube theoretical equation can not be applied directly, by making several simplifying assumptions Nusselt[6] derived a modification for predicting the mean condensate film heat transfer coefficient of a vertical column of horizontal tubes. When written as a ratio of the mean condensate film heat transfer coefficient for a vertical column of n tubes ($\overline{h}_{cn}$) to that of the top tube (h_N) as calculated from Equation (13), the following simple relationship was obtained:

$$\frac{\overline{h}_{cn}}{h_N} = n^{-0.25} \qquad (15)$$

The assumptions required (in addition to those used for the single tube derivation) were:

1. Condensate drains as a laminar sheet from a tube bottom to a tube top such that the velocity and temperature gradients are not lost in the fall between tubes.

2. The condensation rates for all tubes in the column are equal.

In contrast to the single condenser tube derivation, neither simplifying assumption corresponds to actual conditions in a steam condenser. With regard to the first assumption, investigators have reported that rather than laminar sheets, the condensate collects in discrete regions on the undersides of tubes, and drains as individual drops or streams, presumably also mixing in the process.[9,10] It has also been noted[11] that the drops and/or streams do not strike only the tops of lower tubes but strike anywhere on the upper half. With regard to the second assumption, the condensation rate per tube, rather than being a constant, is itself dependent on h_c. The magnitude of the variation depends on the magnitude of the condensate film compared to the other resistances. This latter effect is conveniently handled by converting Equation (15) into a form which gives the performance of a single lower tube in terms of the Nusselt equation prediction at that lower tube condensing rate, rather than the rate of the top tube. This is done by the following steps.

Starting with the expression for the mean value of the condensing coefficient for a column of n tubes:

$$\frac{\bar{h}_{cn}}{h_N} = n^{-0.25}, \tag{15}$$

the mean of the (n-1) tubes above the nth tube is:

$$\frac{\bar{h}_{c(n-1)}}{h_N} = (n-1)^{-0.25}. \tag{16}$$

Then, noting that from the definition of the mean, one can write:

$$h_{cn} = n\,\bar{h}_{cn} - (n-1)\,\bar{h}_{c(n-1)}. \tag{17}$$

By substituting Equation (15) and Equation (16) into Equation (17), one obtains the desired relation:

$$\frac{h_{cn}}{h_N} = n^{0.75} - (n-1)^{0.75} \tag{18}$$

with h_N evaluated at the condensation rate of the nth tube rather than as in Equation (15) from the top tube.

In a similar manner, the mean condensate film coefficient for the bottom five tubes of a 5m high column of tubes (where m is a positive integer) can be obtained as a function of the mean value of a five tube high column, all based on Equation (15). Thus, the mean coefficient for a 5m tube high column is:

$$\frac{\bar{h}_{c5m}}{h_N} = (5m)^{-0.25}, \tag{19}$$

for a 5(m-1) tube high column it is:

$$\frac{\bar{h}_{c5(m-1)}}{h_N} = [5(m-1)]^{-0.25}, \tag{20}$$

and for a five tube high column it is:

$$\frac{\bar{h}_{c5}}{h_N} = 5^{-0.25} \tag{21}$$

Defining the mean coefficient of the bottom five tubes of a 5m high column as:

$$(\bar{h}_{c5})_{bottom} = \frac{1}{5} \sum_{s=5(m-1)+1}^{5m} h_{cs} \tag{22}$$

and noting that, from the definition of the mean:

$$5m\ \bar{h}_{c5m} = 5(m-1)\ \bar{h}_{c5(m-1)} + \sum_{s=5(m-1)+1}^{5m} h_{cs} \tag{23}$$

the bottom five tube mean coefficient, in terms of the top tube is:

$$\frac{(\bar{h}_{c5})_{bottom}}{h_N} = \frac{(5m)^{0.75} - [5(m-1)]^{0.75}}{5} \tag{24}$$

and therefore, the desired ratio is:

$$\frac{(\bar{h}_{c5})_{bottom}}{\bar{h}_{c5}} = \frac{(5m^{\ 0.75} - [5(m-1)]^{0.75}}{5^{0.75}} \tag{25}$$

The latter expression is used in comparing the Nusselt theory to the experimental data obtained in the present work, in which a five-tube high bundle was utilized.

Equations (15) and (18) have been compared in the literature with experiments involving single vertical columns of tubes and also triangular spaced staggered tube arrays. In several of the studies, recycled condensate rained onto the top of the array to simulate even deeper bubbles. Agreement between theory and experiment has generally not been good, with the data nearly always yielding higher values than predicted. In Figure 4 are curves representing data from several authors.[9,10,12-15] It is noted that the experimental results differ from each other by significant amounts as well as deviating from Nusselt theory. These disagreements between investigators, although noted previously,[10] have not been the subject of further theoretical analysis. Instead, the experimental results have been fitted in most cases by empirical equations which are essentially modified forms of Equation (15) in which the exponent is empirically determined:

$$\frac{\bar{h}_{cn}}{h_N} = n^{-s} \tag{26}$$

Values of s in the range 0.07 to 0.20 have been reported.

Equation (26) can be used to derive an expression for the mean condensate film heat transfer coefficient for the bottom five tubes in a deeper array which is analogous to Equation (25) but in general form:

$$\frac{(\bar{h}_{c5})_{bottom}}{\bar{h}_{c5}} = \frac{5m^{1-s}-[5(m-1)]^{1-s}}{5^{1-s}} \tag{27}$$

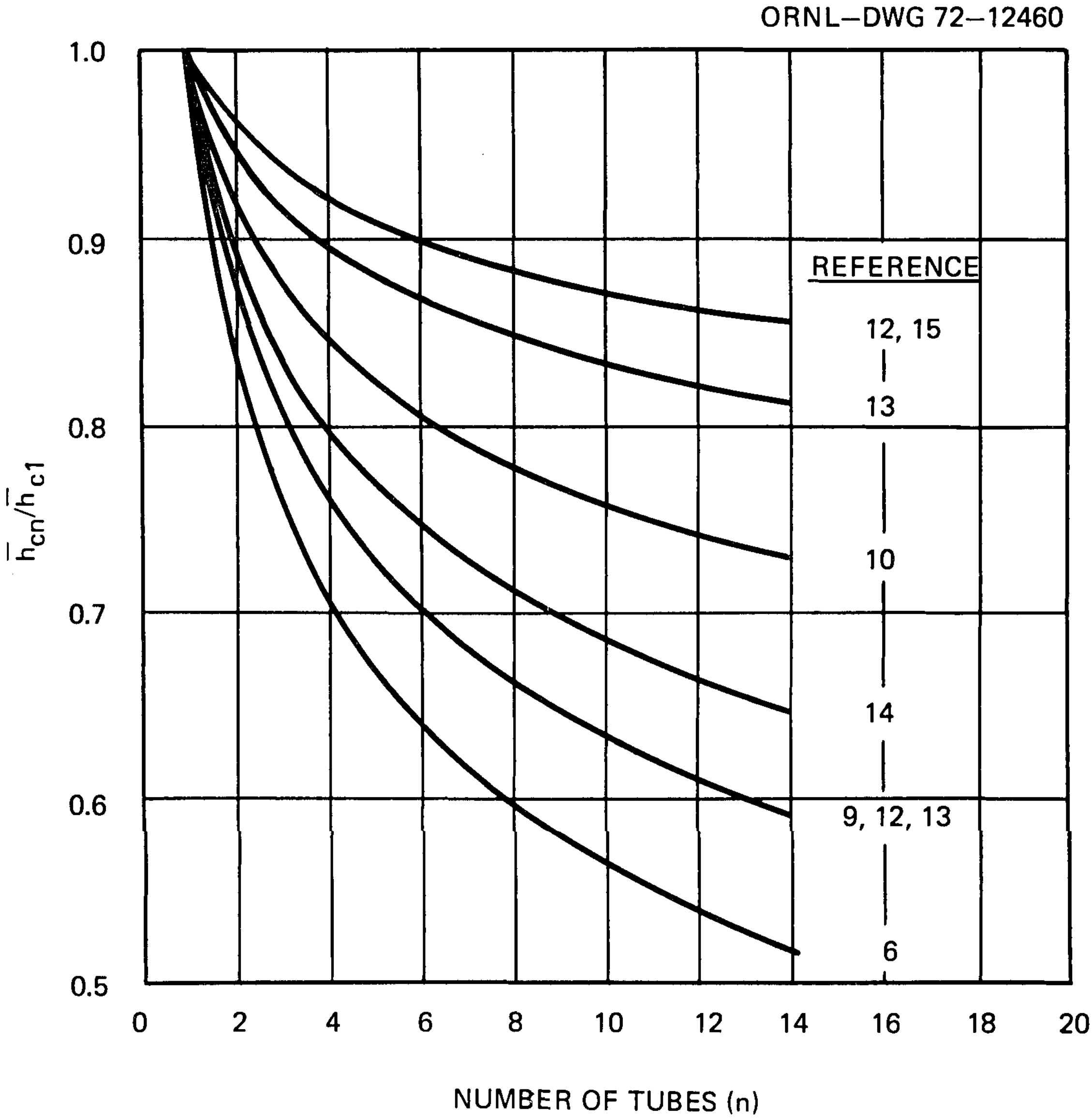

FIGURE 4

EFFECT OF CONDENSATE RAIN ON THE MEAN CONDENSATE FILM HEAT TRANSFER COEFFICIENT ACCORDING TO VARIOUS AUTHORS

This expression was used in correlating the experimental data obtained in the present work.

Derivation of the Side Drainage Model

In the literature, the conflicting experimental effects of condensate rain are reported without any explanation of the differing results obtained with a single vertical column of tubes and with arrays in which the tubes are oriented variously with respect to each other, that is, in-line or staggered triangular pitch, with varying centerline distances. In each case, all that defined the tube bundle for correlation purposes was the number of tubes in a vertical column. This procedure unnecessarily ignores tube-condensate interactions which can influence the magnitude of the condensate drainage effect. As part of the present work, a new phenomenological model has been developed which accounts for this effect and which hopefully can provide a more accurate measure of the condensate rain effects for a variety of tube bundle layouts.

In Figure 5 are illustrated schematically the two common orientations of tubes in tube bundles. In each instance, tube numbers for a representative column are shown to illustrate the counting scheme. The side drainage model proposed here deals with the differences in condensate drainage patterns as between these two orientations.

Figure 6 illustrates an equilateral triangular staggered layout with a spacing (S/d_o) of 1.33 (a common spacing for steam condensers). For 3/4 in. to 1 in. OD tubes, the gap between adjacent horizontal tubes is thus 1/4 in. - 1/3 in. Shown in such a gap is a droplet of condensate of 1/8 in. diameter, a size that is typical of those falling from tubes.

ORNL–DWG 72–12448

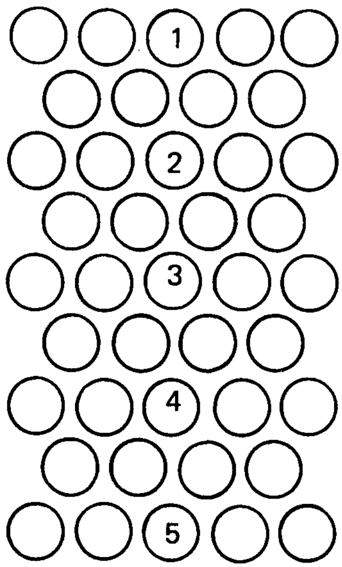

STAGGERED

(a)

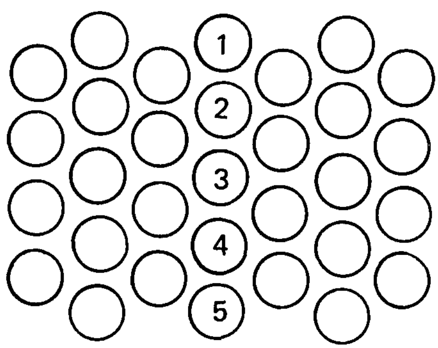

IN–LINE

(b)

FIGURE 5

ALTERNATE HORIZONTAL CONDENSER TUBE BUNDLE ARRANGEMENTS

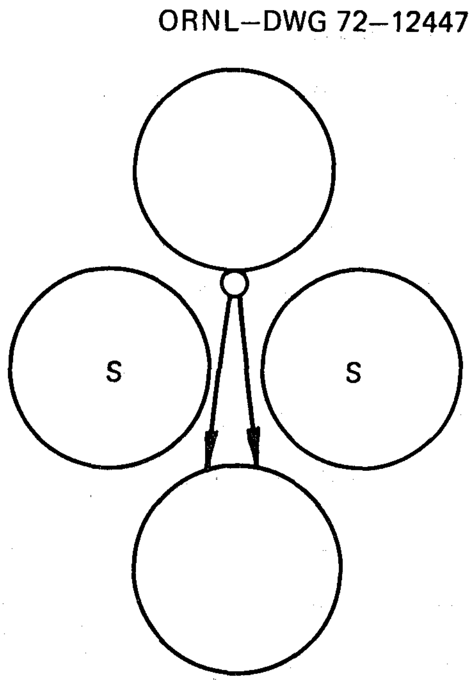

FIGURE 6

SIDE DRAINAGE MODEL

Also shown is the limit of trajectory (shown as the centerline trajectory) within which a drop from tube one will not strike either of tubes "S" (the side tubes). It is noted that in order for the Nusselt theory to be applicable, all of the drops must avoid striking tubes "S."

Since the tubes in a condenser are continuously coated with a film of condensate, any drop which falls outside of the limits shown and strikes either of the tubes "S" can be drawn by surface tension wholly or partially onto them. These drops will strike somewhere close to the tube midpoint of the side, and once absorbed will join the rest of the condensate on "S." Since all tubes in a condenser have the same geometric arrangement, this event, referred to as "side drainage," can occur with equal probability on any tube.

The frequency of side drainage will depend on the probability of a trajectory lying outside of the limits shown. Qualitatively, this in turn may depend on the interactions of the following:

1. Orientation. A triangular staggered pattern should lead to more side drainage than in-line. Isoceles triangles (acute angle up) should lead to more side drainage than equilateral triangles.

2. Spacing. The smaller the S/d_o, the more frequent should be the side drainage.

3. Momentum. The greater the horizontal component of momentum of the drops leaving a tube, the greater the side drainage. Horizontal momentum will be greater when discrete rivulets flow over the surface, and will increase with increased condensate flow rate.

4. Steam Velocity. When steam flows horizontally across tubes at sufficient velocity, the drop trajectory will reflect the added lateral

momentum. When steam flows vertically, its direction change with each tube may also impart lateral momentum to the drops.

5. Misaligned Tubes. A tube misaligned in a bundle may receive a greater or lesser amount of condensate depending on its orientation with respect to the side tubes. Drainage from a misaligned tube may all fall onto a side tube, leaving the tube beneath it free of drainage.

Some of the above factors could cause condensate to strike the side of the tube immediately below when no side tubes are present. In that case, the limitation on the trajectory would be determined by the vertical spacing between the tubes, with a small spacing practically insuring a drop striking near the top of the lower tube. Thus simply rotating an equilateral triangular array from staggered to in-line should significantly reduce side drainage. Since the net effect of side drainage on condensation will be to reduce the effect of condensate rain, it should lead to an increase in the condensate film heat transfer coefficient of lower tubes. This can be quantitatively predicted using the following theoretical analysis.

Analysis of Side Drainage

If all tubes in a bundle drain condensate via side drainage and if the condensate strikes the sides of tubes at their midpoint, then the top half of all tubes will receive no drainage -- that is, they will all behave as top tube top halves. Kern[1] notes that the top half of a single horizontal condenser tube will theoretically condense at a rate 1.2 times that of the entire tube based on the Nusselt assumptions. Thus the condensate formed on the top half of all tubes in a bundle with side drainage will be 1.2 x 0.5 or 0.6 that of a top tube. The condensate rate for the bottom half of each tube can be approximated from the following. Again assuming only side drainage, individual drops that leave each tube will strike either right or left side tubes. This, on the average, will lead to condensate striking the lower half of each tube (except the top tube) from both sides at a flow rate equal to twice the condensate load if all drainage had been normal (tube bottom to tube top). This can be visualized by drawing the hypothetic track of a single drop, Figure 7. If all paths were of this type, each tube bottom would receive the average drainage from two vertical columns instead of one. If it is assumed that the effect of the added condensate on the bottom halves of all tubes is correctly predicted by the Nusselt theory, then the mean coefficient for the bottom halves will be:

$$\left(\frac{\bar{h}_{cn}}{h_N}\right)_{\text{bottom}} = (2n)^{-.25} \tag{28}$$

or, since half the tube area is involved, the contribution to the mean tube bundle coefficient is half that amount. Thus, the predicted sum of the contributions of top and bottom halves of tubes will be:

$$\frac{\bar{h}_{cn}}{h_N} = 0.60 + \frac{0.50}{(2n)^{.25}} \tag{29}$$

The prediction of condensate drainage given by Equation (29) represents a theoretical minimum effect, hypothetically possible in staggered tube bundle arrays only when there is complete side drainage. Actual staggered tube bundles will be expected to have a distribution of drop trajectories such that some fraction of the condensate falls as side

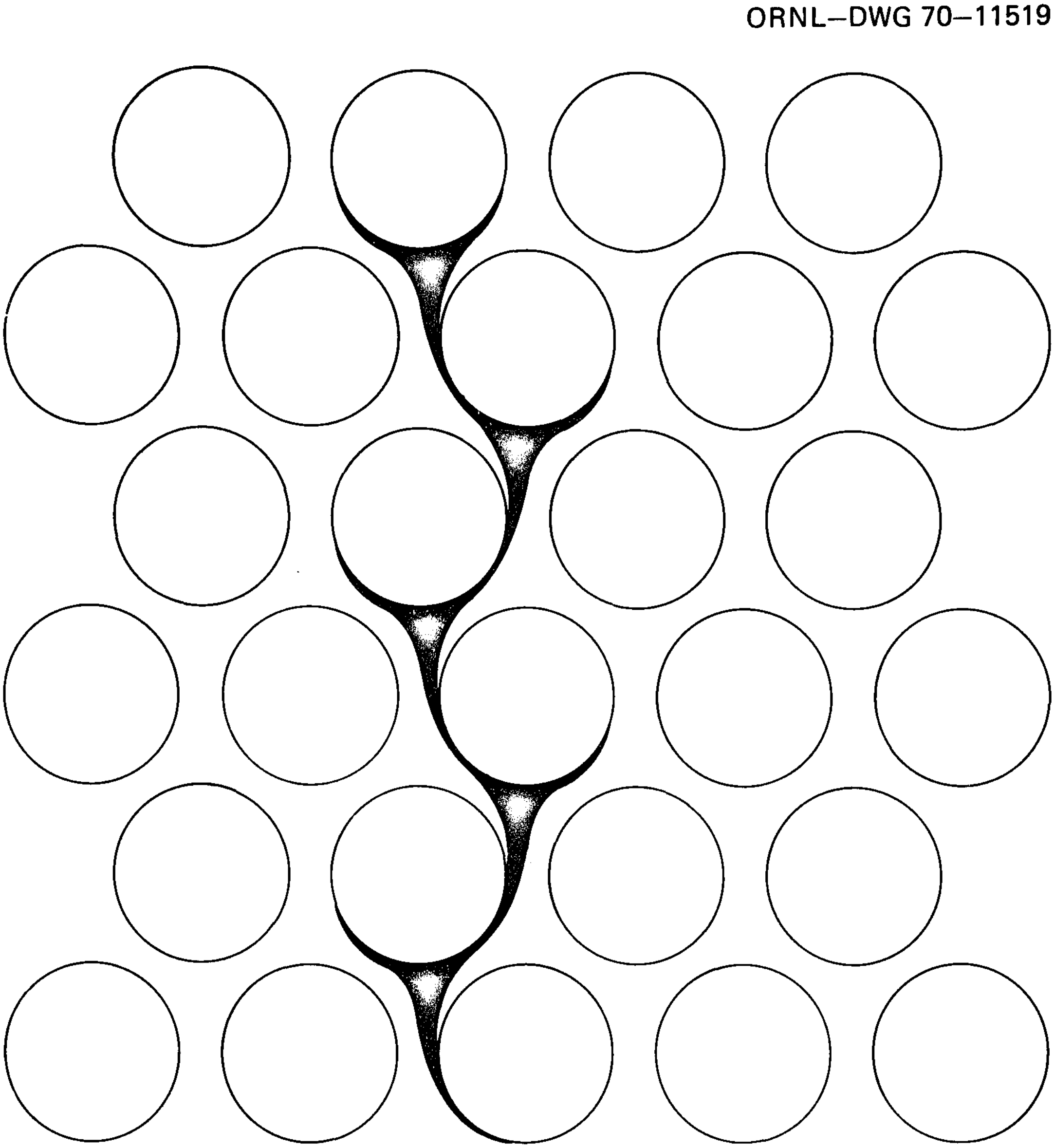

FIGURE 7

DROPLET PATH THROUGH A TUBE BUNDLE WITH SIDE DRAINAGE

drainage and the rest by top drainage, the fraction being determined by the factors listed previously. At the other extreme, bundles consisting of single vertical columns or of in-line wide spaced arrays will according to this model have a $\bar{h}_{cn}$ as predicted by the Nusselt theory.

To analytically express bundle performance which lies between the theoretical maximum and minimum conditions, the parameter F_d has been defined as the fraction of the condensate everywhere in a bundle which occurs as side drainage. Thus:

$$\bar{h}_{cn} = F_d\,(\bar{h}_{cn})_{side} + (1-F_d)\,(\bar{h}_{cn})_{top} \tag{30}$$

Substituting Equation (29) and Equation (15) for $(\bar{h}_{cn})_{side}$ and $(\bar{h}_{cn})_{top}$ respectively, and simplifying, one obtains the parametric equation:

$$\frac{\bar{h}_{cn}}{h_N} = 0.6\ F_d + \frac{1-0.58\ F_d}{n^{0.25}} \tag{31}$$

This equation and its adjustable parameter F_d provides a correlating method which can be used in place of the purely empirical Equation (26).

A pair of tests performed by Ferguson and Oakden[12] provides experimental support for the predictions of the model. The tests were performed using a single vertical column of 3/4 in. tubes and a small staggered triangular array of tubes of the same dimensions. In each case there was downflow of steam past the tubes at various velocities. The effect of the number of tubes on the condensate film heat transfer coefficient is shown in Figure 8 along with lines representing Equations (15) and (29), equivalent to F_d equal to zero and to unity, respectively. It is seen that each set of data agreed fairly well with one of the limiting equations.

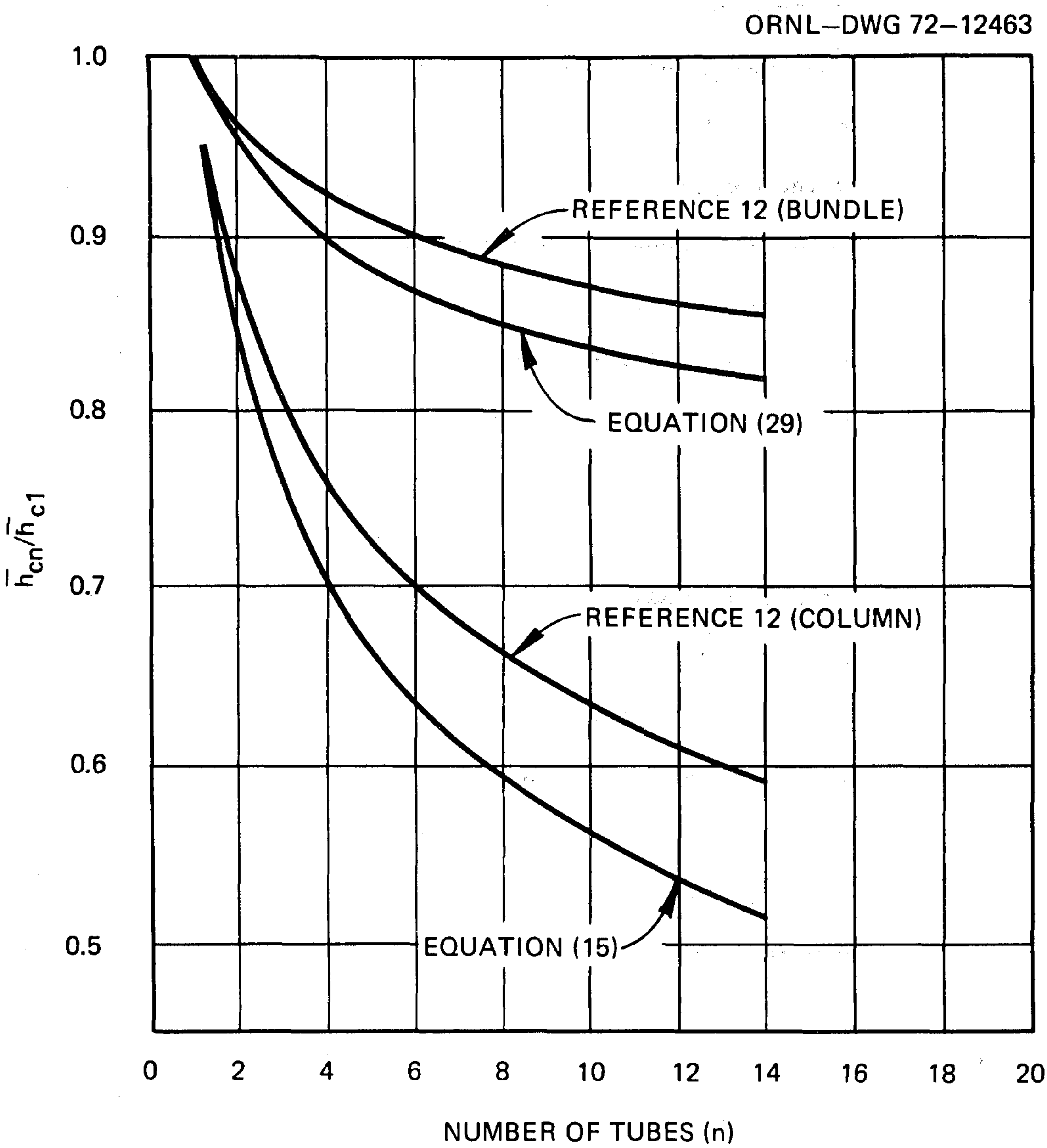

FIGURE 8

COMPARISON OF DATA OF FERGUSON AND OAKDEN WITH THEORETICAL EQUATIONS

Data sets by the other investigators included in Figure 4 were mostly for staggered arrays, with various tube spacing, diameters and operating conditions. The data generally lie in the region between the values of F_d of 1 and 0. From an examination of the experimental parameters, no relationship could be found between F_d and any parameters.

Another study which indirectly gives support to another aspect of this model is that of Young.[13] Experiments were carried out using triangular staggered arrays which were narrow (three tubes wide) and high (seven to nine tubes). Tests were reported for two tube bundles with smooth tubes. One of the bundles gave a value of F_d of close to unity and the other a value closer to zero. No explanation for this difference was offered by the author,[16] but in analyzing the results, it was found that for the bundle with $F_d = 1$, a replotting of the data in the form of h_{cn} versus n produced a pattern whereby several tubes had higher values of h_{cn} than either the tube above or below. This is consistent with the misaligned tube hypothesis of enhancement due to side drainage, whereby a tube misses receiving its condensate load from upper tubes because it, or the tube above it, is misaligned. This effect was missing for the case of the bundle with F_d nearer to zero.

It is concluded from the analysis of the available data that the model of side drainage provides a potentially valuable framework for accounting for and predicting the effect of condensate drainage in staggered triangularly arrayed tube bundles. It is hoped that future experiments will shed light on the factors which determine F_d. The present experimental program was limited to only one tube size and spacing, so that it could not be used for that purpose.

Effect of Steam Velocity

The Nusselt derivations for single tube and tube bundle condensate film heat transfer coefficient both assume that the velocity of the steam flowing past the tubes is negligible. However, in steam condensers, the velocity everywhere in the bundle and especially near the front face tubes is appreciable, so that its effect needs to be determined, and if significant, properly taken into account.

There are two mechanisms that have been proposed whereby steam velocity can influence the condensate film heat transfer coefficient. First, the vapor shear on the condensate film and on the falling drops could influence the mean flow rate or the flow direction of the condensate and thus affect the thickness of the condensate film.[12] Second, the vapor shear could cause the surface of the condensate film to become turbulent and thus increase the effective thermal diffusivity of the film.[17] The magnitude of the first effect will depend on the direction of the steam flow -- downward flow increasing the condensate velocity while up flow having the opposite effect (and at sufficiently high velocity, flooding the condenser in a manner analogous to a packed column). Horizontal flow would tend to transport condensate laterally without directly affecting the film thickness. The second effect, that of turbulence enhancement, increases the rate of condensation in proportion to the increase in turbulence it causes and the fraction of the tube on which is promotes the turbulence. It should be independent of the steam flow direction.

Several experimental studies of the effect of steam velocity in horizontal tube bundles have been reported. In one study, Fuks[18] used an eleven-tube-high staggered bundle containing 72 tubes with an S/d of

1.475. He measured both the effect of condensate drainage and steam velocity, the latter directed downward over the bundle. For the conditions investigated (steam temperature in the range 85 to 212°F and mass velocity between 220 and 2100 lb/hr-ft^2), the condensate film heat transfer coefficient for the top tube (where the effect of condensate rain would not be present), was found to vary directly with the velocity head (G^2/ρ) to the 0.08 power. This is also equivalent, at constant steam temperature, to a variation with the mass velocity of $G^{0.16}$.

A study by Berman and Tumanov[17] gave the effect of a downward flow of steam past a tube located within a dummy bundle with S/d_o of 1.475. The authors covered a range of steam temperatures from 75°F to 175°F and steam mass velocities from 60 to 1000 lb/hr-ft^2. They found an increase in the condensate film heat transfer coefficient with increased steam velocity, correlating the results by the empirical equation:

$$\frac{h_c}{h_N} = 1 + 9.5 \times 10^{-3}\, Re_s^{\,11.8/\sqrt{Nu_N}} \qquad (32)$$

where Re_s is the vapor Reynolds number defined using the tube outside diameter and the superficial steam velocity, and Nu_N is a condensation Nusselt number, defined as:

$$Nu_N = \frac{h_N d_o}{k_f} \qquad (33)$$

The authors also presented their data as a power function relationship. For the range of mass velocity covered they found that the condensate film heat transfer coefficient varied directly with $G_s^{0.15 \pm 0.05}$, where the exponent increased with increasing condensing rate.

Rachko[19], using two 11-tube-high staggered arrays with different tube spacings, studied the combined effects of bundle depth, tube spacing, condensing rate, steam velocity (downward) and steam temperature. He correlated the separable effect of steam velocity in power law form, finding that the condensate film heat transfer coefficient varied directly with $G^{0.125}$ for the bundle with S/d_o of 1.475 and with $G^{0.22}$ for S/d_o of 1.625.

All of the reported experiments dealt with the downflow of steam through staggered arrays. They are in agreement that the condensate film heat transfer coefficient varied directly with the steam velocity. As noted by Berman,[17] the use of a simple multiplicative term to express the steam velocity effect is mechanistically wrong, since it does not extrapolate at zero velocity to the Nusselt equation, and thus can be regarded as valid only within the range of velocities covered by the experimenters.

The difference between steam flow down versus horizontal across a horizontal bundle has not previously been studied. If the mechanism of enhancement by steam velocity is by a thinning of the condensate film, it is likely that a horizontal steam flow will have a smaller effect than downflow. In the present experiment, the effect of horizontal flow was studied.

Non-Condensable Gas Film Heat Transfer Coefficient

The effect of non-condensable gas on steam condensation is to decrease the temperature of condensation from the saturation temperature at the total pressure in the condenser (for the case of pure steam) to the saturation temperature at the partial pressure of the steam at the cooled surface. There are two separable effects which occur, that due to the concentration of the gas in the bulk steam-gas mixture, and that due to the buildup in its concentration in the vicinity of the tube wall where the condensation is occurring.

The first effect is handled in detailed condenser performance calculations by using a ΔT_{lm} based on the steam saturation temperature for the bulk steam-gas mixture flowing by that region as calculated from the local gas concentration. The second effect, the gas film temperature drop, results from the gradient of steam partial pressure in the vicinity of the tube. This gas film temperature drop is related to h_g, the non-condensable gas film heat transfer coefficient by:

$$Q_T/A_T = h_g \, \Delta T_g \tag{34}$$

The correlation of h_g is not carried out using heat transfer parameters, since the process occurring is one of mass transfer of the steam across a partial pressure gradient to the cooled surface. There is no detectable temperature drop (and thus no resistance) involved in the actual phase change occurring at the surface. The conventional approach has been to relate h_g to a mass transfer coefficient. The simplest one, and the one adopted in this work is defined by the equation:

$$h_g \, (T_b - T_c) = \lambda \, k_g \, (p_{sb} - p_{sc}) + h_o (T_b - T_c) \tag{35}$$

so that the condensation rate is given by:

$$W_s = k_g \, (p_{sb} - p_{sc}) \tag{36}$$

For small differences in partial pressure across the film, and neglecting the sensible heat transfer which occurs coincidentally with the mass transfer of the vapor, one can write:

$$h_g = \lambda\ k_g \frac{(p_{sb} - p_{sc})}{(T_b - T_c)} \tag{37}$$

Although there is always a small amount of sensible heat transferred during condensation in the presence of gas, for the usual case where the steam enters the condenser saturated, the sensible heat transferred is a negligible fraction (about 0.1 percent) of the latent heat, and has been neglected.

Colburn Analogy

One of the first and the most commonly used method for predicting mass transfer coefficients for a wide variety of flow geometries is the j-factor analogy proposed initially by Chilton and Colburn[20] based on approaches by Nernst[21] and Lewis.[22] By analogy with the Colburn equation for turbulent convective heat transfer:

$$j_H = \frac{h_o}{C_p G} (Pr)^a = f\ (Re) \tag{38}$$

they proposed that the mass transfer coefficient could be correlated by an equation of the type:

$$j_M = \frac{k_g \overline{P}_g M_b}{G\ M_s} (Sc)^a = f\ (Re) \tag{39}$$

where both f(Re) and a are the same as for heat transfer in the same flow geometry.

For the case of cross flow on the outside of tube bundles, the Colburn heat transfer equation is:

$$\frac{h_o}{C_p G} (Pr)^{2/3} = 0.33\ Re^{-0.4} \tag{40}$$

for the flow orientation in the present work (flow through a triangular spaced array in the in-line direction.[23] Thus the j-factor equation applicable to the present work based on the Colburn analogy is:

$$\frac{k_g \overline{p}_g}{G} \frac{M_m}{M_s} (Sc)^{2/3} = 0.33\ Re^{-0.4} \tag{41}$$

Stagnant Film Model

Chilton and Colburn, in presenting their j-factor equation of mass transfer, noted that the use of $\overline{p}_g$, the mean gas partial pressure, defined by:

$$\overline{p}_g = \frac{p_{gc} - p_{gb}}{\ln \frac{p_{gc}}{p_{gb}}} \tag{42}$$

was justified as being a consequence of the molecular diffusion process occurring in a thin stagnant film adjacent to the cooled surface. This can be demonstrated by the following derivation for one-dimensional diffusion of one fluid through a stagnant region containing a second fluid.

The system considered is shown in Figure 9. The diffusion equation, written in terms of mole fractions and molar flow rates is:

$$N_s = \frac{-\rho D}{M_b} \frac{d\ X_s}{dz} + X_s\ (N_s + N_g) \tag{43}$$

ORNL–DWG 72–12452

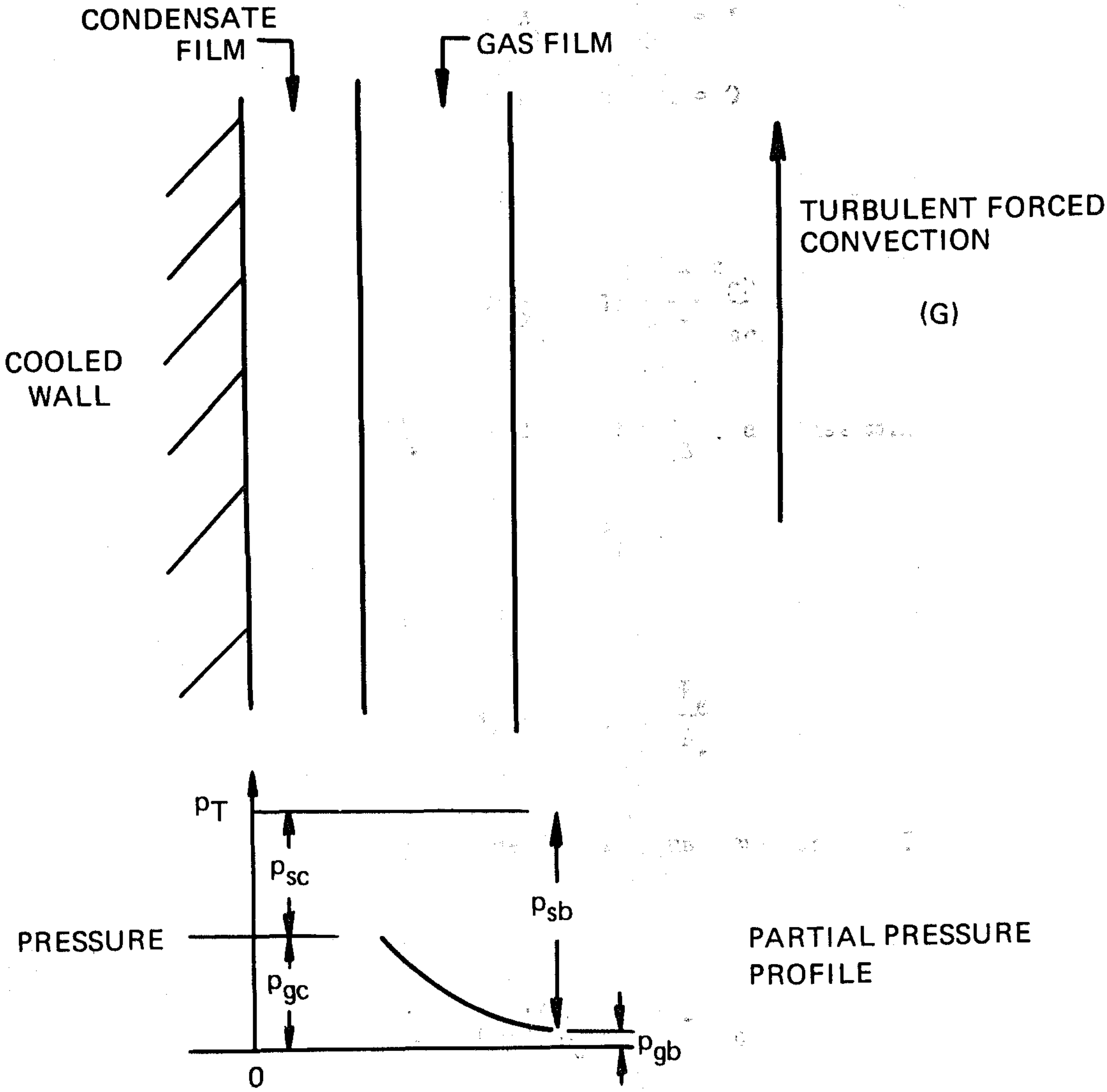

FIGURE 9

STAGNANT FILM MODEL

For the case of a stagnant gas, N_g is equal to zero, and the equation can be integrated with the boundary conditions:

$$X_s = X_{sb} \quad \text{at} \quad z = \delta$$

$$X_s = S_{sc} \quad \text{at} \quad z = 0$$

to yield:

$$N_s = \frac{\rho D}{M_b \delta} \ln \frac{1 - X_{sb}}{1 - X_{sc}} \tag{44}$$

Replacing $1-X_{sb}$ by X_{gb} and $1-X_{sc}$ by X_{gc}, and assuming Dalton's Law:

$$p_g = X_g p_T \tag{45}$$

results in:

$$N_s = \frac{\rho D}{M_b \ \delta} \ln \frac{p_{gb}}{p_{gc}} \tag{46}$$

which, after substituting the defining equation for $\overline{p}_g$ (Equation 40), results in:

$$N_s = \frac{\rho D}{M_b \ \delta \ \overline{p}_g} (p_{gc} - p_{gb}) \tag{47}$$

Since from Dalton's Law:

$$p_{gc} - p_{gb} = p_{sb} - p_{sc} \tag{48}$$

the resulting equation is:

$$N_s = \frac{\rho D}{M_b \ \delta \ \overline{p}_g} (p_{sb} - p_{sc}) \tag{49}$$

or, in terms of mass flow units,

$$W_s = \frac{\rho D\ M_s}{\delta\ \bar{p}_g\ M_b}\ (p_{sb} - p_{sc}) \tag{50}$$

Comparison with Equation (34) yields the expression for the mass transfer coefficient:

$$k_g = \frac{\rho D}{\delta\ \bar{p}_g}\ \frac{M_s}{M_b} \tag{51}$$

This result can be applied to the case of mass transfer from a turbulent flow of a steam gas mixture parallel to a cooled surface by assuming that within the turbulent region there is perfect mixing of the steam and gas and it acts as an infinite source of steam. Assuming that the same stagnant film thickness applying to forced convection sensible heat transfer also applies to the case of forced convection mass transfer, and noting that the film thickness for sensible heat transfer is given by:

$$\delta = \frac{k}{h_o} \tag{52}$$

the Colburn heat transfer j-factor can be written:

$$j_H = \frac{k}{\delta\ C_p\ G}\ (Pr)^{2/3} \tag{53}$$

in terms of δ.

Substituting for δ the relation obtained from Equation (51), one gets:

$$j_H = \frac{k\ k_g\ \bar{p}_g}{\rho D\ C_p\ G}\ (Pr)^{2/3}. \tag{54}$$

Multiplying by $(Le)^{1/3}$ where Le is the Lewis number, the ratio of the thermal to the mass diffusivities:

$$Le = \frac{Pr}{Sc} = \frac{C_p \rho D}{k}$$

one obtains the Colburn mass transfer j-factor:

$$j_M = \frac{k_g \bar{p}_g}{G} \frac{M_b}{M_s} (Sc)^{2/3} \tag{55}$$

The Lewis number is introduced simply as a means of replacing thermal diffusion parameters with mass diffusion parameters by a dimensionless exchange. The dependence of sensible heat transfer on the Prandtl number was arbitrarily assumed by Colburn to carry over as an identical dependence of diffusive mass transfer on the Schmidt number.

This analysis verifies that in order to obtain the desired relation between j_H and j_M, Chilton and Colburn assumed that the governing mechanism of mass transfer was molecular diffusion through a stagnant fluid, and that the same thickness of film applied to mass transfer as to heat transfer. The validity of the mass transfer analogy rests, as with all of the semi-theoretical turbulent flow correlations, on experimental verifications.

Experimental Verification of the Colburn Analogy

The Colburn heat transfer-mass transfer analogy has been found valid for a number of flow geometries,[24] including turbulent flow inside tubes, flow past flat plates, and flow around spheres and cylinders. The mass transfer processes used in all of these experiments involved either evaporation,absorption, or sublimation, with very low mass transfer rates used in all cases. In a recent study[25] the analogy was found to adequately correlate the data for condensation from a steam-gas mixture in turbulent annular flow. Thus there appears to be good reason to consider that the Colburn j-factor correlation would provide a suitable basis for predicting h_g for steam-gas condensation on the shell side of condensers.

Spalding Analogy

Within the overall conceptual framework of the mass transfer-heat transfer analogy, it is possible to derive a set of j-factors based on an alternate to the stagnant film model; namely, the Reynolds flux model. Originally postulated by Reynolds,[26] it has more recently been elaborated by Spalding[27] and discussed, with application to steam-gas condensation, by Silver.[28] The model is based on the concept as stated by Reynolds, that the processes of heat transfer, mass transfer and momentum transfer occurring near a phase interface are:

> very much like a bombardment of the interface by fluid, plucked out of the main stream and brought at least partially to equilibrium with the interface. The effectiveness of the flow in promoting friction, heat (and mass) transfer could be measured by giving a number to the bombardment rate.[27]

Spalding called the bombardment rate the Reynolds flux, and derived a general equation for describing both heat and mass transfer in terms of the Reynolds flux, which with specific modifications would be applicable to a number of industrial processes. In the derivation to follow, the terminology will refer to steam-gas condensation.

Referring to Figure 10, the control volume represents a region close to and at equilibrium with the condensate film. The (molar) flow rate of bulk fluid (considered, as in the stagnant film model, to be flowing in turbulent flow) which enters the volume is the Reynolds flux (g_R)

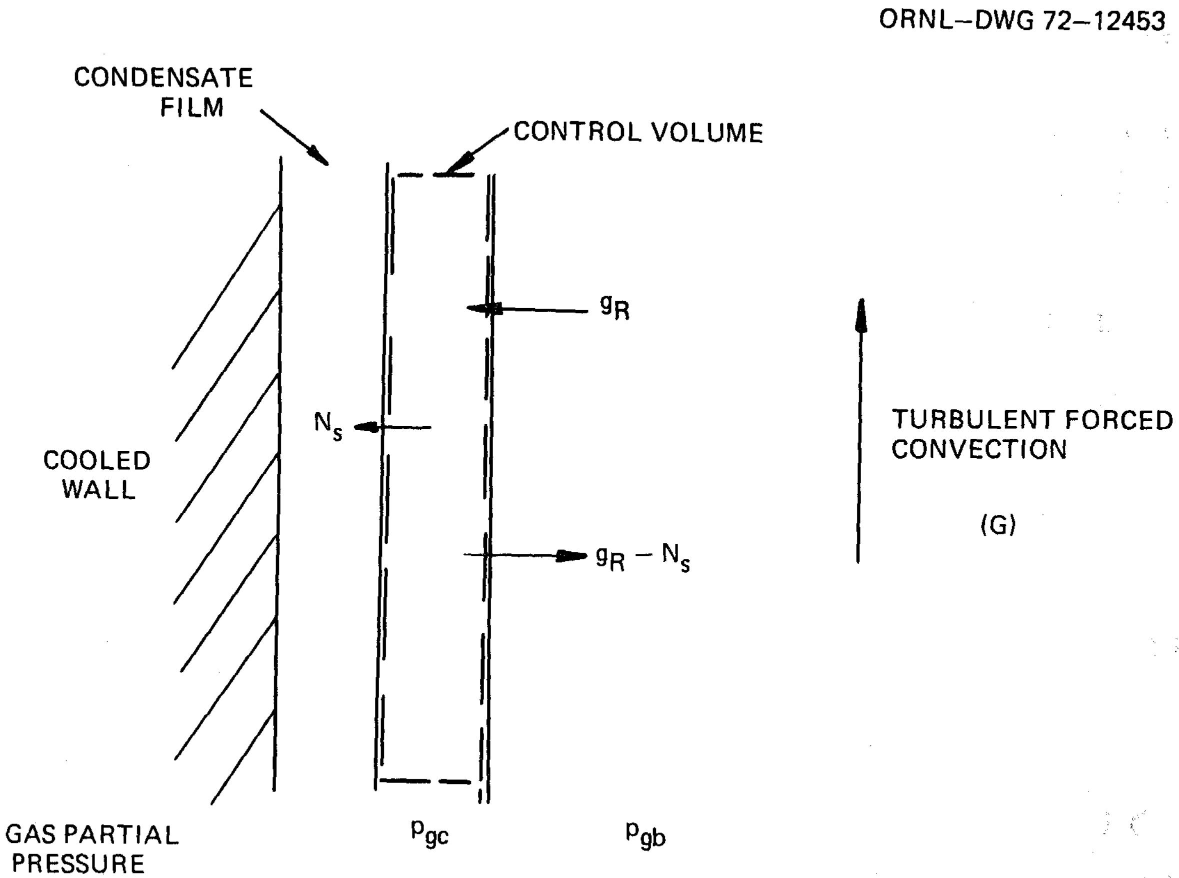

FIGURE 10

REYNOLDS FLUX MODEL

with its composition that of the bulk flow. In the case of heat transfer, this fluid equilibrates in temperature with the wall and then returns at the same flow rate. The heat transferred is then related to the Reynolds flux by:

$$g_R = h_o/C_p \tag{56}$$

With condensation the fluid leaves by two paths - the quantity condensed (N_s) flowing to the wall, while the remaining (g_R-N_s) re-entering the bulk stream.

A molar flow balance for steam around the control volume yields:

$$g_R X_{sb} = (g_R - N_s) X_{sc} + N_s \tag{57}$$

solving for N_s:

$$N_s = g_R \frac{X_{sb} - X_{sc}}{1 - X_{sc}} \tag{58}$$

and assuming Dalton's Law:

$$N_s = g_R \frac{p_{sb} - p_{sc}}{p_{gc}} \tag{59}$$

Converting to mass rather than molar flow rate, and assuming that the mean molecular weight of the Reynolds flux is:

$$M_g = \frac{M_b + M_c}{2} \tag{60}$$

the mass flow equation is obtained:

$$W_s = \frac{g_R M_s}{p_{gc} M_g} (p_{sb} - p_{sc}) \tag{61}$$

which results in the mass transfer coefficient-Reynolds flux relationship:

$$k_g = \frac{g_R}{p_{gc}} \left(\frac{M_s}{M_g}\right) \tag{62}$$

The basis of the analogy between mass and heat transfer is the equality of the Reynolds fluxes, along with, as in the case of the stagnant film model, replacing the Prandtl number by the Schmidt number. Equating the Reynolds flux for sensible heat transfer, from Equation (56) to the Reynolds flux for mass transfer:

$$(g_R)_{mass} = k_g \; p_{gc} \left(\frac{M_g}{M_s}\right) \tag{63}$$

transforms the sensible heat transfer j-factor equation for the case of cross flow in the in-line direction across tube banks into the analogous Spalding mass transfer j-factor equation:

$$\frac{k_g p_{gc}}{G} \left(\frac{M_g}{M_s}\right) (Sc)^{2/3} = 0.33 \; Re^{-0.4} \tag{64}$$

Equation (64) differs from that based on the stagnant film model in the use of p_{gc} M_g in place of $\overline{p}_g$ M_b. Spalding in an attempt at further generalizing the Reynolds flux model showed that by modifying the basic assumption of a single control volume to that of an infinite number of small control volumes, he could also obtain a result identical with the stagnant film model. The Reynolds flux model thus appears to provide a more general approach to the heat-mass transfer analogy than the stagnant film model. It also provides a better phenomenological model for the specific case of flow across tube bundles. This is discussed in the next section.

Cavity Flow Model

When a fluid flows normal to the tubes of a closely spaced tube bundle (that is, for $S/d_o < 2.0$) particularly when the flow is in the in-line direction, as shown in Figure 11, the flow pattern cannot be considered analogous to flow parallel to a surface, or even to flow past a single cylinder. Specifically, a large fraction of the tube surfaces bound regions which are not along the flow path, as indicated by the shaded portion in the illustration. These regions are referred to as pseudo-cavities, and the flow characteristics displayed by such a tube bundle are taken to represent an example of turbulent convective flow past cavities.

A cavity is described in this context as a volume all of whose boundaries are solid surfaces except one, which itself is an extension of another solid surface parallel to which a fluid flows in turbulent forced convection. The shape of the cavity is not considered important provided that the included volume is the same order of magnitude as the flow volume through which the fluid travels in passing the cavity. A pseudo-cavity is one which is open at two parallel boundaries, and which is symmetrical with respect to the plane at the center of the two open boundaries. It can be taken as representing two cavities back to back, with no net flow between them, with the same laws applying as with cavities.

ORNL-DWG 72-12455

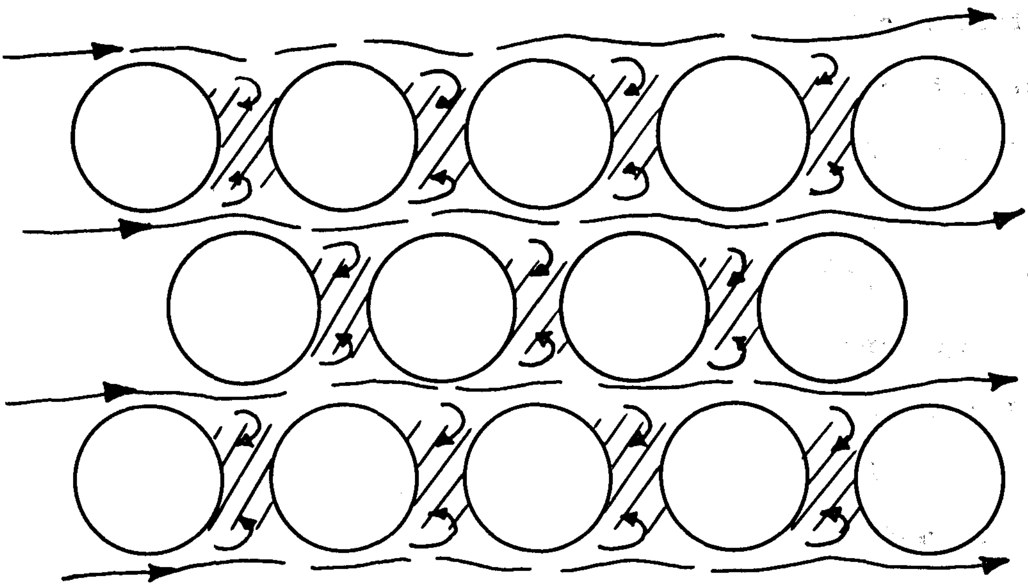

FIGURE 11

HYPOTHETICAL STEAM FLOW PATH THROUGH A TUBE BUNDLE

A hypothetical cavity is drawn in Figure 12, along with an indication of the bulk flow past it. It can be seen that the mechanism of heat and mass transfer for the surface outside of the cavity will be considerably different from that on internal surfaces. Whereas the former could be described either by the stagnant film model or the Reynolds flux model, the latter of necessity must be based on the Reynolds flux, since the large cavity size precludes a high rate of diffusion flow, and since significant flow into and out of the cavity will take place by eddies originating in the bulk. By drawing the control volume boundary around the cavity, one phenomenologically justifies the use of the Reynolds flux derived j factor for the case of mass transfer due to flow past cavities. Insofar as flow across tube bundles can be represented by the cavity model, then the Reynolds flux model appears to be the more appropriate one to use in correlating the steam condensation data. The present experiments provided a suitable test for that determination.

The analogy between sensible heat transfer and mass transfer based on the Spalding j factor assumes that the same Reynolds flux that brings heat into the control volume (the cavity) also transports the mass (the steam to be condensed, in the present case). If the mass transfer rate is large compared to the Reynolds flux, very little flow will return out the entrance to the cavity. In the limit, the return flow will be zero. Under this hypothetical condition, there is no mechanism for transporting out of the cavity the non-condensing gas portion of the incoming Reynolds flux, and its concentration will rise within the cavity until the partial pressure of steam falls so low that condensation ceases. This process describes a possible mechanism for the familiar gas blanketing of

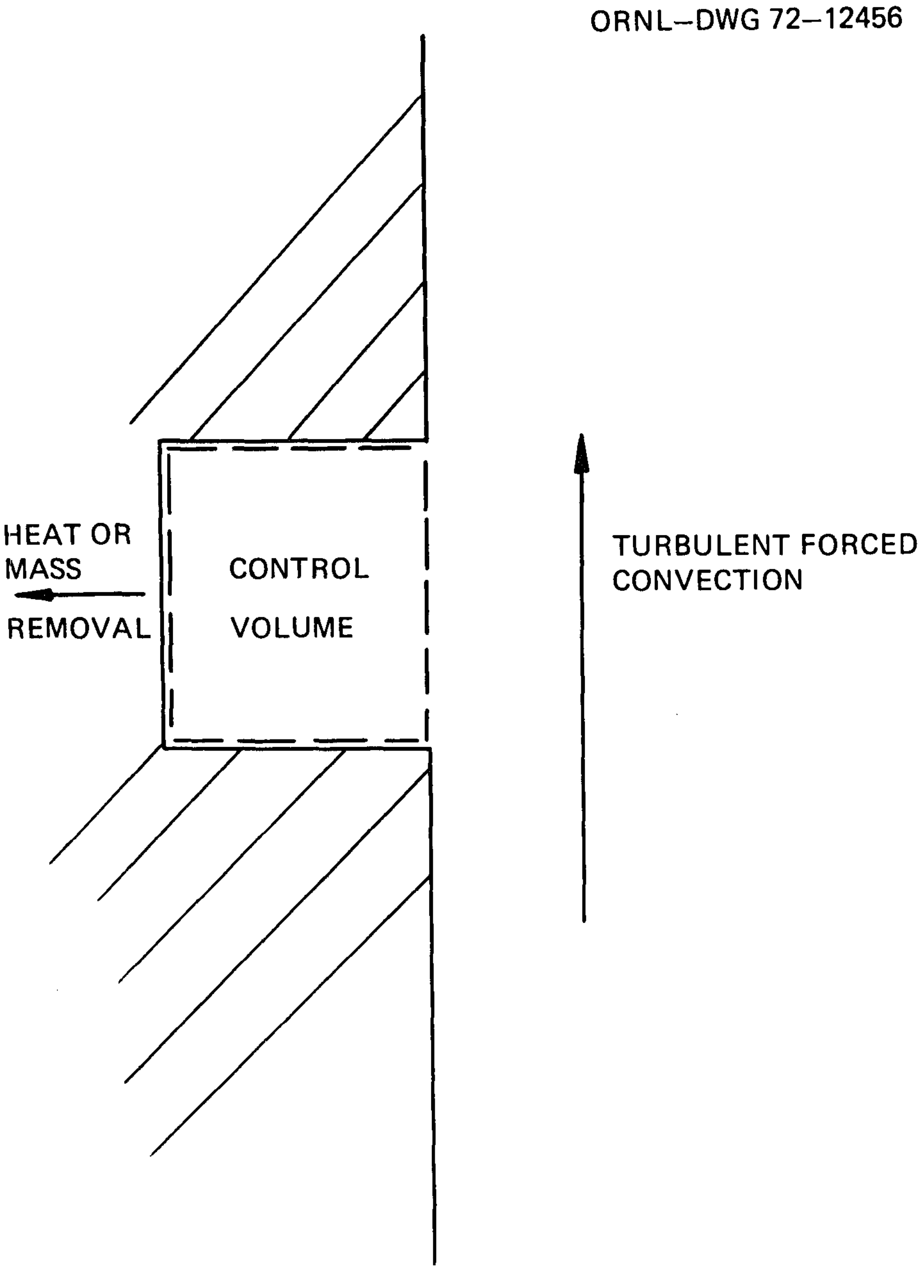

FIGURE 12

CAVITY FLOW MODEL

condensers in which part or all of a condenser bundle will stop condensing due to a steady state accumulation of gas.

In the present experiments, the predicted Reynolds flux, as calculated from Equations (63) and (64), was in the range 5-20 lb/hr-ft^2 for steam mass velocities between 100 and 1000 lb/hr-ft^2 at a steam temperature of 230°F. For an overall heat transfer coefficient of 1000 Btu/hr-ft^2-°F, and a ΔT_{lm} of 10°F, the condensing rate (in the absence of non-condensing gas) would be 10 lb/hr-ft^2. Thus, the present experiments clearly represent those where the mass transfer rate is large compared to the Reynolds flux. It is noted that there have been no other reported experiments testing the analogy at large mass transfer rates.

CHAPTER III

DESCRIPTION OF EXPERIMENT

Condensation Research Program

The present research had as its principle objective the operation of an experimental steam condenser over a wide range of operating conditions of interest to the multistage flash distillation process in order to provide verification of design correlations for predicting the two shell side film heat transfer coefficients. The work consisted of the design, construction, and operation of an instrumented condenser and associated loops, and the acquisition of data in the following areas:

1. The effect of condensate rain, steam velocity and temperature on the condensate film heat transfer coefficient.

2. The effect of non-condensable gas concentration, steam velocity, temperature and condensing rate on the gas film heat transfer coefficient.

A secondary objective was to verify the performance of enhanced tubes in increasing the convective film heat transfer coefficient above that for smooth tubes. The tube type used had previously been tested only in a single tube condenser. The method of enhancement (in the form of a shallow indentation) did not affect condensation in single tube tests, so that the use of the tube was not expected to interfere with the primary objective of the work.

Equipment Design Criteria

A horizontal multitube experimental steam condenser was designed specifically for present work, and included the following tube bundle features:

1. Overall heat transfer coefficients were to be obtainable for five horizontal 1 in. OD by 8 ft long condenser tubes arrayed vertically within a staggered triangularly spaced bundle.

2. The five instrumented tubes were surrounded by 27 other identical active tubes.

3. The active tubes were surrounded (upstream and downstream) by dummy tubes providing entrance and exit steam flow conditions for the active array.

4. Condensate collection rates from beneath the active bundle and from beneath the upstream and downstream dummy bundles were to be measured separately.

5. The entire bundle was baffled and contained in a pressure vessel. The baffling distributed steam from the inlet pipe uniformly across the full width of the bundle minimizing bypassing of the steam around the bundle. The pressure vessel was designed for operation over the steam temperature range 130°F to 260°F.

6. A viewport and optical periscope were provided for examining the shell side of active tubes while in operation and thus determining the mode of condensation (dropwise or filmwise) and the presence of solids fouling.

7. Spray tubes were installed above the active bundle for recycling condensate spray onto the top tubes of the active bundle.

External piping loops were constructed to provide the following:

1. Clean saturated steam at temperatures from 130°F to 260°F at rates to 10,000 lb/hr.

2. Recirculating cooling water to provide tube side water velocities of 2 to 20 ft/sec at cooling water inlet temperatures between condenser steam temperature and ambient process water temperature.

3. Heated condensate at temperatures 0 - 5°F below steam temperature at rates up to 20 gpm to supply the spray tubes.

4. A barometric direct contact vacuum condenser to condense steam leaving the test condenser at rates to 10,000 lb/hr.

5. A gas addition system to inject controlled amounts of nitrogen gas into the steam feed to the test condenser.

Most of the equipment, including the shell of the test condenser and the clean steam generator, consisted of modified surplus pressure vessels, heat exchangers and open tanks. As a result the design and layout of the components reflected the compromises necessary to use the surplus equipment.

The layouts of the equipment and the detailed design of the components were prepared prior to construction and are documented on a series of drawings on file at Oak Ridge National Laboratory. A simplified flowsheet is shown in Figure 13. What follows are short descriptions of the principal components and systems along with their operating characteristics and capabilities.

Condenser Design

Shell

The steam condenser shell is a 3 ft diameter, horizontal 8 ft long Inconel cylindrical pressure vessel of approximately 1/2 in. wall thickness with a circumferential flange near the (axial) midpoint. Cooling

MAJOR COMPONENTS

1. TEST CONDENSER
2. BAROMETRIC CONDENSER
3. SPRAY WATER HEATER
4. ENTRAINMENT SEPARATOR
5. BOILER
6. CONDENSATE STORAGE TANK
7. COOLING WATER STORAGE TANK
8. COOLING WATER HEATER
9. MAKEUP DEAREATOR
10. STEAM JET EJECTOR

SYMBOLS

M DEMINERALIZED WATER

S STEAM

CW COOLING WATER

D DRAIN

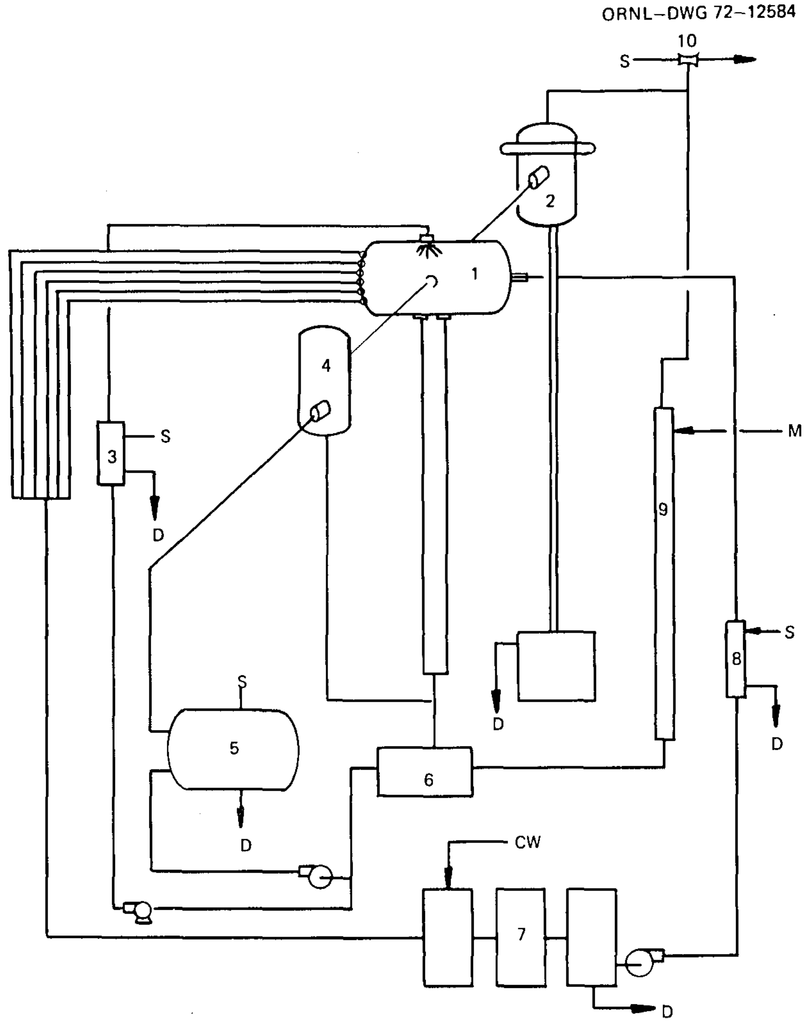

FIGURE 13

SIMPLIFIED FLOWSHEET OF TEST CONDENSER LOOP water enters the shell at one end through a single 4 in. Schedule 40 pipe and leaves at the opposite end through five 1 in. Schedule 40 pipes and a single 4 in. Schedule 40 pipe. Steam enters and leaves the shell at right angles to the water tubes through two 8 in. Schedule 40 pipes located opposite each other horizontally at about the midpoint of the tube bundle. All cooling water and steam pipes connections use Flexmaster couplings. Other shell penetrations include condensate drain lines, temperature and pressure taps, and a flanged 1 in. ID hole for viewing the condensing side of several tubes during operation using an optical periscope. Figure 14 is a photograph of the installed vessel.

Steam Distribution Baffles

Steam enters the shell through a 6 1/4 in. ID inlet sleeve, strikes a baffle plate and is diverted into two streams flowing parallel to the tubes and contained in distribution boxes. The distribution boxes themselves contain internal baffles and are perforated with holes in the direction of the tube bundle in order to promote a uniform flow velocity across the bundle and absorb the inlet velocity head. Downstream of the distribution box discharge holes is a flow straightener consisting of a 4 in. thick aluminum 1/4 in. honeycomb grid.

At the steam exit are two flow distribution boxes and an exit sleeve essentially the same as at the inlet.

Bundle Configuration

The test bundle, shown in a schematic cross section in Figure 15 consists of a square array of one hundred sixty-three 1 in. OD by 0.035 wall 90-10 cupronickel tubes spaced on a 1.33 equilateral

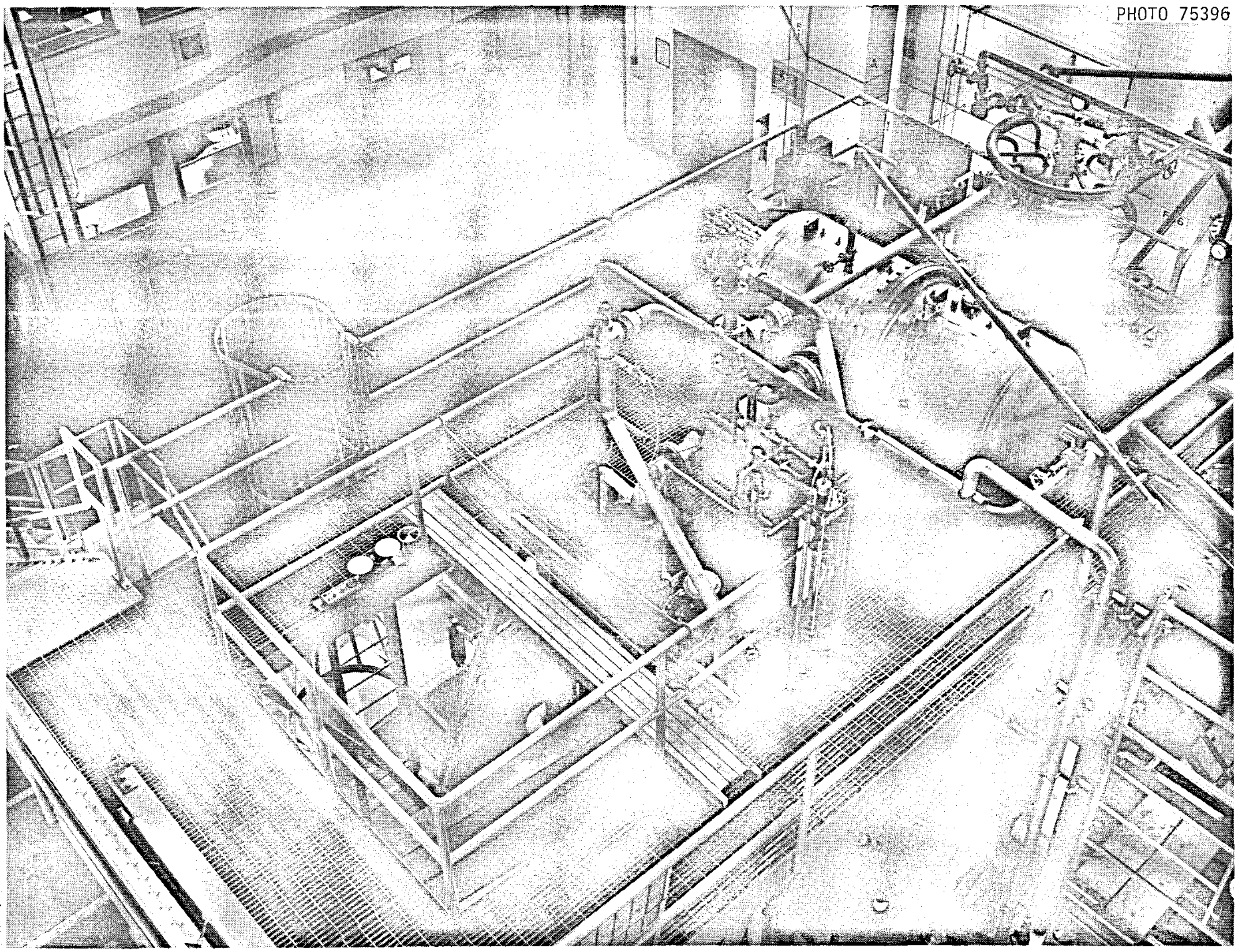

FIGURE 14

PHOTOGRAPH OF MAIN COMPONENTS OF TEST CONDENSER LOOP

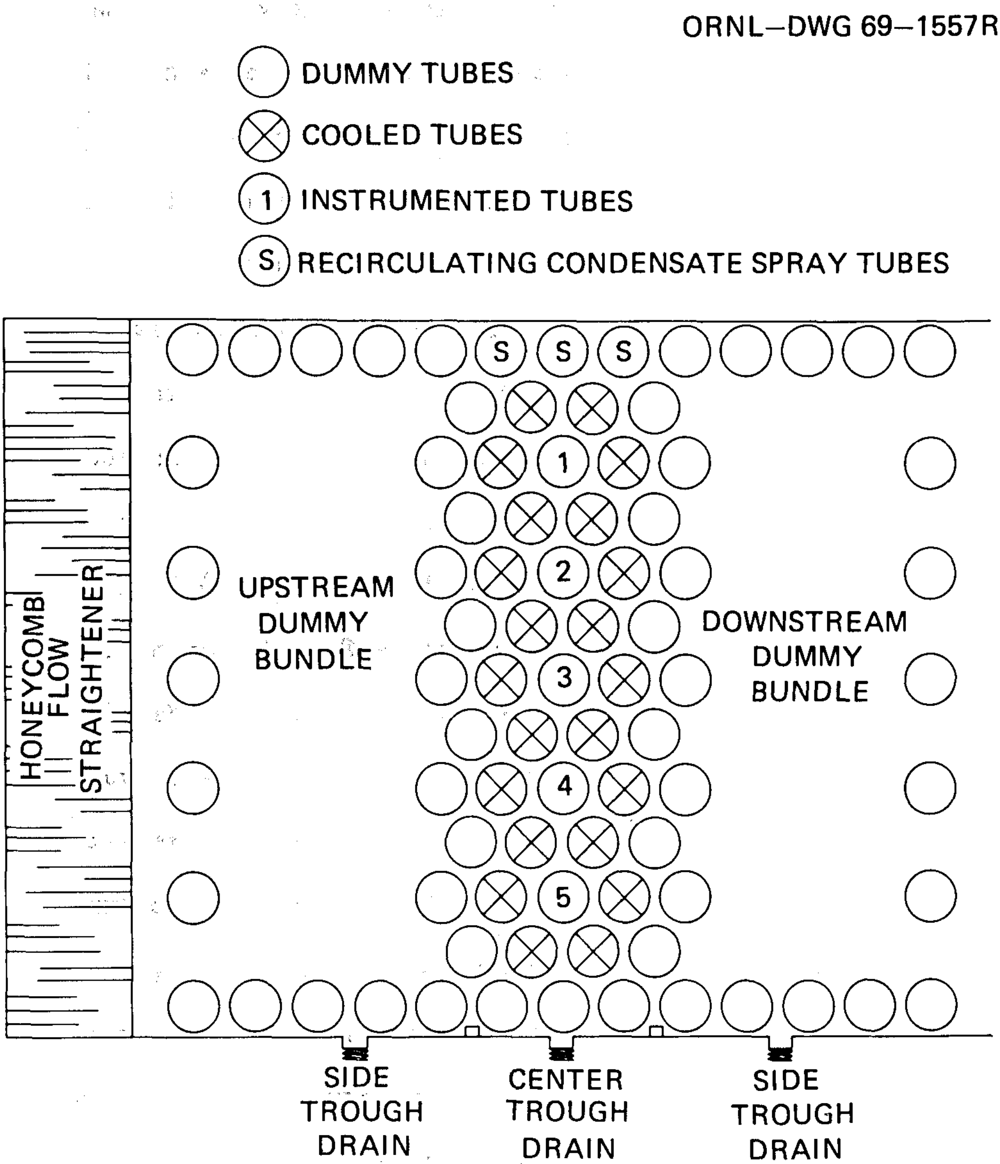

FIGURE 15

SCHEMATIC CROSS SECTION OF TEST CONDENSER TUBE BUNDLE triangular pitch. Steam flow is horizontal and in-line (parallel to the triangle side) while condensate drainage is staggered. The length between tube sheets is 6.73 ft giving a heat transfer area per tube of 1.76 ft^2 or a total active tube heat transfer area of 47.56 ft^2. The superficial flow area for steam at the faces of the bundle was 8.45 ft^2. The flow area between tubes measured along centerlines between adjacent tubes (A_s) was 2.24 ft^2. Two full intermediate support baffles are provided which divide the shell into three equal parts. The 27 active tubes are located centrally in the bundle (Figure 15) in five staggered vertical columns. All columns except the central one terminate at both their upstream and downstream ends in common water boxes and are sealed with rubber O-ring gaskets. The five central tubes pass through the downstream tube sheet with O-ring seals and then through the water box and the pressure vessel using drilled out Swagelok fittings with Teflon seals and Flexmaster couplings, respectively. These five tubes were used for the measurement of heat transfer coefficients.

Directly above the active array and aligned with the same pitch and orientation are three perforated 1 in. OD by 1/16 wall stainless steel spray tubes in a horizontal row headered together at one end. The middle tube of the three penetrates the shell through a Flexmaster seal. The portion of the middle tube within the bundle contained 1/8 in. holes on 3 in. centers drilled in two staggered rows along lines 30°F from the tube bottom in the direction of the central tube.

The remaining 133 tubes are dummy tubes, used for establishing a flow pattern for the active tubes similar to that inside a deep bundle. The dummy tubes were fabricated of 1 in. OD thin wall stainless steel tubing.

Optical Periscope

An access space was left in the dummy tube bundle for installing a periscope. The space resulted from omitting 3 in. long sections of 13 of the dummy tubes on the downstream side of the active tube bundle. Small tube sheets support the ends of the sectioned tubes on each side of the access. The optical periscope could be lowered through the flange with its mirror system facing upstream to observe condensation on the downstream half of 5 of the active tubes for about 2 ft of their lengths with a minimum of disruption of the steam flow pattern.

The optical periscope (Figure 16) consists of a 3 ft long 1 in. diameter barrel containing periscope optics. A nitrogen sweep of the periscope optics provided cooling,and a high temperature sealant for the protective window was used. The periscope was inserted and removed only during shutdowns.

Support System Design

Cooling Water

The cooling water system supplies heated recirculated process water at flow rates sufficient to give water velocities within the tubes of up to 10 ft/sec. The system consists of three Monel storage tanks connected in parallel with a total capacity of 1000 gal, a centrifugal pump of 400 gallons per minute flow rate, a steam mixer pipe for initial preheat of the recirculating water (using the building 50 psi steam supply) and a cold water supply and hot water overflow system at the storage tanks for rejecting the heat picked up by the recirculating water. The system piping contains three bypass loops and associated flow control valves.

PHOTO 75423

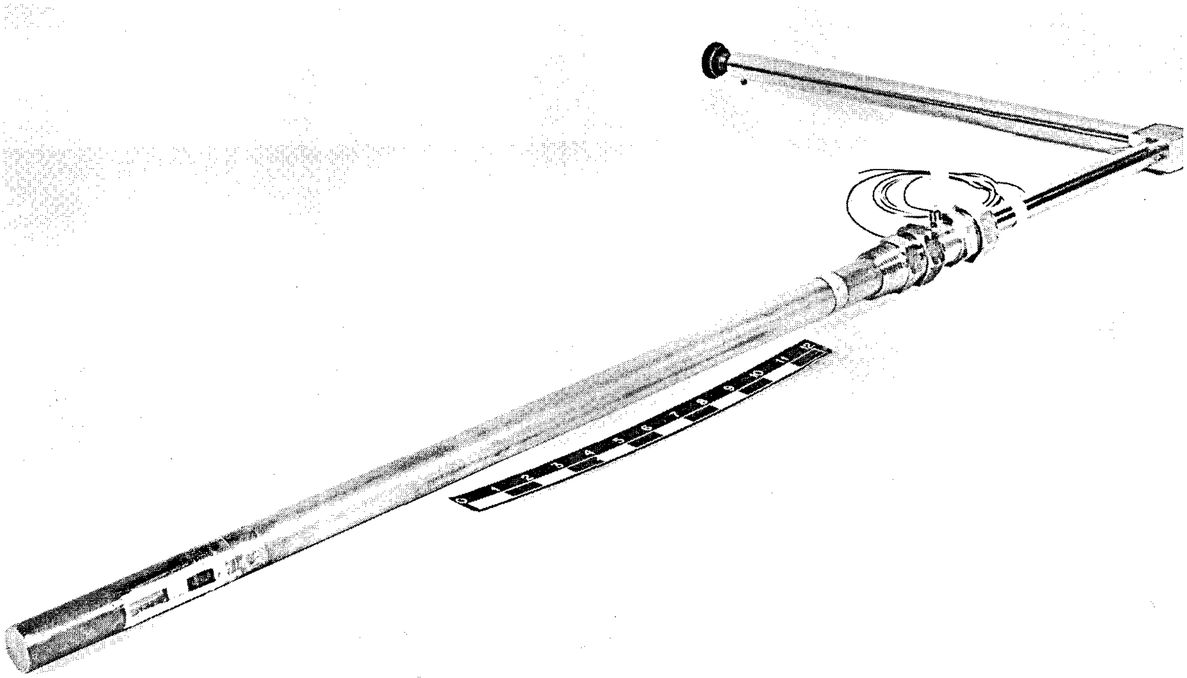

FIGURE 16

OPTICAL PERISCOPE VIEWING DEVICE

One loop contains a filter for removing rust and other particles from the circulating water. The second loop contains a small heat exchanger for removing pump heat during standby operation of the cooling water system. The third loop is used to control independently the pressure and flow rate of water in the main flow piping at the condenser. Most of the piping in the cooling water system, including the 4 in. water supply lines to the condenser and the 4 in. and 1 in. discharge lines from the condenser are made of mild steel.

The flow of water into the active tubes was regulated with hand-operated valves. The cold water makeup valve was pneumatically operated and was controlled by a temperature controller which senses the inlet water temperature to the test condenser.

Thermocouples are installed in wells located in the inlet and discharge 4 in. lines and are inserted into each 1 in. tube through elbows located at the discharge side. The thermocouple junctions are located on the tube axes approximately 5 in. downstream from the ends of the heated portions of the tubes to provide a mixing length of 5 L/D. At this axial location, the tubes are within the downstream water box. Since the temperature difference between the cooling water inside and outside of the tube is small (approximately 1°F), within the water box, the heat loss or gain in this section is negligible.

Steam and Spray Water

The steam and spray water system controls the environment for the shell side of the active tubes. This includes independent control of the steam pressure, steam mass flow rate leaving the condenser, non-condensable concentration entering the bundle, and rate of inundation of the active tubes by the spray tubes located immediately above the active bundle.

The steam supplied to the condenser is generated in the tubes of a 10 MW stainless steel U-tube heat exchanger. Building steam at up to 250 psi pressure on the shell side is used to boil the water which is fed to the tubes with a high head centrifugal pump. The wet steam formed in the tubes passes through a pneumatically operated throttling valve and into a 2 ft diameter entrainment separator containing an impingement plate and 8 in. of stainless steel Yorkmesh. Pressure upstream of the throttling valve is kept at a sufficiently high level so that the valve is maintained in approximately a half-open position. By locating the throttling valve upstream of the entrainment separator, superheat is eliminated by adjusting the feedwater flow rate and the steam pressure so that wet steam is generated.

Nitrogen gas is metered into the steam inlet piping through 1/4 in. tubing from a station consisting of six nitrogen cylinders connected to a common pressure regulator and gas rotameter. The location of the nitrogen addition point is just downstream of the entrainment separator, providing a distance of 10 pipe diameters plus the condenser inlet baffling to obtain good mixing with the inlet stream.

Water drained from the entrainment separator is returned, along with condensate from the test condenser, to a 360 gal Monel boiler feed storage tank. Makeup water supplied to the tank from the building demineralized water system is deaerated in a vacuum deaerator.

Uncondensed steam leaving the test condenser passes through an 8 in. manually operated condenser vent valve into the barometric condenser. This consists of a 3 ft diameter spray chamber mounted on a 40 ft high by 12 in. diameter barometric leg draining into a 10 ft diameter open tank. The tank discharges through an overflow to the building waste. Two parallel steam jet ejectors maintain a 28 in. vacuum in the spray chamber. The chamber contains two rings of spray nozzles which spray a metered flow rate of building tap water into the spray chember. The mixed spray water and steam condensate drains through the barometric leg. A stainless steel rupture disc is located in a 4 in. OD stainless steel bypass line running from the inlet steam line to the discharge line downstream of the condenser steam discharge valve. The disc was sized to rupture at a pressure differential of 50 psi. Since the downstream side of the disc was always at a vacuum, this permitted operation of the condenser to saturation temperatures of 250°F.

A 5 gpm pump taking its suction from the boiler feed storage tank provides water for the spray water system. Since the temperature of the water in the storage tank will be lower than the condensate temperature due to the amount of cold demineralized water makeup added, a steam jacketed single tube heat exchanger preheated the spray water entering the test condenser to the desired temperature of 1 - 3 degrees below the condenser steam temperature.

Tubing Description

The enhanced tubing (Figure 17) installed as active tubes in the test condenser (rope tubes) were fabricated of 1 in. OD 90-10 cupronickel with 0.035 in. wall. The original smooth surface of the tubing has been modified by indenting a pattern consisting of three equally spaced, parallel, smooth contoured spirals approximately 1/2 in. apart. Tests performed by Oak Ridge National Laboratory[29] have shown that this tubing

PHOTO 76288

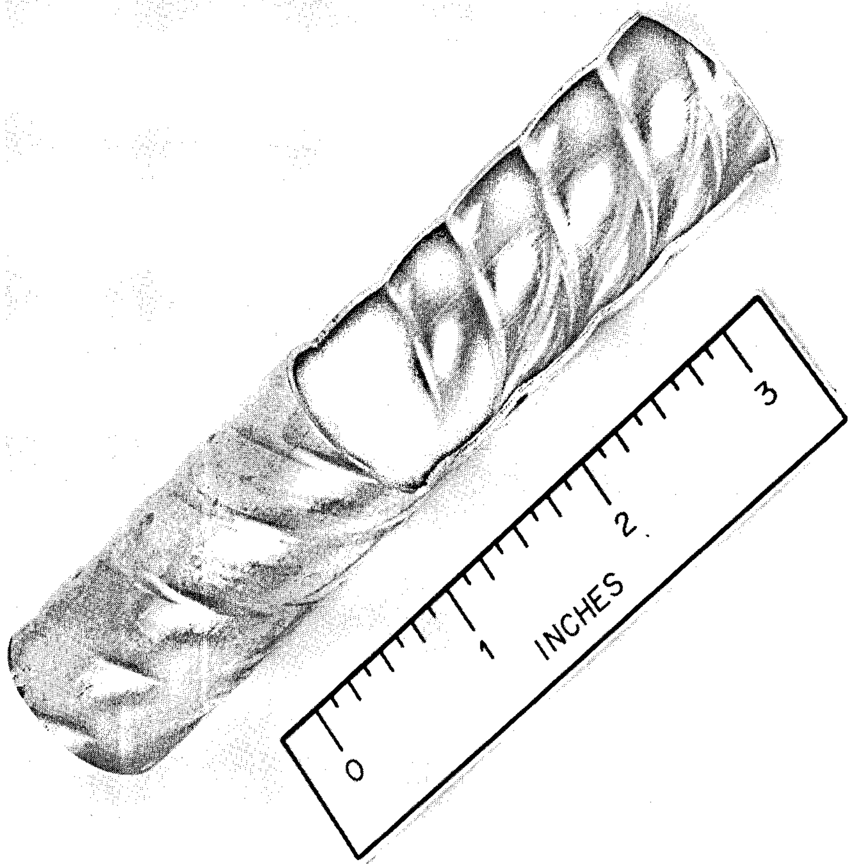

FIGURE 17

SPIRAL INDENTED (ROPE) TUBE

type provides an increased convective film coefficient of up to a factor of two times smooth tubing while increasing the friction factor an equal amount. No enhancement of the condensing side was observed.

A sample of tubing from the same batch as used in this condenser gave a value of convective film constant C_i [for Equation (12)] of 0.047 in tests conducted in a single tube test condenser using the Wilson plot method of evaluating individual coefficients.[30]

Instrumentation

The instruments used in the multitube condenser were of three categories according to their function in the system:

1. Instruments used in determining the overall heat transfer coefficients of the five test tubes.

2. Instruments used in determining the values of the experimental conditions to which the five tubes are exposed.

3. Instruments used to monitor the loop operation.

The overall heat transfer coefficient for each test tube is calculated from measurements of the individual tube coolant water flow rate and outlet temperatures and the common inlet water and bundle steam temperatures. The cooling water flow rates were measured by variable orifice meters (rotameters) chosen to cover the flow rate range of interest. Each rotameter was calibrated at room temperature over its entire range prior to installation. At least once during the experimental program, each rotameter was removed from the loop and its calibration rechecked, with no deviation from the original calibrations found.

Temperatures of inlet and outlet cooling water, of steam entering and leaving the condenser shell and of steam at the downstream side of the active tubes within the bundle were measured using 1/8 in. OD stainless steel sheathed chromel-alumel thermcouples installed directly into the flowing streams through pressure fittings. The voltage of the thermocouples were read in random sequence using a Leeds and Northrup K-3 Universal potentiometer and were also monitored with a Beckman expanded scale voltmeter connected to a Brown Elektronik recording voltmeter. All thermocouples were calibrated prior to installation at the ORNL Calibration Laboratory over the full temperature range of interest (100-300°F) along with their thermocouple connecting leads, multiple position switch, and cold junction. To provide a periodic check on the thermocouple accuracy, an 8 in. OD by 12 in. high solid copper cylinder wrapped with nichrome heaters and insulated, was used to cross calibrate thermocouples as described in Appendix C.

In addition to the temperature and flow measurements needed for calculating overall heat transfer coefficients, calibrated flow and temperature sensing instruments were used to define the experimental conditions in the neighborhood of the five instrumented tubes. They included two gas rotameters of different ranges for metering N_2 into the steam entering the test condenser, a rotameter and thermocouple to measure the flow rate and temperature of condensate fed into the three spray tubes, and an orifice plate with a differential pressure cell and thermocouples to measure the flow rate and temperature rise of the cooling water used to condense the vented steam.

Calibrated rotameters were also used to meter the condensate flow draining from directly beneath the active bundle and from upstream and downstream dummy bundles. This enabled an independent determination of the total condensate produced, and an estimate of the fraction of the condensate which disperses as it drains through the bundle. It also provided a better estimate than the spray tube flow rate of the effective inundation resulting from operating the spray tubes, since some of the spray water spattered onto the dummy bundles.

Fouling Prevention

It was desirable that there be no solids fouling of the condenser tubing. In order to prevent fouling on the shell side, only stainless steel and Inconel pipe and equipment were used (with the exception of several brass valves). In addition demineralized deaerated water was used for makeup for the steam supply system and a nitrogen blanket was maintained on the condenser shell during all shutdowns. Initially no precautions were taken to prevent fouling of the tube inside and there was no indication of loss of performance with time. However, after one long shutdown, iron oxide which formed on the steel piping during the shutdown deposited on the tube walls, causing a measurable loss in tube performance. This was corrected (after investigating several alternative methods) by cleaning the circulating water system piping with 5 percent citric acid, passivating with a proprietary sodium polyphosphate (Nalco 345) and maintaining a circulating concentration of about 200 ppm of a proprietary chromate inhibitor (Nalco 270).

System Operation

The condenser was normally operated only during the day time. During overnight shutdown, the cooling water supply to the test condenser active tubes and to the vent condenser spray nozzles were left set at their normal settings and a nitrogen blanket was maintained on the shell side of the condenser.

To heat the system, building steam was bled into the recirculating cooling water to the active tubes using the steam mixing pipe, and the temperature raised to about 30°F below the desired steam temperature. The steam bleed was then discontinued, and steam was admitted to the shell side of the steam generator, the feed pump started, and its flow adjusted (manually) to be greater than the expected steam demand for the following runs. As the pressure of the shell side of the test condenser rose, the condenser vent valve was opened and the jet ejector of the vent condenser activated. The steam flow control valve was then set at the desired shell side (steam) temperature. If the valve was not controlling properly the pressure of the steam on the shell side of the steam generator was readjusted as necessary to provide the pressure drop across the control valve that was needed (at the flow rate of interest) to maintain the valve in a partly opened condition.

As the circulating water temperature increased and approached the desired range, cold makeup water was admitted into the recirculating water system using a normally controlled valve. As the inlet water temperature reached its desired value, the makeup water flow was put on automatic operation based on the inlet water to the test condenser. The vent rate from the shell side of the condenser was readjusted as needed and the system given several hours to reach a steady condition.

Runs normally consisted of taking one set of temperatures and flows at a steady operating condition which generally took about 15 minutes. The initial temperature measurement was rechecked following reading of the last data point and if the reading had changed by more than 0.3°F, the data were discarded and another set obtained.

The normal procedure for a series of runs was to establish a steady steam temperature, cooling water inlet temperature and steam velocity for the first run. Then one parameter was varied, that is, nitrogen flow rate, steam velocity, spray water flow rate, or cooling water velocity with about an hour allowed for equilibrium before data were taken. In this way, about four or five runs were made in one day. The last run of each day generally duplicated the initial run conditions.

Error Analysis

There are three separable types of errors in the experimental data. These were:

1. Errors due to the inherent inaccuracy of the measuring instruments, including the calibrated thermocouples.

2. Errors due to the inability to maintain constant experimental conditions during the data taking period.

3. Errors in calibration of the measuring instruments.

The errors inherent in the measuring instruments were estimated as follows. The flowmeters (rotameters and magnetic flowmeter) were estimated to be accurate to within 1 percent of full scale. The orifices were estimated to be accurate to within 2 per cent of full scale. In general, the flowmeters and orifice readings were in the range 50 to 100 per cent of full scale, leading to errors of the order of 1 to 2 percent of the indicated flow for the flowmeters and 2 to 4 percent for the orifice plate.

The thermocouples were all initially calibrated. The inherent stability of the calibrated thermocouples (their ability to duplicate a reading after frequent cycling of their temperatures) is not known, but based on the results of the cross calibrations, their accuracy was about ±3 microvolts, equivalent to ±0.15°F. The thermocouples were read using a Leeds and Northrup Model K-3 potentiometer that can be read accurately to 0.1 microvolts, an order of magnitude less error than from the thermocouples and therefore not of significance.

During the time that a set of data were taken, the loop parameters were held as steady as possible. However, fluctuations were observed in loop temperatures, probably reflecting minor variations in flow through the inlet and vent steam valves. Thermocouple voltage fluctuations, with cycle times of the order of 5 to 10 sec. and magnitudes of the order of 5 microvolts (0.2°F) were normally present. In order to minimize the effect of these fluctuations, a Beckman expanded scale voltmeter with a sensitivity of 2 microvolts was used to monitor the bundle steam temperature while readings of cooling water temperatures were made. The latter were read at those times when the steam temperature had cycled to a fixed value. By this procedure, a consistent set of thermocouple data were obtained in 10 min, without the loss of accuracy due to the loop fluctuations.

Water flow rate fluctuations, with cycle times of less than one sec. and magnitudes of up to 5 percent of full scale were observed in the rotameters. The mean value of the flow could be read to within 1 percent of full scale however, so that these fluctuations were not considered to reduce the overall accuracy of the heat transfer data.

At least once during the test program each of the rotameters was removed from the loop and recalibrated, with no shifts in calibration curves found. The thermocouples were cross calibrated at operating temperatures nine times during the test program using the copper cross calibration block. A set of mean second-order thermocouple corrections (the difference between each thermocouple apparent temperature and the mean of all of the calibrated thermocouples) was prepared (Appendix C) and applied to all of the data before calculation of heat transfer coefficients. On several occasions, thermocouples were replaced or switched during the experimental program when anomalies in the data were suspected of being due to calibration shifts. The new thermocouples in all cases were calibrated spares.

The overall accuracy of the separate tube calculated heat transfer coefficients reflects the sum of the accuracies of each measurement. Since the accuracies of measurement varied from run to run (due to differences in flow and LMTD), the reported values of overall heat transfer coefficient varied in accuracy. The range of accuracy of U was estimated to be ±15-30 percent with the lowest accuracy associated with data taken at the lowest temperature differences. Coefficients obtained at temperature differences above 10°F were accurate to at least ±20 percent. The error in the five tube mean, assuming that the errors were normally distributed, would be about $1/\sqrt{5}$ times that of a single tube, or between 7 and 15 percent.

Solids Fouling

Measurable solids fouling occurred during loop operations on several occasions. It was detected indirectly as a time dependent decrease in overall heat transfer coefficient for all the active tubes below that expected based on previous data at the same operating conditions. When there was no such downtrend with time, no significant fouling was assumed to be present on either tube outside or inside.

The fouling, when it occurred, was found in each instance to be associated with deposits, primarily of iron oxides, on the inside surfaces of the tubes, as determined during shutdown by disassembling the outlet fittings for one or more instrumented tubes and observing visually and with a borescope. Cleaning and passivation was carried out as described in Chapter III.

No fouling was observed throughout the entire experiment to have built up on tube outside surfaces, as determined by visual observations during loop operation using the optical periscope. The tubes consistently maintained the characteristic pink color of the 90-10 cupronickel alloy throughout the experiment.

A number of runs were carried out during the time that the loop was known to be fouled on the tube side. Most of these runs were for diagnostic purposes. However, several sets of gas addition runs were also made during this period, since they provided a check on the method of correlation of the gas film heat transfer coefficient. Properly correlated, the effect of gas concentration on the gas film heat transfer coefficient should be independent of the presence or absence of solids fouling.

<u>Bypassing of Steam Around Test Condenser</u>

Following completion of the experimental program, an inspection of the steam system revealed that the rupture disc originally located in the bypass line around the test condenser was no longer in place. The evidence indicated that it had either been improperly installed or that it had corroded during loop operation, and that during operation, it had broken loose and been carried away by the bypass steam flow. The vacuum backup plate used in conjunction with the rupture disc was still intact, however, thus restricting the flow rate of steam through the line to that which passed through six small radial strips, and accounting for the fact that the bypass flow was undetected during loop operation. The bypass flow was estimated by two procedures - the steam flow to the barometric condenser was measured while the test condenser discharge valve was completely shut, and the expected flow rate was calculated for each operating temperature by assuming choking (critical) flow through the backup plate openings. The calculations are described in Appendix D. Correction terms to account for the bypass flow were added to the data reduction program. The magnitude of the correction term was between one and fifty percent of the measured steam flow to the barometric condenser. If the error in estimating the bypass flow were of the order of 25 percent, this introduces an error of the order of less than 12 percent in the measure mass velocity through the test condenser.

Data Reduction

The raw data were converted into overall heat transfer coefficients for each of the five test tubes, for their average, and also the following derived parameters:

1. Steam mass and molar velocity at the plane of the test tubes.
2. Nitrogen mole fraction at the plane of the test tubes.

3. Inundation ratio.

4. Log mean temperature difference for the bundle.

5. Cooling water velocity.

6. Mass balance ratio around the test condenser.

The calculations were performed twice, once as a preliminary check shortly following each run using a computer program written in BASIC and run on a time-sharing computer, and the second time after completion of the entire series using the FORTRAN program CONTST. The latter program (Appendix A) also contained additional data reduction subroutines used in developing and testing correlations. The equations used in calculating the overall heat transfer coefficients and the system parameters are described in the following sections.

Overall Heat Transfer Coefficient

The value of the overall heat transfer coefficient for each test tube was calculated from the equation:

$$U = \frac{WC_p}{A_T} \ln \frac{T_b - T_i}{T_b - T_o} \tag{65}$$

with the heat capacity of the cooling water evaluated at its mean bulk temperature. The same water inlet temperature and shell side steam temperature was used in calculating U for each tube. The mean value of U for the five test tubes was calculated from the same equation using averaged flow rates and tube discharge temperatures.

Steam Mass and Molar Velocities

The steam mass velocity at the plane of the test tubes (G) was calculated as the arithmetic average of the steam mass velocities at the entrance and exit faces of the bundle. The steam mass velocity at the exit face was obtained from the steam vent rate using the equation:

$$G = \frac{W_{sv}}{A_s}, \tag{66}$$

where the flow area A_s was as shown in Figure 18. The steam vent rate was obtained from the heat removal rate in the vent condenser after subtracting out the bypass flow:

$$W_{sv} = \frac{W_b \; C_p \; (T_o - T_i)}{\lambda} - W_{corr.} \tag{67}$$

The entering steam mass velocity was also calculated from Equation (66), where the steam mass rate was the sum of the vent rate and the tube bundle condensation rate. This latter was calculated from the sum of the heat removal rates of all of the active tubes. For the cases in which nitrogen gas was continuously added, its mass flow rate was added to that of the steam in calculating the mass velocities. The steam molar velocity was calculated by converting the steam and nitrogen mass velocities into molar quantities and adding.

Non-Condensable Gas Fraction

The non-condensable gas mole fraction at the plane of the test tubes (F_m) was the ratio of the nitrogen molar addition rate to the total molar flow rate (steam plus nitrogen) at the plane of the test tubes.

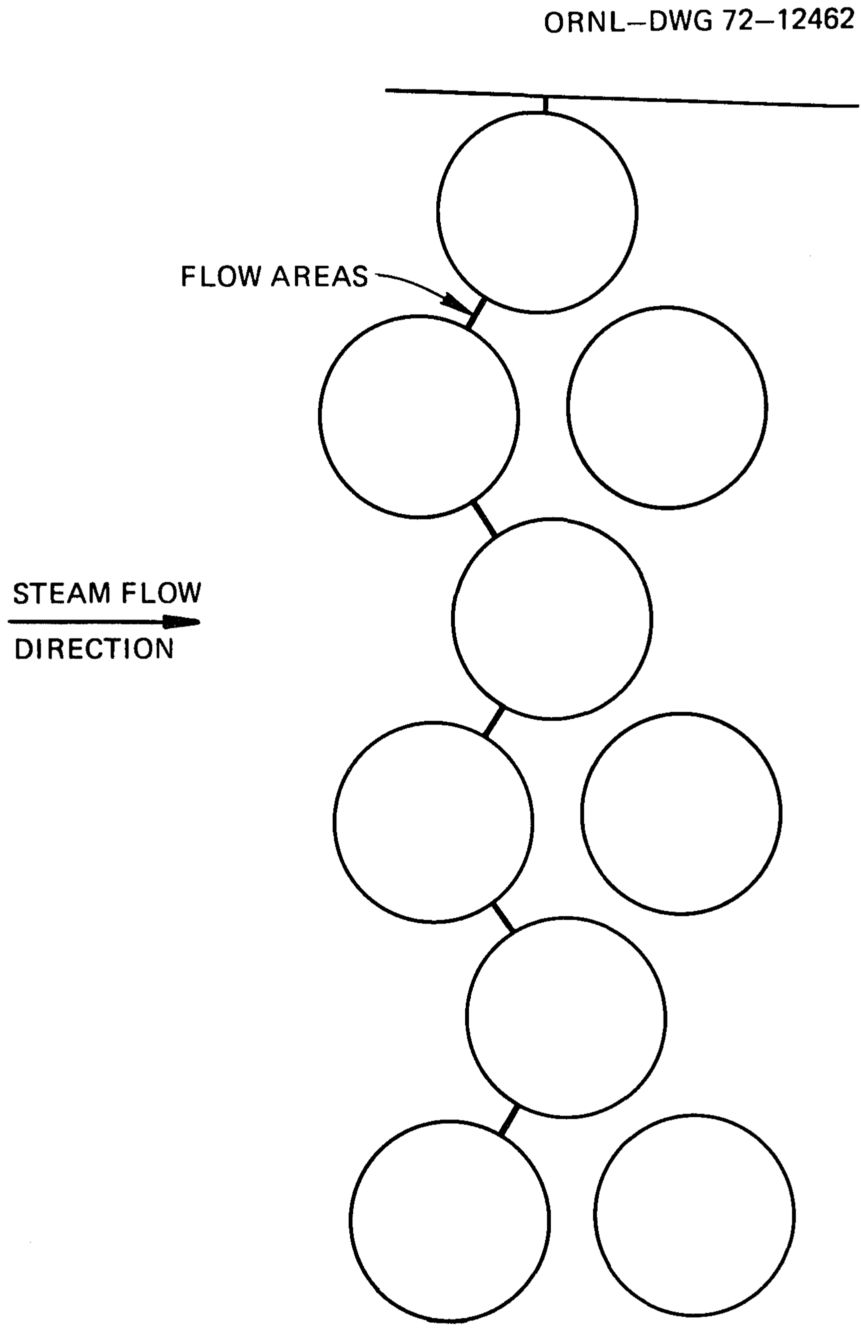

FIGURE 18

STEAM FLOW AREAS USED IN CALCULATING STEAM MASS VELOCITY

Inundation Ratio

When condensate was recycled over the active tubes, the measure of the effective condensate rain was the inundation ratio, defined as the ratio of the rate of collection of water from the center trough to the actual condensation rate in the bundle. Since the dummy tube bundles upstream and downstream of the active bundle drained into separate troughs (side troughs), the inundation ratio would be expected to have a value of slightly less than unity when no spray water was used, because of lateral dispersion of condensate out of the active bundle.

The three spray tubes, when used, sprayed recycled condensate at 45° angles against the two active tubes that comprised the top row of the active bundle. From these tubes the water rained onto lower tubes following a random pattern which because of the narrow bundle, allowed some of the recycled water to also flow into the dummy tube bundles upstream or downstream of the active bundle in a manner similar to that for the condensate formed on the tubes.

From the definition of the inundation ratio, only the condensate passing through the bundle and collected in the trough beneath the bundle was counted. Although this may have underestimated the amount draining through the upper active tubes, it was considered a better estimate than the measured amount of recycled condensate sprayed onto the top tubes because it provided a means of eliminating the effect of steam velocity on the inundation ratio, since only condensate rain which was not carried away by the steam flow was measured as inundation ratio.

Log Mean Temperature Difference

The log mean temperature difference was obtained from:

$$\Delta T_{lm} = \frac{T_o - T_i}{\ln \dfrac{T_b - T_i}{T_b - T_o}} \qquad (5)$$

Cooling Water Velocity and Wilson Plot Parameters

The cooling water velocity was calculated for each test tube based on the tube maximum inside diameter. It was varied in order to establish the convective film coefficient of the five instrumented tubes using a modified Wilson Plot method. For this purpose,the Wilson plot parameter:

$$Re_L^{-0.8} \quad Pr_L^{-1/3} \left(\frac{\mu_w}{\mu_L}\right)^{-0.14}$$

was also calculated, where the fluid properties were taken to be that for pure water at the mean temperature in the tube.

Mass Balance Ratio

A mass balance ratio around the test condenser was calculated for each run. This compared the rate of input and production of condensate in the active bundle (due to condensation on the active tubes and to spraying of recycled condensate) to the rate of removal (the sum of the rates of flow of condensate from the center trough and side troughs).

CHAPTER IV

EXPERIMENTAL RESULTS

A total of 489 runs were carried out with the condenser operating in the range of parameters given in Table I. Of these runs, only 340 were

TABLE I

RANGE OF PARAMETERS

Controlled Variable	Range
Steam Temperature	160-230°F
Steam Mass Velocity	150-2000 lb/hr-ft^2
Non-Condensable Volume Percent	0-8%
LMTD	6-30°F
Inundation Ratio	1-6
Cooling Water Velocity	1-10 ft/sec

considered useful from the standpoint of condensation heat transfer. The remaining included equipment and instrumentation shakedown runs, runs where there were appreciable solids fouling deposits on the inside wall of the tubes, and runs that contained obvious errors in data recording.

No particular schedule was followed in examining the effects of the variables. Initial tests were at 230°F in order to avoid problems with inleakage of air while determining whether the data were sufficiently precise that correlations would be obtained. The subsequent scheduling of tests were carried out on a week-to-week basis, reflecting the results of the previous week. This was possible because all of the preliminary data reduction was carried out the same day as the data were collected.

The schedule of runs included frequent repeats taken in order to establish and repeat baseline conditions. These were used particularly to monitor loop performance before and after gas runs, and also to insure that no fouling had occurred and that the instruments were operating correctly.

The experimental results were converted to values of the overall heat transfer coefficients for the five separately instrumented tubes, their mean value, and values of the experimental parameters described in Chapter III, by means of the computer program CONTST listed in Appendix A. A sample output sheet is given in Figure 19. A tabulation of parameters of interest to the calculation of correlating variables, as extracted from the output sheets, is included in Appendix B as Table B-I.

Mass Balance Ratio

An examination of the mass balance ratios provides a measure of both the accuracy and the precision of the bundle heat transfer coefficients, and by implication of the five tube mean overall heat transfer coefficients. The mass balance ratios for each run listed in Appendix B have been analyzed to determine the presence of bias and to compare the scatter with that expected from the instrument accuracy. To do this, the runs were divided into groups of ten, and group mean values of the mass balance ratio calculated. In calculating the means, runs with gas additions or with recycled condensate were omitted, since the former generally gave lower mass balance ratios, and the latter introduced an additional source of error because of the recycle water rotameter. The gas runs apparently had lower ratios because there was insufficient time during each run for the condensate storage tank beneath each trough to reach equilibrium.

ORNL-DWG 72-12594

RUN SUMMARY SHEET

RUN NO. 244

FLOWS			TEMPERATURES		
BOILER FEED	4.125	GPM	BUNDLE IN	149.092	DEG F
ENTRAIN SEPAR	2.600	GPM	TUBE ONE OUT	152.019	DEG F
SPRAY WATER	0.0	GPM	TUBE TWO OUT	151.912	DEG F
CENTER TROUGH	0.800	GPM	TUBE THREE OUT	152.139	DEG F
SIDE TROUGH	0.079	GPM	TUBE FOUR OUT	151.911	DEG F
TUBE ONE	11.780	GPM	TUBE FIVE OUT	151.721	DEG F
TUBE TWO	11.644	GPM	BUNDLE OUT	152.022	DEG F
TUBE THREE	11.657	GPM	STEAM IN	159.555	DEG F
TUBE FOUR	11.690	GPM	STEAM OUT	159.526	DEG F
TUBE FIVE	11.730	GPM	CONDENSER STEAM	159.522	DEG F
BUNDLE	260.000	GPM	SPRAY WATER	1.000	DEG F
BARO CONDENSER	16.150	GPM	BARO CONDENSER IN	68.000	DEG F
NITROGEN GAS	0.0	CFM	BARO CONDENSER OUT	80.000	DEG F

BUNDLE PARAMETERS

BUNDLE LMTD	8.885	DEG F
STEAM TEMP	159.522	DEG F
STEAM MASS VEL	171.391	LB PER HR-SQ FT
STEAM MOLAR VEL	9.522	MOL PER HR-SQ FT
STEAM VELOCITY HEAD	0.0055	LBF PER SQ FT
NITROGEN MOL FRAC	0.0	
BUNDLE WATER VEL	5.582	FT PER SEC
INUNDATION RATIO	0.841	
MASS BALANCE	1.081	IN OVER OUT

OVERALL U		DATA REDUCTION	
BTU/HR-SQFT-DEG F		FIVE TUBE AVERAGES	
BUNDLE	1084.	OVERALL U	1050.
TUBE ONE	1089.	LMTD	8.93
TUBE TWO	1030.	INSIDE HTC	2723.
TUBE THREE	1130.	OUTSIDE HTC	2265.
TUBE FOUR	1034.	CN 5	1.167
TUBE FIVE	956.		

FIGURE 19

SAMPLE OUTPUT SHEET

The results have been plotted in Figure 20. An experimental bias of +5-10 percent is seen to be present. Superimposed on the bias is a random scatter of an additional ±5 per cent. There appears to be no trends.

Analysis of Experimental Bias

The bias in the mass balance ratio most probably resulted from one or both of the following sources: a calibration shift associated with the inlet cooling water thermocouple not compensated by the cross calibration term, or an error in calibration or in reading the center drain trough flowmeter. The magnitude of the error in thermocouple calibration needed to account for the bias is +0.15 to +0.25°F. An error in the flowmeter calibration of 1 percent of full scale would also have accounted for the bias. In each instance, the magnitude of the error was at or near the limit of accuracy of the measurement.

It is noted that the thermocouple cross-calibration described in Appendix C, carried out to account for the possibility of thermocouple drift, contained a mean correction term for the inlet water thermocouple of +0.15°F, but that the later calibrations indicated higher values than the mean by an additional +0.12°F. Thus, this thermocouple had a history of drift over a range of temperature equal in magnitude to that of the observed bias.

The flowmeter calibration curve was examined and there was no basis for expecting a bias. It has been concluded that the most likely cause of the experimental bias was a drift in the calibration of the inlet cooling water thermocouple. Because of the uncertainty involved in the above analysis, the experimental results were not changed to reflect a recorrection of the thermocouple readings.

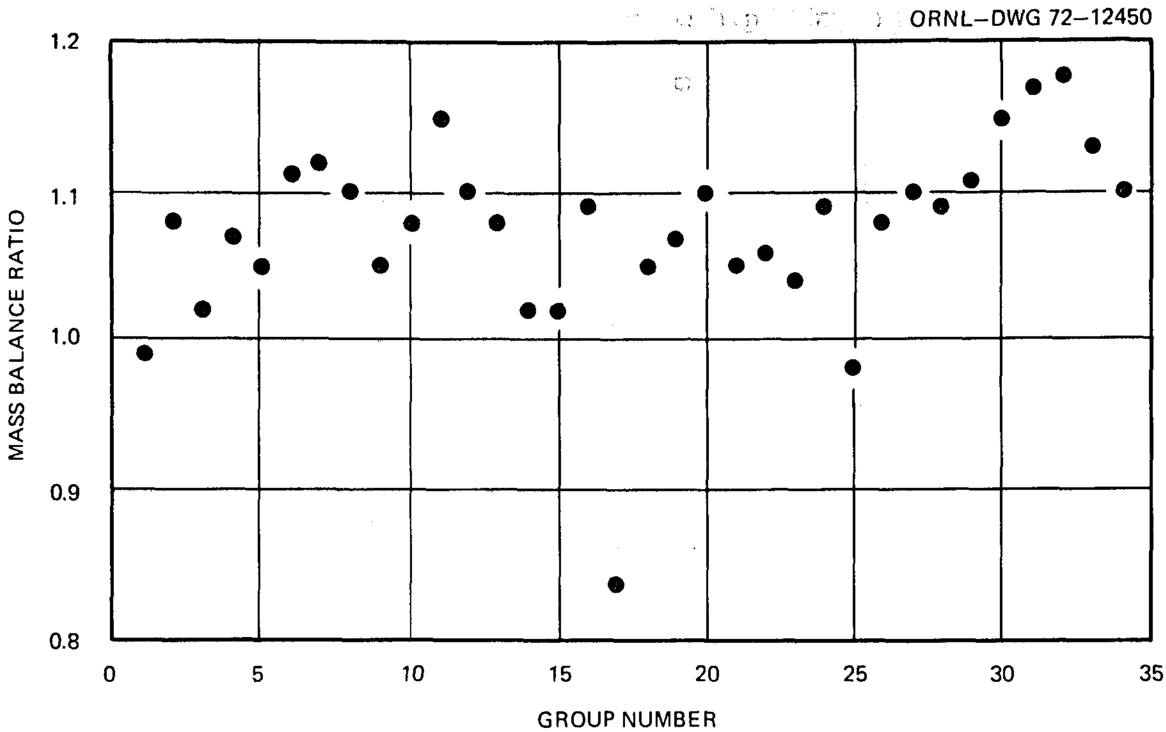

FIGURE 20

AVERAGE MASS BALANCE RATIOS FOR TEN-RUN GROUPS

Sample Data

In order to provide a graphical overview of the experimental data, typical data sets have been plotted in Figures 21 and 22 as overall heat transfer coefficient vs tube number for several sets of operating parameters. It can be seen that the effects of the parameters appear to follow consistent patterns and that the relationship between tube number and performance is consistent from run to run.

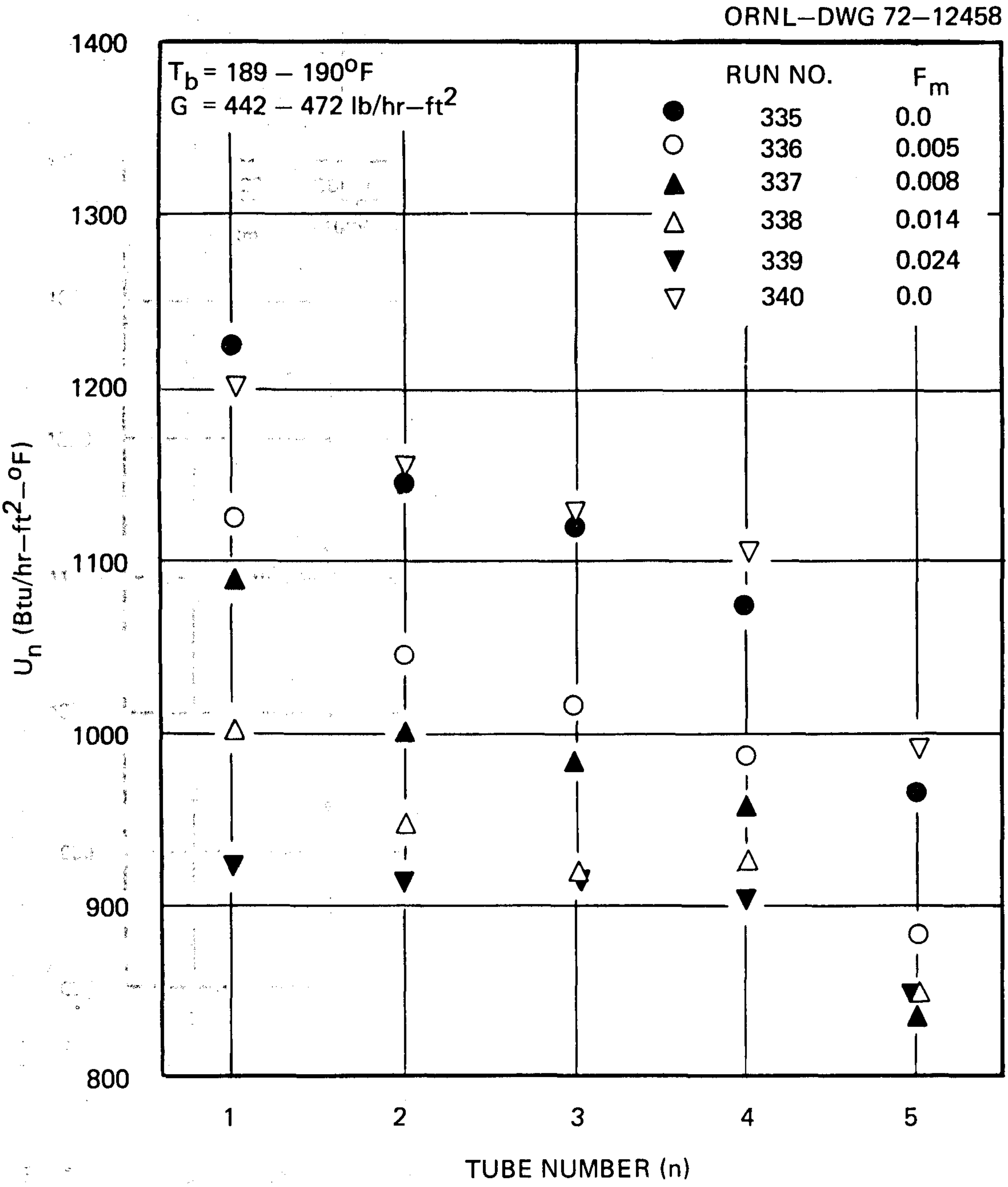

FIGURE 21

EFFECT OF CONCENTRATION OF NON-CONDENSABLE GAS ON THE OVERALL HEAT TRANSFER COEFFICIENT OF SEPARATE TUBES

ORNL–DWG 72–12464

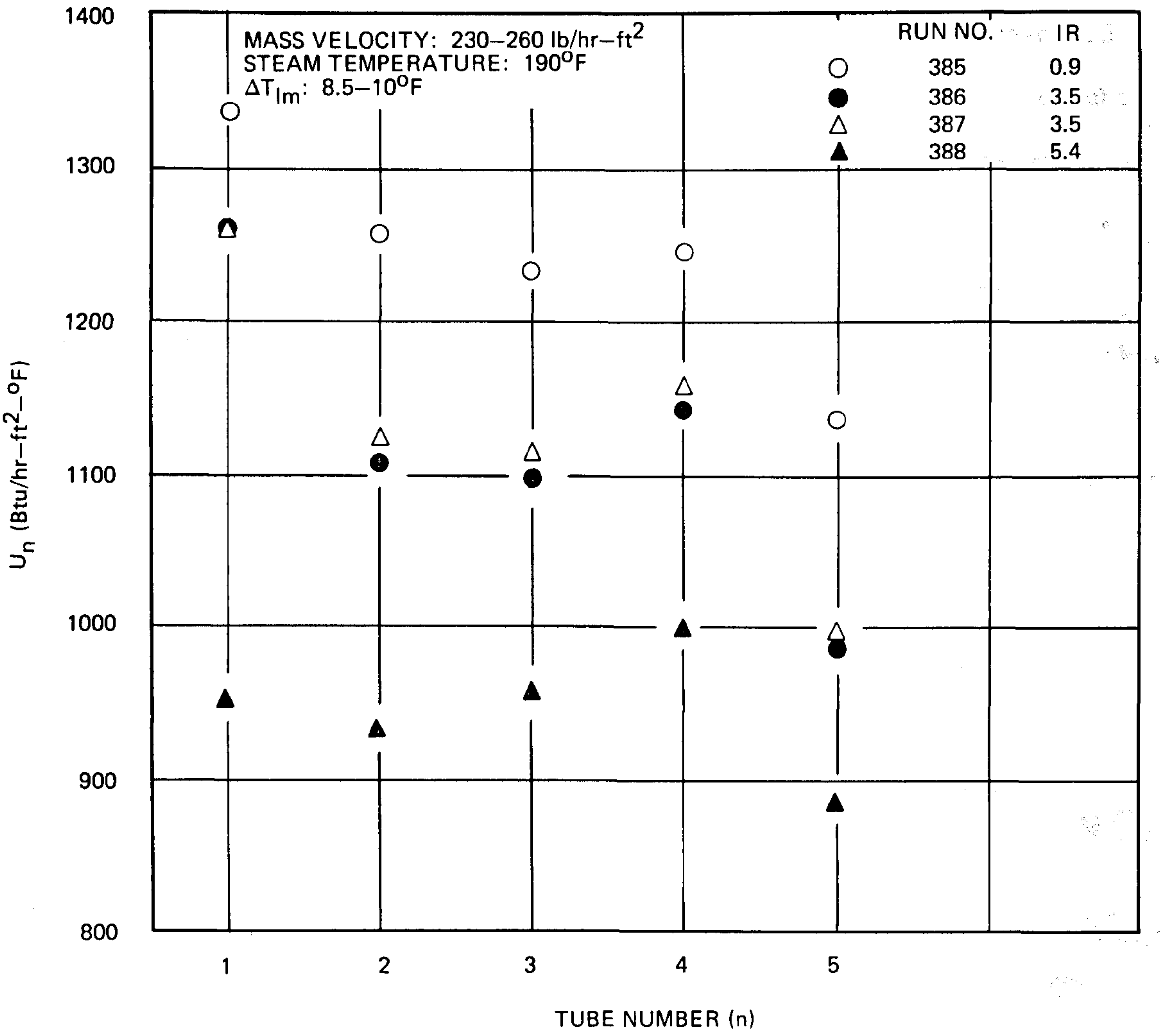

FIGURE 22

EFFECT OF FLOW RATE OF RECYCLED CONDENSATE (INUNDATION RATIO) ON THE OVERALL HEAT TRANSFER COEFFICIENT OF SEPARATE TUBES

CHAPTER V

CALCULATION OF SHELL SIDE FILM HEAT TRANSFER COEFFICIENTS

In this chapter, the methodology used for calculating experimental values of the shell side heat transfer coefficients from the measured overall coefficients is described. In the calculations, the five-tube mean values, ($\overline{U}_5$), rather than separate tube values, (U_n) were used, since all five instrumented tubes were exposed to the same shell side parameters of gas concentration, steam temperature and mass velocity, cooling water inlet temperature and velocity, and spray water flow rate, and the use of $\overline{U}_5$ reduced the experimental error.

The following sequence of assumptions and calculations were used to obtain individual film heat transfer coefficients:

1. The solids fouling resistance was assumed to be zero.

2. The tube wall heat transfer resistance was calculated from Equation (11).

3. The Wilson plot runs were used to derive the correlating equation for the convective film heat transfer coefficient based on Equation (12).

4. The condensate film heat transfer coefficient, and its normalized form, the Nusselt Correction Factor, were calculated for runs with no gas additions.

5. The gas film heat transfer coefficient was calculated for runs with gas addition.

The above calculations were carried out as part of the computer program CONTST and JFACT listed in Appendix A. In the following sections, the calculations involved in steps 2 through 5 are described.

Tube Wall Resistance

The wall resistance for all active tubes in the test condenser was calculated from Equation (11). Using a wall thickness of 0.035 in. and a thermal conductivity of 310 Btu/hr-ft^2-°F/in.[23] results in a wall resistance of 0.000117 °F/Btu/hr-ft^2.

Correlating Equation for the Convective Film Coefficient

The modified Wilson plot method was used to obtain the correlating equation for predicting h_i. In using the Wilson plot, the functional relationship between h_i and V must be chosen a priori, and the remaining heat transfer resistances (other than that due to the convective film) must be held constant while the velocity is varied. In the present work, Equation (12) was selected as the functional form of the correlation, with the constant C_i determined empirically. The condensate film resistance was held essentially constant by using a lower tube (usually the third from the top) for the measurements, and maintaining the water velocity in the remaining tubes constant during the measurement period.

The Wilson plot[30] is a graphical solution to a modified form of Equation (6). By substituting Equation (12) into Equation (6) and lumping all resistances other than the convective film into a single residual term ($\sum R$), the equation:

$$\frac{1}{U} = \frac{d_o}{C_i k} \, Re_L^{-0.8} \, Pr_L^{-1/3} \left(\frac{\mu_w}{\mu_L}\right)^{-0.14} + \sum R \tag{68}$$

is obtained. From this equation, it is seen that a plot of 1/U against the term:

$$Re_L^{-0.8} \; Pr_L^{-1/3} \; \left(\frac{\mu_w}{\mu_L}\right)^{-0.14}$$

will be a straight line with a slope of $d_o/C_i k$, and an intercept equal to the sum of the residual resistances. The value of C_i for each Wilson plot run is then obtained from the slope.

The calculation of the Wilson plot parameters and the least squares fit of the slopes were carried out as a subroutine of the computer program CONTST. A Wilson plot for a typical data set, shown in Figure 23, with the good fit to a straight line taken as proof of the accuracy of the functional relationship chosen. Table II contains a summary of the values of C_i obtained from the Wilson plot runs. The mean value was found to be 0.042, or about 1.9 times that obtained for smooth tubes. This agrees well with the value previously obtained for a sample of the tubing run in a single tube condenser; thus confirming that the performance of the rope tube in a multitube condenser is as predicted.

The correlating equation for h_i, for use in calculating the shell side coefficients, was taken to be:

$$\frac{h_i \, d_i}{k} = 0.042 \; Re_L^{0.8} \; Pr_L^{1/3} \; \left(\frac{\mu_w}{\mu_L}\right)^{0.14} \qquad (69)$$

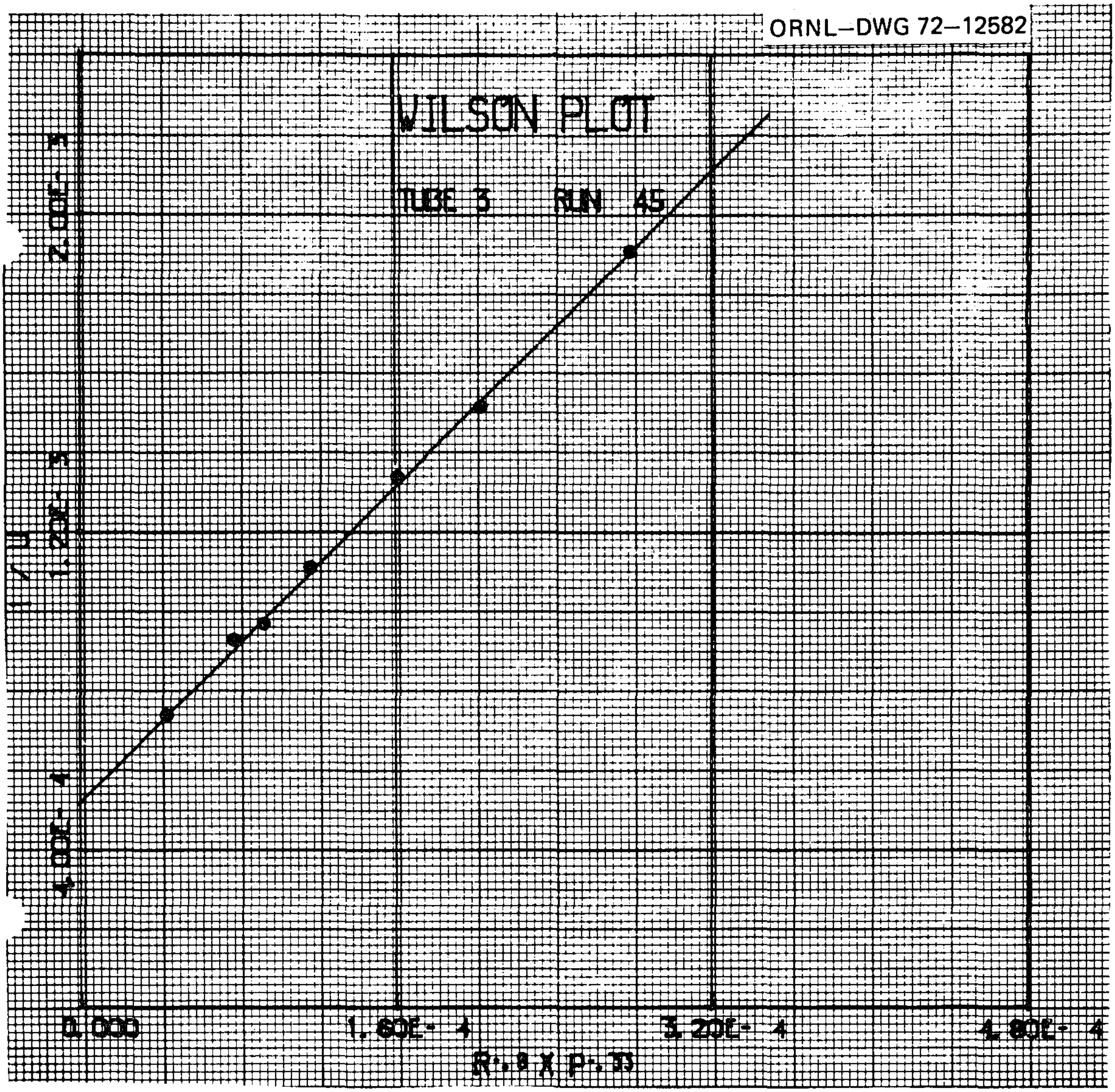

FIGURE 23

TYPICAL WILSON PLOT (RUN NO. 45)

TABLE II

SUMMARY OF WILSON PLOT RUN RESULTS

Run No.	Tube	C_i
38	3	0.0447
39	3	0.0419
40	3	0.0404
41	3	0.0430
42	3	0.0432
43	3	0.0535
44	3	0.0444
45	3	0.0422
46	3	0.0444
48	3	0.0393
49	3	0.0407
50	3	0.0400
51	3	0.0441
56	1	0.0392
57	5	0.0392
59	2	0.0397
60	1	0.0400
61	1	0.0368
61	3	0.0370
301	2	0.0420
301	3	0.0416
302	3	0.0432
302	4	0.0409
302	5	0.0404

Mean: 0.0417
Standard Deviation = 0.0033
$C_i = 0.0417 \pm 0.007$

Calculation of the Experimental Condensate Film Heat Transfer Coefficients

For each run with no gas addition, the experimental five tube mean condensate film coefficient ($\overline{h}_{c5}$) was calculated from the equation:

$$\overline{h}_{c5} = \frac{1}{\frac{1}{\overline{U}_5} - R_w - \frac{d_o}{d_i\ h_i}} \tag{70}$$

where h_i was evaluated at the conditions of the run, and $\overline{U}_5$ was the experimental five tube mean overall coefficient. The values of $\overline{h}_{c5}$ were normalized for correlation purposes by dividing them by the predicted values based on Equation (15) calculated for the run conditions. The resulting ratio was designated as the Nusselt Correction Factor (CN5):

$$CN5 = \frac{(\overline{h}_{c5})_{exp.}}{(\overline{h}_{c5})_{Nusselt}} \tag{71}$$

The usefulness of this dimensionless condensate film heat transfer coefficient stems from the fact noted in Chapter II that Equation (13) has been shown by previous investigators to predict correctly the effects of condensing rate and steam temperature (the latter through its effect on fluid properties). Thus comparisons of experimental values of CN5 do not necessarily have to be made at the same temperature or condensing rate, whereas comparisons of $\overline{h}_{c5}$ would.

Experimental values of $\overline{h}_{c5}$ and CN5 calculated as part of the computer program CONTST are tabulated in Appendix B, Table B-I.

Calculation of the Gas Film Heat Transfer Coefficients

For the case of runs where nitrogen gas was added to the steam, the application of Equation (70) to the overall coefficient results in a combined film coefficient which included the effect of both the gas film and the condensate film. Referring to this as an effective coefficient, ($\bar{h}_{e5}$), it can be shown by reference to Equation (6) to be composed of:

$$\frac{1}{\bar{h}_{e5}} = \frac{1}{h_g} + \frac{1}{\bar{h}_{c5}} \qquad (72)$$

Solving for h_g yields:

$$h_g = \frac{\bar{h}_{e5}}{1 - \dfrac{\bar{h}_{e5}}{\bar{h}_{c5}}} \qquad (73)$$

The effective coefficient was normalized in the same manner as the condensing coefficient:

$$CN5_g = \frac{\bar{h}_{e5}}{(\bar{h}_{c5})_{Nusselt}} \, . \qquad (74)$$

By substituting the experimental values of $\bar{h}_{c5}$ and $\bar{h}_{e5}$ obtained from Equations (71) and (74) into the denominator of Equation (73), an expression for h_g is obtained in terms of experimentally measured quantities:

$$h_g = \frac{\bar{h}_{e5}}{1 - \dfrac{CN5_g}{CN5}} \qquad (75)$$

The values of CN5 used in the equation were obtained from runs without gas additions made immediately preceding and/or following the gas runs. This procedure served to increase the precision of calculation of h_g.

Values of h_g for the gas runs were calculated from the program JFACT listed in Appendix A and have been tabulated in Appendix B, Table B-II.

CHAPTER VI

CORRELATIONS

In this chapter, the relationships between the experimental values of the two shell side coefficients (h_g and $\overline{h}_{c5}$) obtained as described in Chapter V, and the relevant shell side parameters, as determined in Chapter IV, are compared with the correlating equations described in Chapter II. Each of the shell side heat transfer coefficients are discussed separately.

Condensate Film Heat Transfer Coefficient

The effects of three parameters on the condensate film coefficient, the condensate rain, the steam velocity, and the steam temperature were determined. The approach followed in each case was to plot the experimental values of $\overline{h}_{c5}$ or CN5 separately as function of a single parameter, and compare the resulting graph with predictions based on results of previous investigators.

As noted in Chapter V, there was a general lack of closure of the mass balance around the test condenser, such that most mass balance ratios were in the range 1.0 to 1.15. The direction of this bias in the mass balance, if due to thermocouple error, would have resulted in higher values of $\overline{U}_5$ and thus of $\overline{h}_{c5}$. If the bias were due instead to errors in measurement of the condensate drain flow rates, the values of $\overline{U}_5$ and $\overline{h}_{c5}$ would have been unaffected. Thus a direct comparison of the present results with the Nusselt equation predictions is not possible since any departure from agreement could have been the result of the bias. Since the effect of temperature level, condensate rain flow rate, and steam velocity are superimposed on the bias if it is present, the study of their relative effects would not be greatly affected.

Effect of Condensate Rain

The effect of condensate rain was obtained from data taken during the runs in which recycled condensate was sprayed onto the top of the active bundle. A plot of these results is given in Figure 24 as inundation ratio (IR) versus CN5. As noted in Chapter IV, the defining equation for IR includes only water collected beneath the active bundle, and thus underestimates the condensate rain on the upper tubes.

The results are compared with the Nusselt prediction for condensate rain effects, Equation (25), and also the curve obtained from Equation (29). A plot of the former is seen to lie substantially below the data points, confirming that the Nusselt theoretical equation for the effect of condensate rain is too conservative, in agreement with the results of previous investigators. It should be noted that the approximations introduced in the definition of IR is to underestimate the amount of condensate rained onto upper tubes. A correction for this would shift the data to the right in Figure 24, thus making the Nusselt prediction even more conservative.

The present data can be correlated either by an empirical equation of the form of Equation (26), or of the form of Equation (30). By trial and error, the line shown in Figure 24 , which is intended to represent

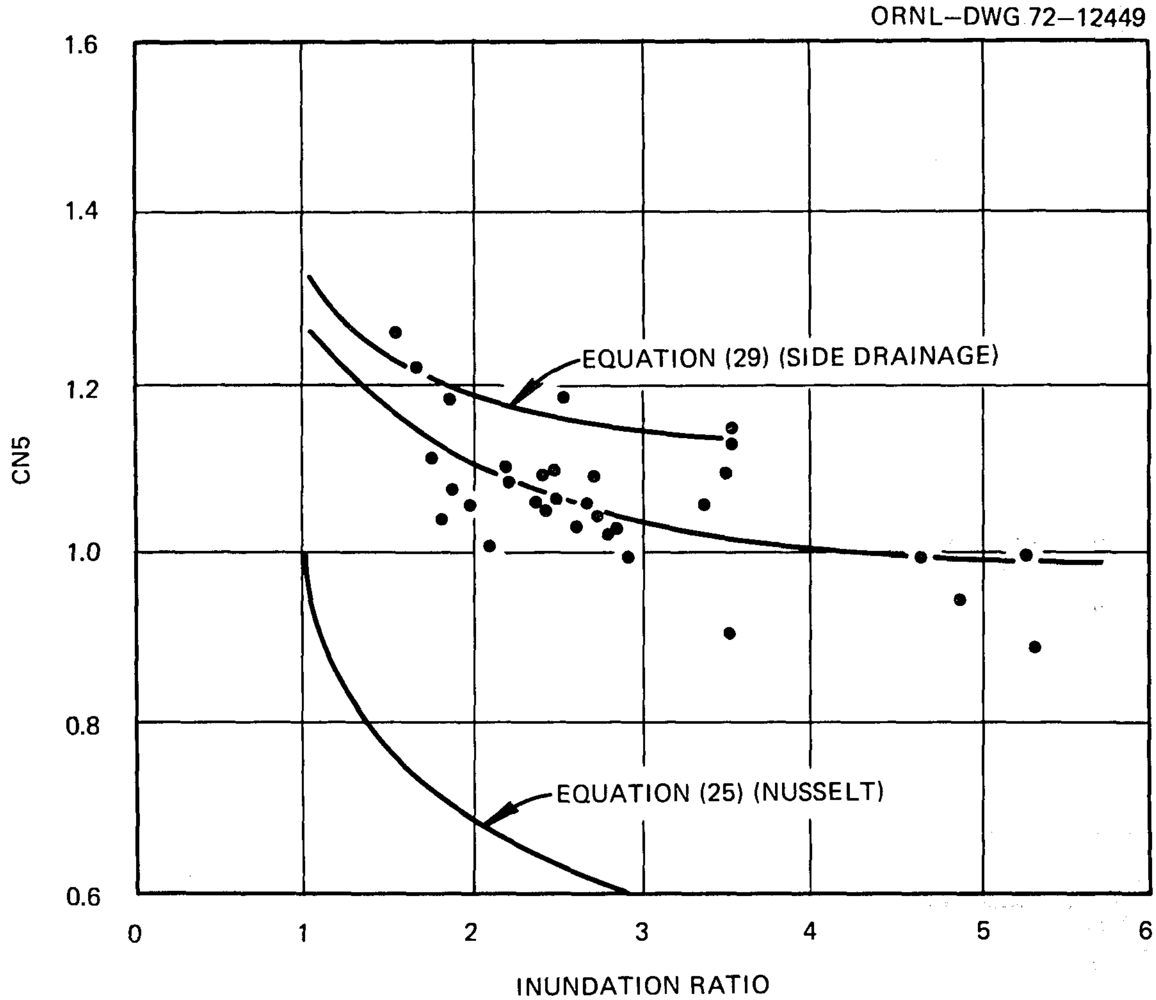

FIGURE 24

EFFECT OF INUNDATION RATIO ON THE NUSSELT CORRECTION FACTOR the best fit to the experimental data while conforming to the correlating equations, was found to be expressed by:

$$\frac{\bar{h}_{cn}}{h_N} = n^{-0.10} \tag{76}$$

and also [by substituting $F_d = 0.8$ into Equation (30)] by:

$$\frac{\bar{h}_{cn}}{h_N} = 0.48 + \frac{0.54}{n^{0.25}}. \tag{77}$$

The scatter in the data around the correlating line of about ±15 percent agrees well with the projected accuracy given in Chapter II. It is noted that the accuracy of CN5 will be lower than that of $\bar{U}_5$ since from Equation (68) there is a subtraction step involved in the conversion from $\bar{U}_5$.

Effect of Steam Mass Velocity

In order to determine the effect of the steam mass velocity, graphs were prepared in Figure 25 of $(\bar{h}_{c5})_{exp.}$ plotted against the mass velocity at the plane of the test tubes. Each graph contains data at only one condensing temperature, and over a restricted range of ΔT_{lm}. Superimposed on the data are lines drawn to represent an equation of the form:

$$\bar{h}_{c5} \propto G^{0.16}, \tag{78}$$

which is the functional relation used by Fuks[18] and Berman[17] for vertical downflow of steam through horizontal tube condensers. There thus appears to be (qualitatively) a similar effect for horizontal as for downward

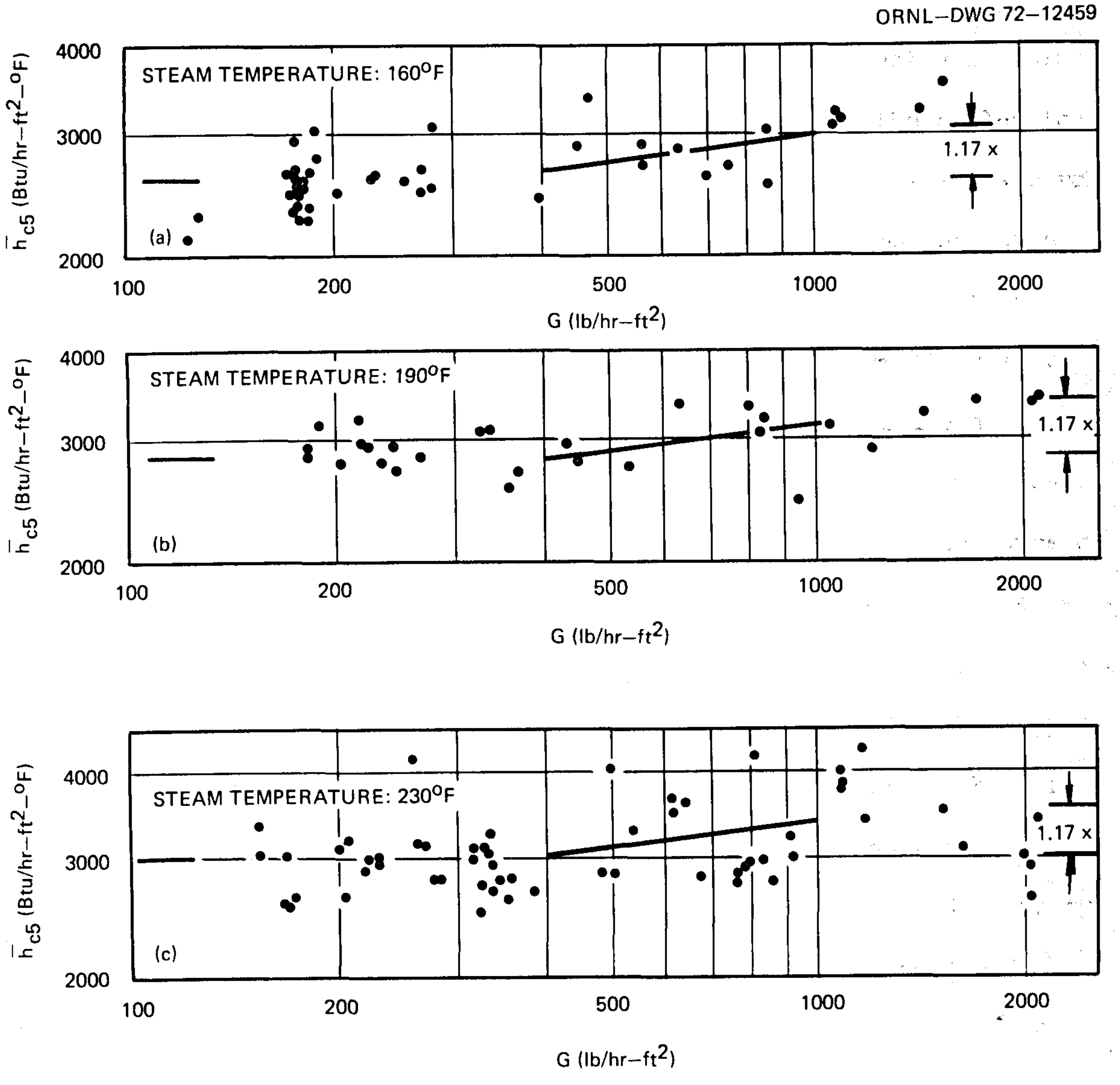

FIGURE 25

EFFECT OF STEAM MASS VELOCITY ON THE CONDENSATE FILM
HEAT TRANSFER COEFFICIENT

cross flow. Because of the scatter, determining a correlating equation for the present data does not appear warranted.

Condensate Carry Over Measurements and Correlation

In reviewing the data for the above runs at the highest velocities, it was observed that there was a significant decrease in the collection rate of condensate from the trough beneath the active bundle and a corresponding increase in the side trough rate. It was concluded that this was due to a directed lateral transport of condensate out of the active bundle in the direction of the steam flow beyond that normally resulting from random dispersion. Since such a loss of condensate could account for part or all of the steam velocity effect, this phenomenon was more carefully studied in several subsequent experiments covering a wide range of steam velocities for each of the three steam temperatures. These experiments were carried out and reported[31] by students of the School of Chemical Engineering Practice of the Massachusetts Institute of Technology with the present author as consultant. The data taken during these runs included separate collection of condensate under the downstream side trough as well as the active bundle trough, both taken with increased accuracy resulting from calibrating the volumes of the collection tanks under each trough and measuring their fill times. The ratio of the observed collection rates,

$$\text{carry over fraction} = \frac{\text{downstream trough rate}}{\text{active trough rate}} \tag{79}$$

was plotted against the steam velocity head, (G^2/ρ), in Figure 26.

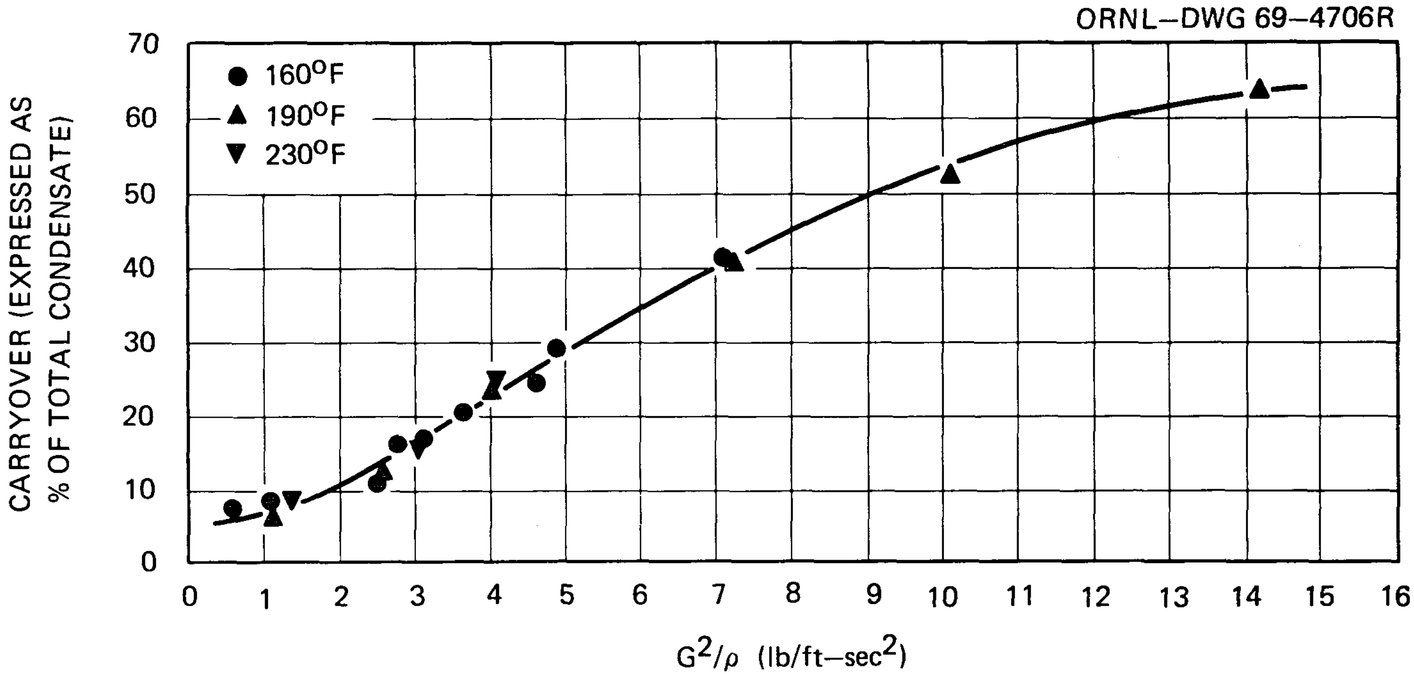

FIGURE 26

EFFECT OF STEAM VELOCITY HEAD ON THE CARRY OVER OF CONDENSATE FROM THE ACTIVE TUBE BUNDLE

The steam velocity head, rather than the mass velocity (G) was found to bring all of the data for the three temperatures onto the same line, thus suggesting that it might provide a better correlating variable for accounting for velocity effects on $\overline{h}_{c5}$ as well. In view of the small magnitude of the effect, however, this does not appear necessary.

The upper theoretical limit to the carry over fraction at high steam velocities was calculated by assuming that all of the condensate drains onto tubes diagonally below in the downstream direction. From geometrical consideration, the condensate from 21 of the 27 active tubes can escape the active bundle trough in this manner. The maximum predicted carry over ratio then is 0.77, which is seen to be in qualitative agreement with the projected asymptote for the data shown in Figure 26 of about 0.65 - 0.70.

If the foregoing analysis were to be applicable to the effect of high velocity steam on $\overline{h}_{c5}$, all of the tubes in the vertical column would behave approximately as top tubes as the velocity of steam is increased. Thus the maximum increase in $\overline{h}_{c5}$ would, for the case of the present experiment, be the inverse of that predicted from Equation (76) for n equal to five, or 1.17x. This is seen to be a reasonable upper limit to $\overline{h}_{c5}$, as shown in Figure 25.

The scatter of the data in Figure 25 is about ±30 percent or less. This scatter is consistent with the projected errors in the measurement of $\overline{U}_5$ described in Chapter II.

It has been concluded that the effect of steam velocity observed in the present work can be accounted for by the transport of condensate away from the active bundle portion of the test condenser.

Effect of Condensing Temperature

The effect of condensing temperature on $\overline{h}_{c5}$ was obtained indirectly by comparison of the data plotted in Figure 25. It is seen that there is an increase in $\overline{h}_{c5}$ with increasing temperature of about 10 percent between 160 and 190°F and about 5 percent between 190 and 230°F. The observed increases are of the same magnitude as the scatter at each temperature. These increases have been compared to those predicted by the Nusselt equations. For the case of constant film ΔT, the condensate film coefficient is a function of the temperature dependent group included in Equation (13a):

$$Nu_I = \left\{ \frac{k_f^3 \, \rho_f^2 \, \lambda_f}{\mu_f} \right\}^{1/4} . \qquad (80)$$

Alternatively, for constant condensing rate, the relevant group from Equation (13b) is:

$$Nu_{II} = \left\{ \frac{k_f^3 \, \rho_f^2}{\mu_f} \right\}^{1/3} \qquad (81)$$

Table III compares the experimental ratios of $\overline{h}_{c5}$ for the different temperatures with those predicted by the Nusselt equation for the cases of constant film ΔT and constant condensing rate.

TABLE III

EFFECT OF TEMPERATURE ON THE CONDENSATE FILM HEAT TRANSFER COEFFICIENT

	Experimental	Nusselt (ΔT_c=Constant)	Nusselt (Condensing Rate Constant)
$\dfrac{\bar{h}_{c5}\ (190^\circ F)}{\bar{h}_{c5}\ (160^\circ F)}$	∿1.1	1.06	1.08
$\dfrac{\bar{h}_{c5}\ (220^\circ F)}{\bar{h}_{c5}\ (190^\circ F)}$	∿1.05	1.05	1.08

Since the data were taken at constant ΔT_{1m}, which is neither constant ΔT_c nor constant condensing rate, the comparison should be made with a value between the ratios for these conditions. The agreement in either case is good considering the scatter, so that it can be concluded that in the temperature range 160 to 230°F, the temperature dependence of the condensate film heat transfer coefficient is adequately expressed by the Nusselt equation.

Non-Condensable Gas Film Heat Transfer Coefficient

The parameters which affect the gas film coefficient (h_g) and which were varied in the present experiments included the condensing rate, the bulk stream gas mole fraction and the steam-gas mixture temperature and mass velocity at the condenser tubes. The correlation approach used was to test the interrelation between these parameters and the gas film coefficient given by the Colburn mass transfer - heat transfer analogy for the same geometry, and by the modified form of the j factor derived by Spalding. For this purpose, the experimental values of h_g were combined with the appropriate other parameters to obtain sets of Colburn mass transfer j factors, Spalding mass transfer j factors, and Reynolds numbers, using the computer program JFACT listed in Appendix A. The steps involved in the program are described below.

Mass Transfer j-Factor Calculation

The Colburn mass transfer j factor is defined as:

$$j_M = \frac{k_g \bar{p}_g}{G} \frac{M_b}{M_s} (Sc)^{2/3} \tag{55}$$

where, from Equation (37):

$$k_g = \frac{h_g}{\lambda} \frac{(T_b - T_c)}{(p_{sb} - p_{sc})} \tag{82}$$

and

$$\bar{p}_g = \frac{p_{gc} - p_{gb}}{\ln \frac{p_{gc}}{p_{gb}}} \tag{42}$$

and the required molecular weights are:

$$M_b = 18 (1 - F_m) + 28 F_m \tag{83}$$

and

$$M_s = 18. \tag{84}$$

The Schmidt number for the steam-nitrogen mixtures was assumed constant and equal to 0.61 over the entire temperature range of interest based on steam-air data.[32]

From the defining equation for the gas film coefficient (Equation 10), the temperature at the condensate film boundary with the gas film is:

$$T_c = T_b - \frac{\overline{U}_5 \, \Delta T_{lm}}{h_g} \tag{85}$$

The corresponding partial pressures of the steam at that temperature (p_{sc}) and at the bulk steam temperature (p_{sb}) are obtained from empirical correlating equations assuming saturation conditions.

The gas partial pressure in the bulk stream is:

$$p_{gb} = \frac{F_m}{1-F_m} \, p_{sb} \tag{86}$$

and the gas partial pressure at the condensate film is:

$$p_{gc} = p_{sb} + p_{gb} - p_{sc} \tag{87}$$

Substituting p_{gb} and p_{gc} into Equation (42) gives $\overline{p}_g$.

The Spalding mass transfer j factor:

$$j_{ms} = \frac{k_g \, p_{gc}}{G} \, \frac{M_g}{M_s} \, (Sc)^{2/3} \tag{88}$$

is obtained in the same manner with the exception that p_{gc} substitutes for $\overline{p}_g$.

Reynolds Number Calculation

The shell side Reynolds number was calculated from:

$$Re_v = \frac{d_o G}{\mu} \tag{89}$$

where the viscosity was assumed to be that of the steam at the condenser temperature.

Comparison of j-Factor Plots

Plots of the Colburn and the Spalding mass transfer j factors versus the shell side Reynolds number are given in Figures 27 and 28. Shown also is the predicted line based on the Colburn analogy (Equation 41).

Two pertinent observations can be made regarding the two curves:

1. The Spalding mass transfer j-factor plot shows about one-half the dispersion of data as the Colburn plot.

2. The Colburn mass transfer j-factor plot lies close to the heat transfer j-factor line.

The agreement between the Colburn j factor and the predicted sensible heat transfer line appears to substantiate the validity of that form of correlation. However, the merits of having a correlation with a lower dispersion of the data is in the final analysis more compelling. An analysis of the lower dispersion in the Spalding j-factor plot is shown in Figure 29, in which several sets of data are plotted both as Spalding and as Colburn j factors. These data sets were each taken during one day, with the final run being a repeat of the initial, both being runs with no gas addition. It is seen that the Spalding j factor leads to a more

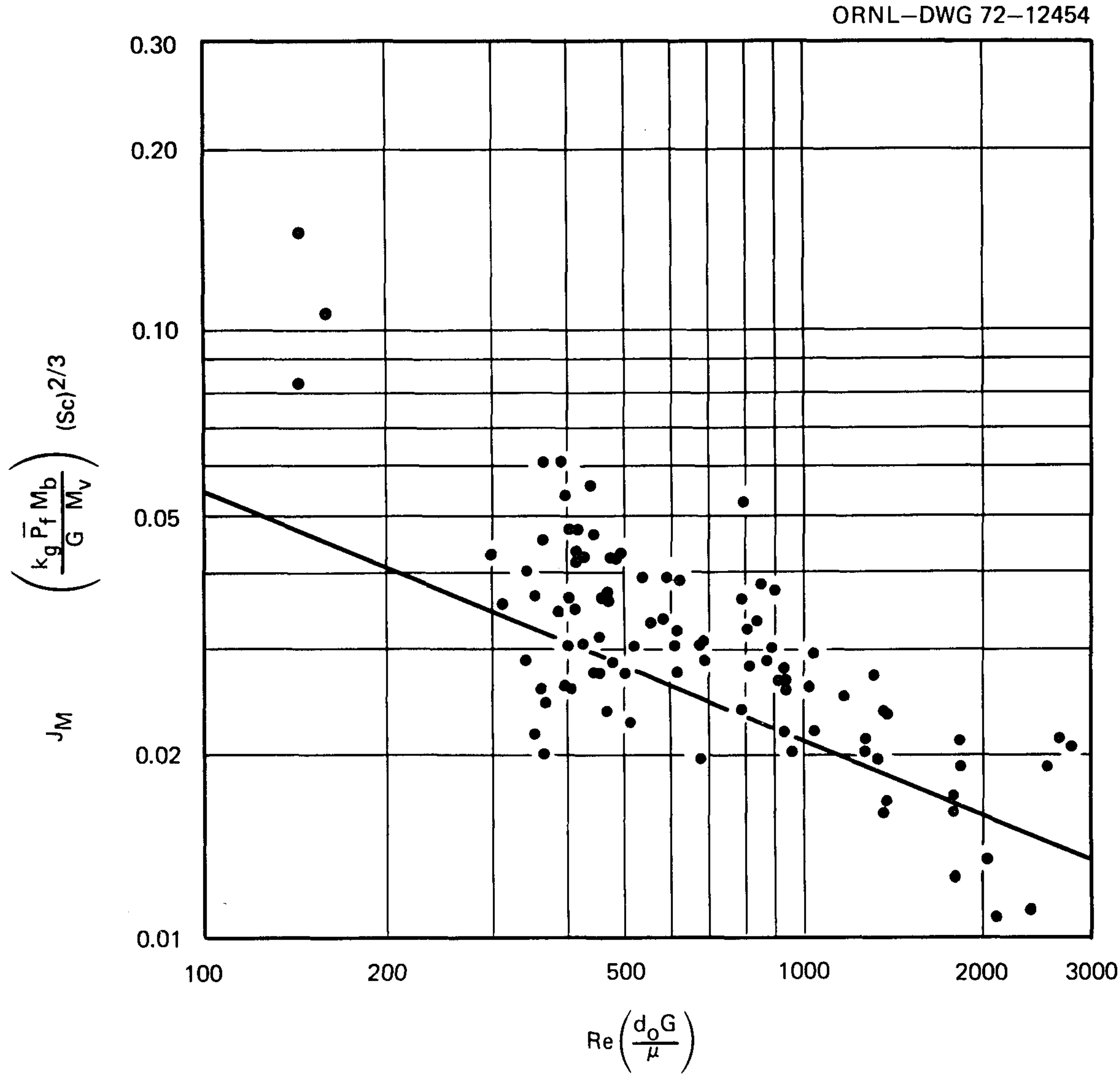

FIGURE 27

CORRELATION OF THE EFFECTS OF NON-CONDENSABLE GAS BASED ON THE COLBURN MASS TRANSFER J FACTOR

ORNL–DWG 72–12451

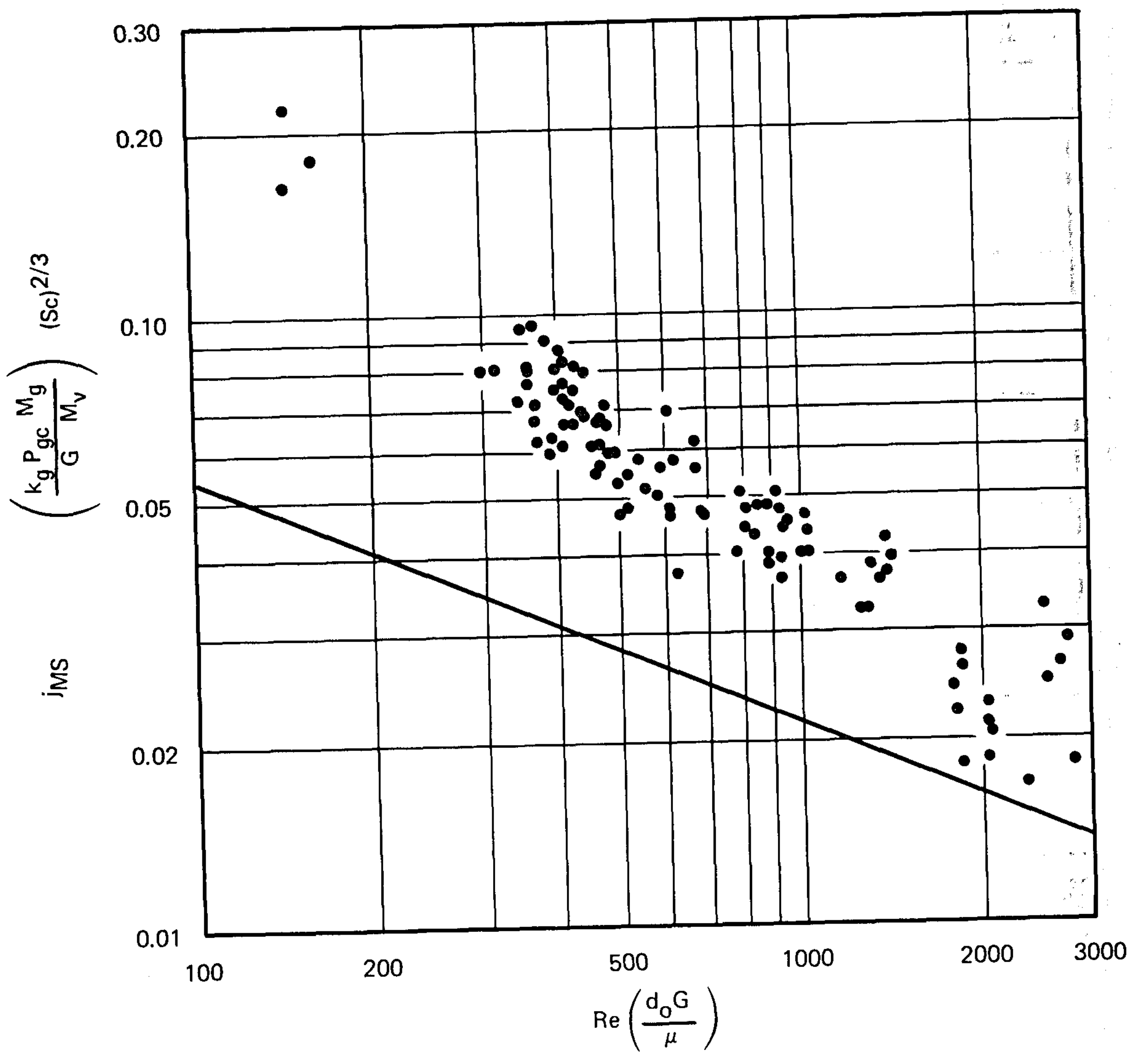

FIGURE 28

CORRELATION OF THE EFFECTS OF NON-CONDENSABLE GAS BASED ON THE SPALDING MASS TRANSFER J FACTOR

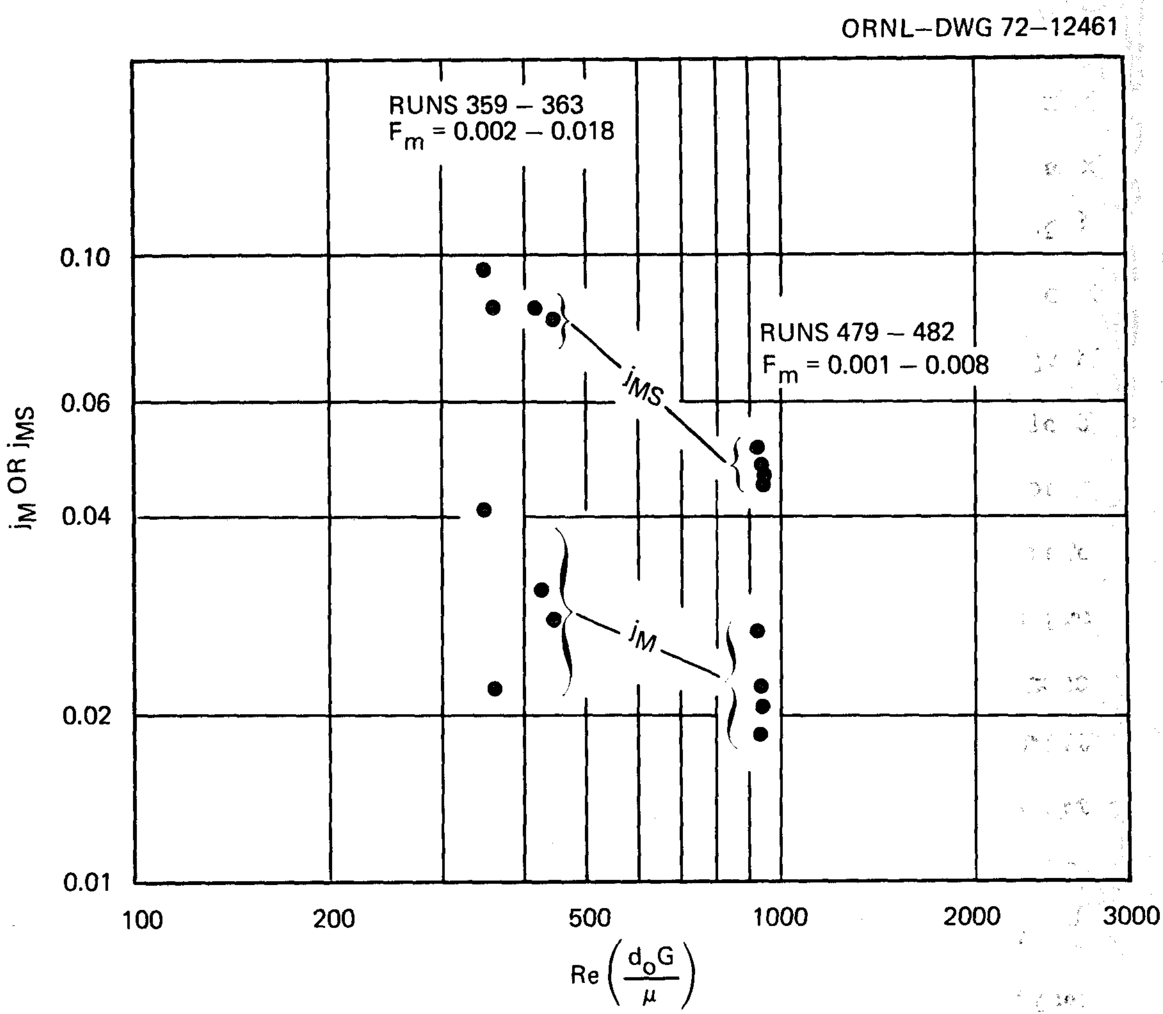

FIGURE 29

COMPARISON OF THE EFFECTS OF GAS CONCENTRATION ON THE COLBURN J FACTOR AND THE SPALDING J FACTOR closely grouped set in each case, although in one case there is still a monotonic relation between the gas concentration and the j factor for constant mass velocity, steam temperature and condensing rate.

There is an apparent explanation of the Spalding mass transfer j-factor data lying about a factor of two above the analogous heat transfer line. It is noted that the mass transfer rates used in the present experiment (in the absence of gas) were in the range 7-20 lb/hr-ft^2, which is the same order of magnitude as the Reynolds fluxes generated at the Reynolds numbers used in the experiments. As calculated from Equation (56), they would be in the range 5-15 lb/hr-ft^2 for Reynolds numbers in the range 300-2000. In Spalding's derivation of the j factor, he assumed that the incoming Reynolds flux was independent of the mass transfer rate. If in fact, the incoming Reynolds flux were increased in proportion to the mass transfer rate, then this would alsc shift the analogous heat transfer j-factor line upward. The magnitude of the expected shift could be enough to account for the difference between the Spalding j-factor data and the indicated heat transfer line, which can be considered as a zero mass transfer line. This explanation also can account for the steeper slope of the mass transfer data, particularly at the higher Reynolds number. In that region, the mass transfer rate is a smaller fraction of the Reynolds flux, so that the data should more closely approach the heat transfer line.

The overall dispersion of data shown in the Spalding j-factor plot is seen to be about ± 30 percent. Noting that the expected error in $\overline{h}_{e5}$ and in $\overline{h}_{c5}$ are each about 20 percent, and that to obtain the j factor, the difference between their inverses are involved, the dispersion in the

Spalding j-factor plot is seen to be well within that expected from the random errors in measurements of temperature and flow. In view of the analysis of cavity flow described in Chapter III, in which the Reynolds flux model appeared more appropriate for condensation in tube bundles, it has been concluded that the Spalding j-factor plot is both experimentally and mechanistically more sound than the Colburn j-factor plot.

CHAPTER VII

CONCLUSIONS AND RECOMMENDATIONS

In this chapter conclusions are developed from the comparisons of the test condenser heat transfer results with the correlating equations for the condensate film and the gas film heat transfer coefficients, and recommendations made for predicting heat transfer performance for condensers of this type based on the conclusions.

Condensate Film Heat Transfer Coefficient

Correlations obtained for the condensate film heat transfer coefficient in this work have been based on the single tube Nusselt equation. The validity of this basis was only indirectly checked because of an apparent bias in the experimental data, and because the correlations were examined based on the five tube mean heat transfer results only. Extrapolation of the condensate rain correlating plot to the single tube case and extrapolation of the steam velocity plots to high velocities both indicated apparent agreement with the single tube prediction equation of Nusselt within the scatter of the data. The effect of temperature on the five tube condensate film heat transfer coefficients in the range 160-230°F was also found to be consistent with the Nusselt single tube prediction.

Condensate Rain Effect

The effect of condensate rain was found, as expected from previous investigations, to be considerably less than predicted by Nusselt theory. A model which accounts for the reduced effect based on the probability of drainage occurring from tube bottoms to tube sides (side drainage) was derived, and a method of correlating the test results based on a single parameter derived from that model were presented. Comparison of this model with literature data indicated qualitative agreement. However, no quantitative correlation was possible.

It is concluded that observed deviation of the condensate rain effect from the Nusselt equation is due to the flow pattern of condensate through the tube bundle, such that the Nusselt theoretical equation applies only to the special case where drainage occurs from tube bottom to tube top. Although an equation for predicting the effect of spacing parameters was derived, it has not been tested in the present work by comparison with different tube bundles.

Steam Velocity Effect

The increase of the condensate film heat transfer coefficient with increasing horizontal steam cross flow in the present condenser was accompanied by the removal from the active tube bundle of part of the draining condensate. Since the removal of condensate from upper tubes reduces the average bundle condensate drainage, it was concluded that this process was also responsible for the increase in the measured condensate film heat transfer coefficient. There was no evidence that the increase was due to increased turbulent mixing of the condensate film by the flowing steam. Thus, the present test results lead to the conclusion that for horizontal flow of steam past horizontal condenser tubes at the velocities used, there will be no increase in the condensate film heat transfer coefficient for the usual tube bundles; that is, bundles whose width is greater than a few tubes.

Recommended Design Equations

As a result of the above, the following equations are recommended for predicting the condensate film heat transfer coefficient (h_{cn}) of the nth tube from the top in a horizontal tube bundle with a horizontal flow of steam:

$$h_{cn} - h_N \left\{ 0.6\ F_d + (1 - 0.58\ F_d)\ [n^{0.75} - (1 - n)^{0.75} \right\} \tag{90}$$

where

$$h_N = 0.725 \left\{ \frac{k_f^{\ 3}\ \rho_f^{\ 2}\ g\ \lambda}{\mu_f\ d_o\ \Delta T_c} \right\}^{1/4} \tag{13a}$$

and

$$F_d = \text{tube bundle spacing parameter.}$$

For a tube bundle with a triangular staggered layout with S/d_i of 1.33 and d_o of one inch, F_d will have a value of 0.8. For a single column of tubes or for bundles with a wide spacing between adjacent columns (S/d_o greater than two), F_d will have a value of zero (equivalent to the Nusselt equation).

Non-Condensable Gas Film Heat Transfer Coefficient

Two forms of the mass transfer j factor were used to correlate the experimental gas film heat transfer coefficients with the steam Reynolds number, and to compare the results with the sensible heat transfer j-factor curve for the same bundle geometry predicted from published correlating equations.

The Colburn mass transfer j factor resulted in the data scattering within a relatively wide band close to the predicted sensible heat transfer j factor line. The corresponding Spalding j factor data lay along a line a factor of two above the predicted heat transfer line, but the scatter was about one-half that of the Colburn j-factor plot. Based on examination of individual data sets, and consideration of the model for representing the process of condensation from a steam gas mixture in tube bundles (the cavity model), it was concluded that the Spalding j factor is preferable for both correlation and prediction purposes.

The difference between the Spalding j-factor line and the sensible heat j-factor line probably reflects the effect of the large mass transfer rate on the Reynolds flux entering the pseudo-cavities between tubes in the condenser bundle.

Recommended Design Equations

Based on the data obtained in the present experiment, values of the gas film heat transfer coefficient can be obtained from:

$$h_g = \lambda\, k_g\, \frac{p_{sb} - p_{sc}}{T_b - T_c} \tag{37}$$

where:

$$k_g = \frac{j_{ms}\, G}{p_{gc}} \left(\frac{M_s}{M_g}\right) Sc^{-2/3} \tag{91}$$

and the Spalding mass transfer j factor, j_{MS}, can be obtained as a function of Reynolds number from Figure 29 for the case of a triangular staggered tube bundle with S/d_o of 1.33 and d_o of one inch. For other tube bundle spacings and geometries and for high mass transfer rates in the absence of experimental verification, the following approximate relation between j_{MS} and j_H can be assumed:

$$j_{MS} = 2\ j_H \ . \tag{92}$$

where j_H is the Colburn heat transfer j factor, obtainable for many tube bundle geometries in Reference 33, and j_{MS} is the Spalding mass transfer j factor.

Recommendations for Additional Work

The objective of developing correlations for predicting individual tube heat transfer coefficients for the steam condensers used in distillation desalination plants has been achieved essentially only for the tube bundle geometry used in the present experiments. Thus a major future effort should be directed toward extending the predictions to different bundle geometries. Particular areas of interest are correlations between bundle dimensions and the bundle spacing parameter F_d, and the relation between the Spalding mass transfer j factor and the heat transfer j factor for different tube bundle spacings. The influence of different tubes, both smooth and enhanced on the gas film heat transfer coefficient should also be determined, as well as the effect of vertical versus horizontal tubes.

A second area of more fundamental interest which could provide insight into the relation between heat and mass transfer in tube bundles is the study of both sensible heat transfer and mass transfer in simple cavity flow.

LIST OF REFERENCES

LIST OF REFERENCES

1. Kern, D. Q., Process Heat Transfer, McGraw-Hill Book Co., Inc., New York (1950).

2. McAdams, W. H., Heat Transmission, McGraw-Hill Book Co., Inc., New York (1951).

3. Standards of Tubular Exchanger Manufacturers Association, New York (1959).

4. Kern, D. Q., "Heat Exchanger Design for Fouling Service," Paper 17 Proceedings of the Third International Heat Transfer Conference, AIChE, Chicago (1966).

5. Eissenberg, D. M. and H. M. Noritake, "Computer Model and Correlations for Prediction of Horizontal Tube Condenser Performance in Seawater Distillation Plants," USAEC Report ORNL-TM-2972, Oak Ridge National Laboratory (October 1970).

6. Nusselt, W. Z., "Die Oberflachenkondensation des Wasser dampfes," Zeit. d. ver. deut. Ing., 60: 541, 569 (1916).

7. Dukler, A. E., "Dynamics of Vertical Falling Film Systems," Chem. Eng. Progress, 55: 62 (1959).

8. Young, F. L. and W. J. Wohlenberg, "Condensation of Saturated Freon-12 Vapor on a Bank of Horizontal Tubes," Trans. ASME, 64: 787 (1942).

9. Short, B. E. and H. E. Brown, "Condensation of Vapors on Vertical Banks of Horizontal Tubes," General Discussion on Heat Transfer, Inst. Mech. Engr.-ASME, London (1951).

10. Borishanskii, V. M. and I. I. Paleev, Convective Heat Transfer in Two-Phase and One-Phase Flows, USAEC Report tr-6877 (1969).

11. Eissenberg, D. M., unpublished work.

12. Ferguson, R. M. and J. C. Oakden, "Heat Transfer Coefficients for Water and Steam in a Surface Condenser," Trans. Chem. Eng. Congress (World Power Conference), 3: 640 (1936).

13. Young, E. R., et. al., "The Condensing of Steam on Horizontal Corrugated and Bare Tubes," Report No. 60, Dept. of Chem. and Met. Engineering, Univ. of Michigan, Ann Arbor (1962).

14. Kern, D. Q., "Mathematical Development of Tube Loading in Horizontal Condensers," AIChE Journal, 4: 157 (1958).

15. Watson, R.G.H., J. J. Brunt and D.C.P. Birt, "Dropwise Condensation of Steam," Int. Heat Transfer Conference, Part II, ASME, New York (1961).

16. Young, E. R., personal communication.

17. Berman, L. D. and Yu. K. Tumanov, "Investigation of the Heat Transfer with Condensation of Flowing Steam on a Horizontal Tube," Teploenergetika, 9: 77 (1962).

18. Fuks, S. N., "Heat Transfer with Condensation of Steam Flowing Over a Horizontal Tube Bundle," Teploenergetika, 4: 35 (1957).

19. Rachko, V. A., "A Study of the Process of Condensation of Moving Pure Steam on Arrays of Tubes," Soviet Phys. Tech. Phys., 3: 1151 (1958).

20. Chilton, T. H. and A. P. Colburn, "Mass Transfer (Absorption) Coefficients," Ind. Eng. Chem., 26: 1184 (1934).

21. Nernst, W., "Theorie der Reaktionsgeschwindigkeit in Heterogenen Systemen," Z. Phy. Chem., 47: 52 (1904).

22. Lewis, W. K., "The Evaporation of a Liquid into a Gas," Mech. Eng., 44: 445 (1922).

23. Perry, J. H., et. al., Chemical Engineers Handbook, Fourth Edition, McGraw-Hill Book Company, Inc., New York (1963).

24. Sherwood, T. K. and R. L. Pigford, Absorption and Extraction, Second Edition, McGraw-Hill Book Company, Inc., New York (1952).

25. Dukler, A. E., et. al., "Experimental Program to Improve the VTE Distillation Process," U. S. Dept. of Interior OSW Res. and Dev. Report 487 (1969).

26. Reynolds, O., "On the Extent and Action of the Heating Surface of Steam Boilers," Proc. Lit. Phil. Soc., Manchester, 41 (1874).

27. Spalding, D. B., Convective Mass Transfer, McGraw-Hill Book Company, Inc., New York (1963).

28. Silver, R. S., "An Approach to a General Theory of Surface Condensers," Proc. Instn. Mech. Eng., 178 Pt. 1: 339 (1963).

29. Lawson, C. G., et. al., "Enhanced Heat-Transfer Tubes for Hozizontal Condensers with Possible Applications in Nuclear Power Plant Design," Trans. Amer. Nuclear Soc., 9: 565 (1966).

30. Eissenberg, D. M., unpublished work.

31. Gordin, R. and J. M. Asbeck, "Study of the Effects of Steam Temperature and Mass Velocity on the Condensation Coefficient in a Horizontal Condenser," USAEC Report No. ORNL-MIT-61, Oak Ridge National Laboratory (October 1968).

32. Ede, A. J., Introduction to Heat Transfer, Pergamon Press, London (1967).

33. Kays, W. M. and A. L. London, Compact Heat Exchangers, The National Press, Palo Alto (1955).

34. Eissenberg, D. M., "Multitube Condenser Data Tabulation," USAEC Report No. ORNL-TM-4037 (Oak Ridge National Laboratory), to be published.

APPENDIXES

APPENDIX A

COMPUTER PROGRAMS

```
LEVEL 20.1 (AUG 71)                                   OS/360  FORTRAN H

          COMPILER OPTIONS - NAME=  MAIN,OPT=02,LINECNT=50,SIZE=0000K,
                                    SOURCE,EBCDIC,NOLIST,NODECK,LOAD,MAP,NOEDIT,ID,XREF
                    C   CONVERSION OF BASIC PROGRAM FOR ANALYSIS OF MULTITUBE CONDENSER DATA
                    C** TO FORTRAN
                    C**  ESSB2  CALIBRATIONS FOR TEMP DROPPED FROM BLOCK DATA AND READ IN
                    C**  WITH EACH SERIES OF DATA
  ISN 0002                IMPLICIT REAL*8(A-H,O-Z)
  ISN 0003                INTEGER IND(5)/6,9,12,8,7/
  ISN 0004                COMMON/SUB/CONTMP,D,TEMP(16),T,FL,U,V,P,R,AA,Q,T1,Z,IFLG,IB,IWM
  ISN 0005                COMMON/CAL/XMV(9,16),B(13,50),A(13),FLOW(13),TY(9,16),TM(16),
                         1TTY(9),PRS(5),CON(5),SLP(5),ROTP,IF,IW,J,NTUB
  ISN 0006                COMMON/SQR1/WILA(50,5),WILO(50,5),SLOPE(5),YZERO(5),VARY(5),
                         1VARYB(5),VARS(5),VARYO(5),NOP(5)
  ISN 0007                COMMON/RLTE1/VENT,CONDRT,STMRT,VELENT,VELLVG,SPRT,UNCOND,CEDRT,
                         1SIDRT,SMSVEL,BLMTD,WIN,WOUT,UBND,VBND,UTUB(5),VTUB(5),SPRTIO,IRUN,
                         2MO,IDA,IYR,RMKS(10)
  ISN 0008                COMMON/WILM/AIN,AOUT,AXSEC,DI,DW,DO,RW,SPGRI,SPHTI,WTH,CNDW
  ISN 0009                COMMON/WILM1/REN(50,5) ,PRN(50,5) ,TIN(50,5) ,TCS(50,5) ,
                         1TTC(50,5),    UBR(50,5) ,FLW(50,5) ,CTI(5)     ,CN(5)
  ISN 0010                COMMON/COND1/ GASFL,TDEL,DLMT(5),UBAR(5) , HO5
  ISN 0011                COMMON/OUTP/ GCORR,SPVOL,VHEAD,SMDVEL,BALM,HI(5),HO(5)
  ISN 0012                DIMENSION CORR(16)
  ISN 0013                NAMELIST/CALIBS/XMV,TY,CORR
  ISN 0014              1 FORMAT(8F10.5)
  ISN 0015              2 FORMAT(16I5)
  ISN 0016              3 FORMAT(4I5,20X,10A4)
  ISN 0017              4 FORMAT(9F8.4)
  ISN 0018              5 FORMAT(1H1)
  ISN 0019                CALL ERRSET(217,0,-1,0)
                    C**  READ IN TEMP CALIBRATION VALUES FOR THE SERIES OF RUNS
  ISN 0020                READ(5,4) ((XMV(I,J),I=1,9),J=1,16)
  ISN 0021                READ(5,4) ((TY(I,J),I=1,9),J=1,16)
  ISN 0022                READ(5,1) (CORR(I),I=1,16)
  ISN 0023                WRITE(6,5)
  ISN 0024                WRITE(6,CALIBS)
                    C**
                    C**  READ DATE, RUNNO, REMARKS
  ISN 0025            100 READ(5,3,END=99) MO,IDA,IYR,IRUN,RMKS
                    C**  READ INDEX CARD
                    C**   IF IS FLOW CALIBRATION CODE
                    C**   IW = 1  FOR WILSON PLOT CALCULATION
                    C**   IM = 1  FOR REVISED WILSON PLOT CALCULATION
                    C**   IP = 1  FOR BENSON-LEHNER PLOT OF REGULAR WILSON PLOT
                    C**   IWMP = 1  FOR BENSON-LEHNER PLOT OF REVISED WILSON PLOT DATA
                    C*****
  ISN 0026                READ(5,2) ISW
  ISN 0027                IF(ISW.EQ.1) READ(5,2) IF,IW,IM,IP,IWMP
  ISN 0029                READ(5,1) ROTP,CNDW,D,WALL,TPLE
                    C**
                    C**  READ FLOWMETER READINGS
                    C**
  ISN 0030                READ(5,1) (A(I),I=1,13)
                    C**
                    C**  READ TEMPERATURES IN MV, AND CORRECTIONS
                    C**
  ISN 0031                READ(5,1) (TM(I), I = 1,16)
  ISN 0032                WTH = WALL / 12.
  ISN 0033                DI = D / 12.
```

CONTST

```
ISN 0034            OD = DI + 2. * WTH
ISN 0035            DW = (OD - DI) / DLOG(OD / DI)
ISN 0036            AIN   = 21.1404 * DI
ISN 0037            AOUT = 21.1404 * OD
ISN 0038            AXSFC = .7854 * DI * DI
ISN 0039            RW = WTH * OD / (CNDW * DW)
ISN 0040            DO 18 I = 1,5
ISN 0041            CN(I) = 0.0
ISN 0042            CTI(I) = 0.0
ISN 0043         18 NOP(I) = 0
ISN 0044            IFLG = 0
ISN 0045            IWM = 0
ISN 0046            CALL CALIB
ISN 0047            DO 12 I=1,16
ISN 0048         12 TEMP(I) = TEMP(I) + CORR(I)
              C**
              C    CALCULATE VENT RATE
              C**
ISN 0049            GASFL = FLOW(11) / 359.0
ISN 0050            CALL PSIA(TEMP(9),PP)
ISN 0051            CALL VAPH(TEMP(9),PP,ENT)
ISN 0052            ENTH = ENT - H(0.,TEMP(15))
ISN 0053            GCORR = 140.0
ISN 0054            IF(TEMP(13).LE.220.0) GCORR = 65.0
ISN 0056            IF(TEMP(13).LE.170.0) GCORR = 33.0
ISN 0058            VENT = 20.78 * HTCP(0.,TEMP(16)) / ENTH * (TEMP(15) - TEMP(16))
                   1 * FLOW(13) + GASFL * 28.
              C    1 * FLOW(13) + GASFL * 28. - GCORR / 26.75
              C**
              C    CALCULATE CONDENSING RATE
              C**
ISN 0059            CONDRT = (0.8585D-02 * SPGR(TEMP(7)))*(FLOW(10) * SPGR(TEMP(7)) *
                   1TEMP(7) + FLOW(6) * TEMP(2) + FLOW(9) * TEMP(3) + FLOW(12) *
                   2TEMP(4) + FLOW(8) * TEMP(5) + FLOW(7) * TEMP(6) - TEMP(1) *
                   3(FLOW(6) + FLOW(7) + FLOW(8) + FLOW(9) + FLOW(10) * SPGR(TEMP(7))
                   4 + FLOW(12)))
              C  MEAN STEAM RATE
ISN 0060            STMRT = VENT + CONDRT / 2.
              C*** MEAN MASS VELOCITY ENTERING
ISN 0061            SMSVEL = STMRT * 26.75
              C****  INUNDATION SPRAY RATE
ISN 0062            SPRT = SPGR(TEMP(10)) * FLOW(5) * 8.33
              C**** NONCONDENSABLE MOL FRACTION
ISN 0063            UNCOND = GASFL / (GASFL + VENT/18. + CONDRT/36.)
              C**** CENTER DRAIN RATE
ISN 0064            CEDRT = SPGR(TEMP(13)) * FLOW(3) * 8.33
              C    INUNDATION RATIO
ISN 0065            SPRTIO = CEDRT / CONDRT
              C**** SIDE DRAIN RATE
ISN 0066            SIDRT = SPGR(TEMP(13)) * FLOW(4) * 8.33
              C**** CONDENSING STEAM TEMPERATURE
ISN 0067            CONTMP = TEMP(13)
              C**
ISN 0068            TDEL = DABS(TEMP(8) - TEMP(9))
              C  PRINT OUT OF FLOWS AND TEMPERATURES
ISN 0069            WRITE(6,200)IRUN
ISN 0070            WRITE(6,201)A(1),FLOW(1),A(2),FLOW(2),A(3),FLOW(3),A(4),FLOW(4),
                   1A(5),FLOW(5),A(6),FLOW(6),A(7),FLOW(7),A(8),FLOW(8),A(9),FLOW(9),
```

```
                          2A(10),FLOW(10),A(11),FLOW(11),A(12),FLOW(12),A(13),FLOW(13)
ISN 0071                   WRITE(6,202)TM(1),TEMP(1),TM(2),TEMP(2),TM(3),TEMP(3),TM(4),
                          1TEMP(4),TM(5),TEMP(5),TM(6),TEMP(6),TM(7),TEMP(7),TM(8),
                          2TEMP(8),TM(9),TEMP(9),TM(10),TEMP(10),TM(11),TEMP(11),
                          3TM(12),TEMP(12),TM(13),TEMP(13),TM(14),TEMP(14),
                          4TM(15),TEMP(15),TM(16),TEMP(16),TPLE,TCEL
                C**** BUNDLE LOG MEAN DELTA T
ISN 0072                   BLMTD = (TEMP(7) - TEMP(1)) / DLOG((CONTMP - TEMP(1)) /
                          1(CONTMP - TEMP(7)))
                C**** WIN IS LBS PER MIN IN, WOUT IS LBS PER MIN OUT
ISN 0073                   WOUT = 8.33 * SPGR(TEMP(8)) * FLOW(1) + VENT + CEDRT + SIDRT
                          1 - GASFL * 28.
ISN 0074                   WIN = 8.33 * (SPGR(TEMP(11))* FLOW(2) + SPGR(TEMP(14))* FLOW(5))
                C***  FIND FACTORS FOR BUNDLE
ISN 0075                   T1 = TEMP(1)
ISN 0076                   Z  = CONTMP
                C***  T1 IS COND INLET AND T IS COND OUTLET
ISN 0077                   T = TEMP(7)
ISN 0078                   FL = FLOW(10)
ISN 0079                   IB = 0
ISN 0080                   CALL UCAL
ISN 0081                   UBND = U
ISN 0082                   VBND = V
                C***  FIND FACTORS FOR EACH TUBE
ISN 0083                   IB = 1
ISN 0084                   DO  10 I = 1,5
ISN 0085                   J = IND(I)
ISN 0086                   T = TEMP(I+1)
ISN 0087                   FL = FLOW(J)
ISN 0088                   CALL UCAL
ISN 0089                   UTUB(I) = U
ISN 0090                   VTUB(I) = V
ISN 0091                   IF(CNDW.EQ.0.0) GO TO 10
                C**  FLOODING FACTOR CALL
ISN 0093                   CALL FLFACT(I)
ISN 0094                10 CONTINUE
                C**  CALL NON-CONDENSABLE SUBROUTINE (WILL AUTOMATICALLY BYPASS THIS
                C**  CALCULATION IF THERE IS NO GAS FED TO SYSTEM
ISN 0095                   IF(FLOW(11).GT.0.) CALL NCOND(IND)
ISN 0097                   IF(IW.EQ.0) GO TO 30
ISN 0099                   IFLG = 1
                C***  READ DATA FOR WILSON PLOT
ISN 0100                20 READ(5,2) NOTUB,NPTS,M
ISN 0101                   NOP(NOTUB) = NPTS
ISN 0102                   II = NOTUB + 1
ISN 0103                   J = IND(NOTUB)
ISN 0104                   DO 15 I = 1,NPTS
                C*** READ IN STEAM IN,STEAM OUT,TEMP IN,TEMP OUT,FLOW
ISN 0105                   READ(5,1) TM(8),TM(9),TM(1),TM(II),A(J)
ISN 0106                   CALL CALIB
ISN 0107                   Z = (TEMP(8) + TEMP(9)) / 2.
ISN 0108                   T1 = TEMP(1)
ISN 0109                   T  = TEMP(II)
ISN 0110                   FL = FLOW(J)
ISN 0111                   CALL UCAL
ISN 0112                   WILA(I,NOTUB) = AA
ISN 0113                   WILD(I,NOTUB) = 0
ISN 0114                   REN(I,NOTUB) = R
```

```
ISN 0115          PRN(I,NOTUB) = P
ISN 0116          TCS(I,NOTUB) = Z
ISN 0117          TIN(I,NOTUB) = T1
ISN 0118          TTO(I,NOTUB) = T
ISN 0119          FLW(I,NOTUB) = FL
ISN 0120          UBR(I,NOTUB) = U
ISN 0121       15 CONTINUE
            C**   CALL SQR FOR REGRESSION OF WILSON PLOT DATA
ISN 0122          CALL SQR(NOTUB,NPTS)
ISN 0123          IF(IP.EQ.0) GO TO 40
            C***   PLOTT PREPARES B-L DATA
ISN 0125          CALL PLOTT (NOTUB,NPTS,IRUN)
ISN 0126       40 IF(M.EQ.1) GO TO 20
            C  30 CALL RITE(IW)
ISN 0128       30 CONTINUE
ISN 0129          CALL OUTPUT
ISN 0130          IF(IM.EQ.0.OR.IW.EQ.0) GO TO 100
ISN 0132          IWM = 1
ISN 0133          DO 50 L = 1,5
ISN 0134          IF(NOP(L).EQ.0) GO TO 50
ISN 0136          NPTS = NOP(L)
            C**   WILMOD CALCULATES REVISED WILSON PLOT DATA
ISN 0137          CALL WILMOD(NPTS,L)
ISN 0138          IF(IWMP.EQ.1) CALL PLOTT(L,NPTS,IRUN)
ISN 0140       50 CONTINUE
ISN 0141        9 FORMAT(1H-,T12,2HCN,T30,2HCI)
ISN 0142       11 FORMAT(1H0,T9,F7.5 ,T27,F7.5 )
ISN 0143        7 FORMAT(1H1,T15,25HMODIFIED WILSON PLOT DATA)
ISN 0144        8 FORMAT(1H0)
            C     WRITE(6,7)
            C     WRITE(6,8)
            C     CALL RITE(IW)
            C     WRITE(6,9)
            C     WRITE(6,11)(CN(I),CTI(I),I=1,5)
ISN 0145          GO TO 100
ISN 0146      200 FORMAT(1H1,T15,30HTEMPERATURES AND FLOWS      RUN,I4)
ISN 0147      201 FORMAT(1H0,T13,4HRDGS/
                 11H0,7HFLOW  1,F9.2,F10.2,T30,15HGPM  ENTR SEPAR/
                 21H ,7HFLOW  2,F9.2,F10.2,T30,3HGPM/
                 31H ,7HFLOW  3,F9.2,F10.2,T30,18HGPM  CENTER TROUGH/
                 41H ,7HFLOW  4,F9.2,F10.2,T30,16HGPM  SIDE TROUGH/
                 51H ,7HFLOW  5,F9.2,F10.2,T30,16HGPM  SPRAY WATER/
                 61H ,7HFLOW  6,F9.2,F10.2,T30,11HGPM  TUBE 1/
                 71H ,7HFLOW  7,F9.2,F10.2,T30,11HGPM  TUBE 5/
                 81H ,7HFLOW  8,F9.2,F10.2,T30,11HGPM  TUBE 4/
                 91H ,7HFLOW  9,F9.2,F10.2,T30,11HGPM  TUBE 2/
                 11H ,7HFLOW 10,F9.2,F10.2,T30,11HGPM  BUNDLE/
                 21H ,7HFLOW 11,F9.2,F10.2,T30,13HCFM  NITROGEN/
                 31H ,7HFLOW 12,F9.2,F10.2,T30,11HGPM  TUBE 3/
                 41H ,7HFLOW 13,F9.2,F10.2,T30,16HGPM  WASTE WATER)
ISN 0148      202 FORMAT(1H0,T13,2HMV,T22,5HDEG F/
                 11H0,7HTEMP  1,F9.4,F10.2,T33,12HCONDENSER IN/
                 21H ,7HTEMP  2,F9.4,F10.2,T33,6HTUBE 1/
                 31H ,7HTEMP  3,F9.4,F10.2,T33,6HTUBE 2/
                 41H ,7HTEMP  4,F9.4,F10.2,T33,6HTUBE 3/
                 51H ,7HTEMP  5,F9.4,F10.2,T33,6HTUBE 4/
                 61H ,7HTEMP  6,F9.4,F10.2,T33,6HTUBE 5/
                 71H ,7HTEMP  7,F9.4,F10.2,T33,10HBUNDLE OUT/
```

```
                     81H ,7HTEMP  8,F9.4,F10.2,T33,13HCOND STEAM IN/
                     91H ,7HTEMP  9,F9.4,F10.2,T33,14HCOND STEAM OUT/
                     11H ,7HTEMP 10,F9.2,F10.2,T33,10HSPRAY ROTA/
                     21H ,7HTEMP 11,F9.2,F10.2,T33,12HWATER TO HEX/
                     21H ,7HTEMP 12,F9.2,F10.2,T33,11HBOILER EXIT/
                     31H ,7HTEMP 13,F9.4,F10.2,T33,13HTEST COND INT/
                     41H ,7HTEMP 14,F9.2,F10.2,T33,14HSPRAY WATER IN/
                     51H ,7HTEMP 15,F9.2,F10.2,T33,14HWASTE COND OUT/
                     61H ,7HTEMP 16,F9.2,F10.2,T33,13HWASTE COND IN/
                     71H ,7HTH-PILE,F9.4,F10.4,T33,12HBNDL DELTA-T)
ISN 0149          99 RETURN
ISN 0150             END
```

CONTST

JFACT

```
5 PRINT"NØ.","STEAM TEMP","SPALDING JF","CØLBURN JF","REYNØLDS NØ."
10 READ C,N2
11 REM WHERE N1 IS THE NUMBER ØF DATA SETS AND
12 REM WHERE C IS THE NØ-GAS  FIVE TUBE AVERAGE CN
13 REM DEFINE THE LATENT HEAT AS A FUNCTIØN ØF TEMPERATERE
15 DEF FNH(T)=970*((212-T)*.00064+1)
16 PRINT
17 PRINT
18 PRINT"                    CN5 WITHØUT GAS IS"C
25 PRINT
26 FØR N1=1 TØ N2
30 READ N,T,D,G,F,C1,H,U
32 REM WHERE   N=RUN NUMBER
33 REM         T=STEAM TEMP
34 REM         D=LØG MEAN ØVERALL TEMP DIFF
35 REM         G=STEAM MASS VELØCITY
36 REM         F=VØLUME FRACTIØN NITRØGEN
37 REM         C1=FIVE TUBE AVERAGE CN WITH GAS
38 REM         H=FIVE TUBE AVERAGE CØNDENSING CØEFFICIENT
39 REM         U=FIVE TUBE AVERAGE ØVERALL CØEFFICIENT
40 LET A1=3.346313
50 LET A2=4.14113E-2
60 LET A3=7.515484E-9
70 LET A4=1.3794481E-2
80 LET A5=6.56444E-11
90 LET A6=3206.1604
100 LET A7=2.3025851
110 LET T1=(T+459)/1.8
115 LET A8=647.27-T1
120 LET P=EXP((A7*A8/T1)*((A1+A8*(A2+A8↑2*(A3+A8*A5)))/(1+A4*A8)))
130 LET P1=A6/P
140 LET P2=P1*F/(1-F)
145 LET H1=H/(1-C1/C)
150 LET D2=(U*D)/H1
160 LET T2=(T-D2+459)/1.8
165 LET A8=(647.27-T2)
168 LET P3=EXP((A7*A8/T2)*((A1+A8*(A2+A8↑2*(A3+A8*A5)))/(1+A4*A8)))
170 LET P3=A6/P3
180 LET P4=P1+P2-P3
190 LET P5=(P4-P2)/LØG(P4/P2)
191 REM F1=VØL FRACT N2 AT CØNDX SURFACE
192 REM F2=AVE FRACT N2 IN FILM
193 REM M1= MEAN MØL WT AT CØNDX SURFACE
194 REM M2=MEAN MØL WT IN FILM
196 LET F1=P4/(P1+P2)
197 LET F2=(F+F1)/2
198 LET M1=29*F1+18*(1-F1)
199 LET M2=29*F2+18*(1-F2)
210 LET K=H1*D2/((P4-P2)*FNH(T))
220 LET J1=K*P4*.72*M1/(G*18)
```

JFACT CØNTINUED

```
225 LET J2=K*P5*.72*M2/(G*18)
230 LET J2=J1*P5/P4
232 IF T>180 THEN 235
233 LET R=3.189*G
234 GØ TØ 250
235 IF T>200 THEN 240
236 LET R=2.995*G
237 GØ TØ 250
240 LET R=2.778*G
250 PRINT N,T,J1,J2,R
251 PRINTH1
260 NEXT N1
262 GØ TØ 10
```

JFACT

APPENDIX B

TABULATION OF RUN PARAMETERS AND EXPERIMENTAL RESULTS

The results of processing the experimental data using the computer program, CONTST, consist of a set of output sheets similar to that shown in Figure 19. A complete set is available as Reference 34 and can be obtained from the Information Division, Oak Ridge National Laboratory, P. O. Box X, Oak Ridge, Tennessee 37830. A partial tabulation of the run parameters and experimental results obtained from Reference 34 is included in Table B-I.

The results of further processing of the data for runs with nitrogen additions to the steam using the computer program, JFACT, have been included in Table B-II.

TABLE B-I

SUMMARY OF RUN PARAMETERS AND EXPERIMENTAL RESULTS

Run No.	T_b °F	G lb/hr-ft^2	F_m	I.R.	Mass Balance Ratio	ΔT_{lm} °F	$\overline{U}_s$ Btu/hr-ft^2-°F	$\overline{h}_{c5}$ Btu/hr-ft^2-°F	CN5
39	231	780	0	0.93	1.00	9.6	1321	2959	1.359
40	232	745	0	2.47	1.02	11.5	1139	2186	1.094
41	232	451	0	2.35	1.03	11.5	1112	2100	1.056
42	232	1160	0	2.90	1.01	7.9	1142	2192	0.996
43	232	2028	0	1.51	0.85	6.8	1324	2982	1.256
44	231	1970	0	1.35	1.22	12.8	1144	2209	1.134
45	231	247	0	3.01	1.07	8.8	1147	2217	1.035
49	232	498	0	0.95	1.01	22.1	1065	1967	1.174
50	232	505	0	0.93	1.04	19.6	1144	2246	1.281
51	227	204	0	0.97	0.92	4.7	1424	3524	1.326
55	229	259	0	0.84	1.08	6.8	1343	3100	1.301
56	229	773	0	0.83	1.09	7.4	1311	2899	1.253
57	229	1154	0	-	-	7.6	1332	3041	1.316
59	228	1607	0	0.65	1.17	7.7	1332	3025	1.314
60	229	879	0	2.41	1.02	7.1	1194	2379	1.048
61	229	300	0	2.19	0.61	7.4	1206	2444	1.081
63	230	346	0	1.98	1.04	8.7	1152	2244	1.045
64	230	350	0	1.86	1.04	8.9	1163	2309	1.075
65	229	336	0	1.52	1.06	8.6	1113	2105	0.984
66	229	338	0	0.84	1.07	8.0	1312	2940	1.293
67	229	321	0	0.87	1.04	8.4	1220	2498	1.138
68	229	307	0	1.92	0.99	7.7	1114	2084	0.952
69	229	314	0	1.78	0.96	8.2	1115	2088	0.970
70	229	315	0	2.07	1.00	8.5	1139	2183	1.014
71	230	324	0	0.97	0.96	8.4	1269	2705	1.221
86	229	504	0	0.90	1.02	7.8	1298	2830	1.246
87	229	281	0	0.90	1.02	7.5	1286	2786	1.218

TABLE B-I (continued)

Run No.	T_b °F	G lb/hr-ft^2	F_m	I.R.	Mass Balance Ratio	ΔT_{lm} °F	$\overline{U}_s$ Btu/hr-ft^2-°F	$\overline{h}_{c5}$ Btu/hr-ft^2-°F	CN5
88	228	237	0.001	1.40	0.64	7.2	727	1047	0.503
89	229	253	0.002	0.83	1.08	7.5	1126	2118	0.959
90	229	249	0.003	0.87	1.03	7.7	1048	1869	0.863
91	229	242	0.008	0.88	1.00	7.8	926	1514	0.717
92	229	281	0	0.90	1.02	7.3	1278	2768	1.203
93	229	782	0	0.85	1.08	7.5	1301	2864	1.246
94	229	759	0	0.83	1.09	7.8	1273	2733	1.209
95	229	764	0.001	0.83	1.10	7.5	1385	3322	1.413
96	229	759	0.001	0.88	1.04	7.5	1325	2969	1.288
97	229	755	0.003	0.85	1.07	7.8	1197	2410	1.082
98	229	761	0	0.89	1.04	8.0	1280	2754	1.225
99	229	793	0	0.83	1.10	8.1	1311	2903	1.285
100	229	231	0	0.84	1.08	7.6	1311	2902	1.263
101	229	224	0.001	0.99	0.93	7.3	1254	2636	1.154
102	229	220	0.004	0.87	1.04	7.6	1207	2443	1.091
103	229	218	0.007	0.86	1.05	7.6	1167	2291	1.028
104	229	212	0.011	0.85	1.05	7.3	1128	2149	0.963
105	220	212	0.015	0.81	1.10	7.6	1115	2088	0.950
106	229	219	0	0.91	1.00	6.9	1302	2860	1.220
107	229	223	0	0.83	1.09	7.5	1333	2989	1.296
108	229	204	0	2.68	0.90	7.0	1202	2415	1.056
109	229	211	0.05	2.19	1.03	7.8	1045	1801	0.863
110	228	202	0.052	0.85	1.04	6.3	1150	2204	0.951
111	229	209	0	0.83	1.09	6.9	1362	3146	1.322
112	229	918	0	0.82	1.11	7.7	1325	2965	1.295
113	229	904	0	2.19	1.00	7.3	1228	2504	1.102
114	229	901	0.002	2.33	0.97	7.6	1143	2173	0.985
115	229	919	0.002	0.83	1.10	7.6	1345	3048	1.321
116	229	914	0	0.81	1.11	7.5	1368	3160	1.357

TABLE B-I (continued)

Run No.	T_b °F	G lb/hr-ft^2	F_m	I.R.	Mass Balance Ratio	ΔT_{lm} °F	$\bar{U}_s$ Btu/hr-ft^2-°F	$\bar{h}_{c5}$ Btu/hr-ft^2-°F	CN5
117	229	844	0	0.80	1.13	7.3	1313	2912	1.257
118	229	851	0	1.81	1.00	7.3	1182	2338	1.039
119	229	856	0	1.73	1.09	7.4	1224	2525	1.114
120	229	847	0	2.71	1.01	7.3	1184	2337	1.037
121	229	834	0	4.86	1.04	7.7	1109	2058	0.942
122	229	828	0	5.25	1.03	7.3	1157	2230	0.996
123	229	861	0	0.82	1.10	7.5	1281	2743	1.203
124	229	346	0	0.87	1.06	8.0	1286	2761	1.228
125	229	317	0.011	0.85	1.05	6.9	1206	2414	1.054
126	228	308	0.016	0.89	1.00	6.3	1184	2329	0.999
127	228	299	0.024	0.84	1.04	6.5	1091	1993	0.877
128	229	335	0	0.83	1.09	7.6	1264	2658	1.172
130	229	355	0	0.73	1.23	7.0	1406	3251	1.374
131	229	333	0.010	0.98	0.93	7.3	1230	2457	1.086
132	229	335	0.015	0.90	1.00	7.5	1153	2173	0.985
133	228	315	0.034	0.86	1.02	7.1	1011	1725	0.790
134	228	319	0.043	0.77	1.13	7.9	949	1554	0.739
135	230	337	0	0.81	1.11	7.3	1358	3000	1.292
137	229	150	0.017	1.33	0.68	7.6	1034	1845	0.848
138	229	151	0.022	0.80	1.09	7.9	1002	1749	0.818
139	229	142	0.033	0.77	1.10	7.5	939	1563	0.730
140	228	129	0.051	0.85	1.01	6.5	857	1351	0.617
141	229	169	0	0.82	1.09	7.3	1318	3001	1.284
143	227	200	0.013	0.97	0.94	7.5	1088	2036	0.925
144	227	192	0.021	0.88	1.01	7.7	1035	1854	0.858
145	227	177	0.037	1.07	0.84	7.1	916	1507	0.697
146	226	157	0.082	-	-	6.0	754	1112	0.508
147	227	200	0	0.92	0.984	6.4	1330	3072	1.272
148	229	170	0	0.82	1.10	7.7	1234	2599	1.151

TABLE B-I (continued)

Run No.	T_b °F	G lb/hr-ft^2	F_m	I.R.	Mass Balance Ratio	ΔT_{lm} °F	$\bar{U}_s$ Btu/hr-ft^2-°F	$\bar{h}_{c5}$ Btu/hr-ft^2-°F	CN5
149	229	163	0.001	0.85	1.06	7.8	1125	2157	0.982
150	229	169	0.002	0.80	1.13	8.1	1160	2291	1.045
151	229	168	0.003	0.81	1.11	7.9	1175	2352	1.063
152	229	166	0.003	0.79	1.14	7.6	1199	2442	1.085
153	229	164	0	0.88	1.04	7.2	1258	2699	1.170
154	229	672	0	0.84	1.08	7.1	1274	2771	1.191
155	229	656	0.007	0.80	1.11	7.3	1158	2282	1.012
156	229	652	0.010	0.86	1.04	6.8	1262	2719	1.161
157	229	669	0.021	0.84	1.06	6.9	1200	2448	1.063
158	229	664	0	0.92	0.98	7.0	1226	2562	1.109
166	229	681	0	0.88	1.03	7.2	1220	2530	1.107
167	229	686	0.005	0.88	1.03	7.0	1238	2608	1.129
168	229	651	0.023	0.75	1.176	7.0	1211	2496	1.085
171	229	354	0	0.85	1.04	5.1	1386	3380	1.299
172	229	335	0	0.74	1.21	7.3	1319	3505	1.286
173	229	317	0	0.78	1.15	6.6	1329	3048	1.272
174	229	318	0	0.77	1.17	6.6	1338	3096	1.288
175	229	318	0	0.77	1.17	6.7	1315	2976	1.250
178	230	353	0	0.71	1.27	8.3	1232	2590	1.167
179	230	357	0	0.69	1.31	8.3	1280	2801	1.251
180	230	386	0	0.85	1.11	11.2	1245	2662	1.291
242	160	170	0	0.88	1.04	8.7	1071	2361	1.201
243	160	177	0	–	–	9.2	1049	2258	1.170
244	160	171	0	0.84	1.08	8.9	1050	2265	1.167
245	159	168	0	0.84	1.08	9.0	1072	2384	1.222
246	159	157	0.003	0.95	0.96	9.0	972	1942	1.024
247	159	160	0.006	0.92	0.99	9.4	929	1777	0.958
248	159	157	0.010	0.96	0.95	9.7	898	1672	0.916
249	159	162	0.014	0.90	1.01	10.2	872	1584	0.885

TABLE B-I (continued)

Run No.	T_b °F	G lb/hr-ft^2	F_m	I.R.	Mass Balance Ratio	ΔT_{lm} °F	$\overline{U}_s$ Btu/hr-ft^2-°F	$\overline{h}_{c5}$ Btu/hr-ft^2-°F	CN5
250	159	174	0	0.82	1.11	8.7	1121	2637	1.324
251	160	118	0	0.84	1.08	9.4	1020	2129	1.118
252	160	101	0.002	1.00	0.90	9.6	883	1611	0.881
253	160	109	0.004	0.91	1.00	9.9	888	1630	0.899
254	160	116	0.008	0.85	1.07	10.5	856	1526	0.859
255	159	98	0.018	1.01	0.89	9.6	793	1335	0.746
256	160	94	0.023	0.97	0.93	9.9	747	1214	0.691
257	160	122	0	0.82	1.11	9.3	1054	2287	1.188
258	160	256	0	0.85	1.07	8.9	1096	2485	1.26[illegible]
259	160	256	0.002	0.84	1.08	8.7	1135	2692	1.343
260	160	256	0.003	0.84	1.08	9.0	1072	2366	1.213
261	160	245	0.006	0.87	1.04	9.2	1021	2132	1.115
262	160	250	0.009	0.95	0.97	8.9	1075	2384	1.217
263	160	244	0	0.87	1.05	9.0	1110	2554	1.293
264	160	169	0	0.86	1.06	8.9	1120	2612	1.318
265	160	171	0	0.84	1.08	9.1	1107	2549	1.296
266	159	170	0	0.85	1.08	8.6	1176	2947	1.448
267	160	183	0	0.82	1.11	8.7	1149	2779	1.380
268	159	181	0	0.85	1.07	8.5	1189	3027	1.476
269	161	166	0	0.90	1.01	8.7	1091	2456	1.240
270	160	165	0	0.91	1.00	8.5	1129	2657	1.320
272	161	168	0	0.93	0.98	8.4	1132	2664	1.318
273	161	167	0	0.91	1.00	8.8	1066	2326	1.185
274	161	221	0	0.92	1.00	8.5	1128	2639	1.309
275	161	219	0	0.89	1.02	8.2	1120	2596	1.283
276	161	178	0	0.89	1.02	8.2	1129	2649	1.304
277	161	175	0	0.90	1.00	8.2	1118	2590	1.280
278	160	195	0	0.89	1.04	9.4	1093	2471	1.272
279	160	255	0.010	1.0	0.92	9.0	1024	2148	1.118

TABLE B-I (continued)

Run No.	T_b °F	G lb/hr-ft^2	F_m	I.R.	Mass Balance Ratio	ΔT_{lm} °F	$\bar{U}_s$ Btu/hr-ft^2-°F	$\bar{h}_{c5}$ Btu/hr-ft^2-°F	CN5
280	159	249	0.017	1.05	0.87	8.9	992	2015	1.054
282	160	256	0	0.97	0.95	8.7	1132	2677	1.337
283	159	248	0.010	1.07	0.86	8.1	1096	2486	1.236
284	160	297	0	1.04	0.91	13.9	1033	2218	1.279
285	159	287	0.009	1.04	0.91	12.9	1025	2187	1.243
286	160	312	0	0.95	0	13.7	1086	2485	1.408
287	161	267	0	0.90	1.02	9.3	1100	2501	1.280
288	161	383	0	0.88	1.05	9.5	1083	2416	1.248
289	160	604	0	0.78	1.15	8.8	1169	2892	1.433
290	161	676	0	0.75	1.11	9.4	1121	2613	1.334
292	162	726	0	-	-	7.9	1142	2706	1.315
294	160	827	0	0.667	1.09	9.0	1195	3055	1.508
295	160	788	0.009	0.728	1.01	9.2	1117	2595	1.320
296	160	797	0.012	0.687	1.09	9.3	1120	2615	1.331
297	160	843	0.015	0.698	1.07	9.3	1103	2522	1.291
298	161	825	0	0.70	1.06	9.3	1107	2542	1.300
299	160	1035	0	0.547	1.04	8.6	1203	3110	1.515
300	189	238	0	0.85	1.08	8.6	1195	2709	1.284
303	191	258	0	0.70	1.13	8.5	1220	2825	1.327
304	189	519	0	1.00	0.92	8.4	1195	2713	1.278
305	190	800	0	0.80	0.97	8.1	1259	3053	1.401
306	189	814	0	0.78	1.10	8.0	1284	3201	1.453
307	189	1029	0	0.72	1.07	7.9	1269	3111	1.416
308	190	1392	0	0.55	0.87	7.9	1294	3251	1.468
309	190	1394	0	0.54	0.89	7.7	1296	3258	1.464
311	190	1657	0	0.47	0.76	7.8	1311	3358	1.506
312	190	2014	0	0.36	0.69	7.7	1317	3396	1.515
313	190	2010	0	0.37	0.70	7.7	1304	3315	1.484
314	190	1274	0	0.60	1.14	8.1	1228	2860	1.325
315	160	1837	0	0.77	1.09	9.4	1090	2456	1.265

TABLE B-I (continued)

Run No.	T_b °F	G lb/hr-ft^2	F_m	I.R.	Mass Balance Ratio	ΔT_{lm} °F	$\overline{U}_s$ Btu/hr-ft^2-°F	$\overline{h}_{c5}$ Btu/hr-ft^2-°F	CN5
316	160	1780	0	0.82	1.03	8.9	974	2277	1.148
317	160	1032	0	0.54	1.02	8.8	1220	3216	1.565
318	160	1048	0	0.53	0.97	8.7	1211	3162	1.540
319	160	1383	0	0.48	0.83	8.4	1220	3219	1.552
321	160	541	0	0.82	1.11	9.2	1137	2709	1.367
322	160	542	0	0.81	1.12	9.1	1174	2927	1.460
323	160	451	0	0.79	1.16	9.0	1244	3400	1.651
324	160	436	0	0.83	1.10	9.1	1168	2886	1.441
325	160	170	0	0.85	1.07	9.5	1103	2521	1.296
326	161	167	0	0.89	1.04	9.5	1099	2492	1.286
327	190	210	0	0.84	1.09	8.0	1285	3201	1.455
328	190	198	0	0.87	1.05	8.3	1208	2761	1.293
329	190	216	0	0.87	1.05	8.2	1241	2939	1.361
330	229	325	0	0.85	1.08	8.6	1335	3093	1.375
331	230	328	0	0.95	0.99	8.5	1333	3075	1.362
333	189	428	0	0.83	1.13	18.1	1125	2438	1.415
334	189	427	0	0.83	1.12	17.6	1138	2499	1.436
335	190	472	0	0.85	1.10	18.4	1110	2365	1.384
336	190	453	0.005	0.92	1.02	18.8	1015	1974	1.189
337	190	459	0.008	0.90	1.04	19.7	972	1822	1.121
338	190	448	0.014	0.89	1.04	20.2	928	1678	1.055
339	189	459	0.024	0.87	1.07	20.8	903	1599	1.015
340	190	490	0	0.82	1.14	18.9	1118	2406	1.413
341	189	438	0	0.87	1.07	10.2	1216	2832	1.394
342	189	437	0.005	0.90	1.04	10.1	1190	2697	1.335
343	189	423	0.009	0.94	0.99	10.4	1122	2377	1.204
344	189	425	0.015	0.96	0.97	10.7	1069	2154	1.115
345	188	390	0.038	1.20	0.79	10.8	934	1670	0.894
346	189	421	0	0.86	1.09	10.1	1238	2955	1.443

TABLE B-I (continued)

Run No.	T_b °F	G lb/hr-ft^2	F_m	I.R.	Mass Balance Ratio	ΔT_{lm} °F	$\overline{U}_s$ Btu/hr-ft^2-°F	$\overline{h}_{c5}$ Btu/hr-ft^2-°F	CN5
347	190	180	0	0.86	1.08	9.6	1270	3126	1.491
348	190	152	0.012	1.15	0.81	10.1	954	1726	0.903
349	190	155	0.018	0.95	0.97	11.1	917	1613	0.871
350	189	141	0.030	1.00	0.92	11.7	813	1319	0.738
351	188	137	0.045	1.07	0.86	12.1	731	1119	0.642
352	190	177	0	0.89	1.05	9.9	1231	2904	1.412
353	190	177	0	0.90	1.03	9.3	1219	2828	1.360
354	190	156	0.002	0.94	0.99	9.3	1120	2353	1.159
355	190	161	0.003	0.91	1.02	9.5	1122	2361	1.170
356	189	156	0.007	0.93	1.00	9.7	1075	2166	1.091
357	189	159	0.013	0.95	0.97	9.8	1030	1994	1.018
359	191	173	0	0.89	1.07	17.6	1936	1688	1.018
360	190	120	0.002	1.26	0.75	17.8	706	1067	0.677
361	189	149	0.004	0.92	1.03	19.0	774	1234	0.786
362	188	143	0.007	0.92	1.03	19.2	729	1124	0.726
363	188	116	0.018	1.09	0.86	20.3	601	848	0.570
364	191	181	0	0.95	1.00	18.9	916	1629	1.004
365	190	614	0	0.83	1.10	9.0	1138	2430	1.183
366	190	614	0.004	0.86	1.06	9.1	1080	2180	1.080
367	190	600	0.006	0.83	1.10	9.2	1065	2120	1.058
368	190	598	0.011	0.87	1.05	9.2	1028	1981	0.995
369	190	600	0.025	0.94	0.97	9.2	942	1686	0.865
370	190	635	0	0.80	1.14	9.6	1087	2208	1.104
371	190	699	0	1.1	0.87	16.5	969	1798	1.060
372	191	675	0.003	0.81	1.16	17.4	873	1494	0.910
373	190	681	0.005	9.81	1.16	17.5	887	1536	0.935
374	190	679	0.009	0.85	1.11	17.4	864	1469	0.898
375	190	680	0.022	0.89	1.05	17.0	817	1340	0.823
376	191	140	0	0.83	1.11	15.2	791	1267	0.759

TABLE B-I (continued)

Run No.	T_b °F	G lb/hr-ft^2	F_m	I.R.	Mass Balance Ratio	ΔT_{lm} °F	$\overline{U}_s$ Btu/hr-ft^2-°F	$\overline{h}_{c5}$ Btu/hr-ft^2-°F	CN5
377	190	122	0.002	0.96	0.96	15.5	673	989	0.609
378	190	122	0.004	0.90	1.02	15.8	670	983	0.609
379	190	114	0.009	0.93	0.99	16.4	592	825	0.523
380	189	119	0.018	0.83	1.09	16.6	582	805	0.514
381	191	144	0	0.79	1.17	15.6	807	1307	0.785
382	189	236	0	0.81	1.13	8.5	1244	2973	1.389
383	189	227	0	9.89	1.03	8.2	1206	2760	1.292
384	189	253	0	3.33	1.06	9.9	1058	2100	1.069
385	190	262	0	0.89	1.03	0.85	1244	2972	1.386
386	190	220	0	3.48	1.1	9.0	1118	2342	1.146
387	190	229	0	3.52	1.08	9.1	1131	2401	1.174
388	190	228	0	5.34	1.75	10.0	944	1694	0.886
390	190	247	0	2.4	1.11	16.4	988	1866	1.084
391	190	196	0	2.48	1.11	16.6	970	1802	1.063
392	190	191	0	3.5	1.09	17.9	863	1471	0.906
393	190	256	0	1.05	0.91	14.9	1119	2385	1.322
394	189	161	0	0.90	1.05	16.2	978	1831	1.073
395	189	133	0.002	1.05	0.90	16.0	862	1467	0.880
396	188	136	0.004	1.01	0.93	16.7	832	1386	0.846
397	187	134	0.008	1.03	0.92	16.9	798	1296	0.800
398	186	123	0.017	1.11	0.85	17.7	722	1109	0.704
399	189	155	0	0.93	1.02	15.9	988	1868	1.087
400	190	810	0	0.77	1.15	8.2	1303	3318	1.510
401	190	793	0.003	0.79	1.11	8.3	1268	3104	1.430
402	190	779	0.005	0.79	1.13	8.3	1296	3273	1.494
403	190	779	0.008	0.79	1.11	8.2	1298	3290	1.496
404	189	940	0.13	0.88	0.98	7.8	1196	2710	1.256
405	190	788	0	0.83	1.07	8.2	1209	3356	1.524
407	191	921	0.002	0.77	1.09	16.7	1130	2438	1.384

TABLE B-I (continued)

Run No.	T_b °F	G lb/hr-ft^2	F_m	I.R.	Mass Balance Ratio	ΔT_{lm} °F	$\overline{U}_s$ Btu/hr-ft^2-°F	$\overline{h}_{c5}$ Btu/hr-ft^2-°F	CN5
408	190	920	0.004	0.78	1.07	16.6	1127	2425	1.377
409	190	906	0.007	0.77	1.09	16.6	1095	2286	1.309
410	190	1086	0.005	0.82	1.05	16.6	1045	2080	1.207
411	191	918	0	0.77	1.08	16.7	1122	2404	1.367
412	191	345	0	0.93	1.01	12.4	1156	2533	1.327
414	190	342	0.002	0.92	1.03	12.2	1151	2509	1.313
415	190	347	0.003	0.87	1.08	12.5	1126	2396	1.269
416	190	341	0.006	0.86	1.09	12.6	1113	2341	1.246
417	190	355	0	0.84	1.12	12.3	1184	2672	1.389
418	229	645	0	0.78	1.19	8.6	1415	3502	1.552
419	229	619	0	0.83	1.12	8.6	1400	3470	1.518
420	229	616	0	0.83	1.12	8.4	1424	3617	1.501
421	220	614	0	0.84	1.10	8.3	1429	3656	1.573
422	229	616	0	0.83	1.12	8.5	1402	3483	1.519
423	229	1080	0	0.83	1.05	8.2	1454	3813	1.621
424	229	1082	0	0.82	1.07	8.2	1476	3974	1.680
425	229	1089	0	0.78	1.13	8.2	1473	3951	1.673
426	229	1082	0	0.82	1.07	8.2	1479	3996	1.689
427	229	1080	0	0.83	1.06	8.2	1445	3758	1.604
428	229	1131	0	4.23	1.08	8.4	1093	2042	0.952
429	230	1138	0	2.69	1.05	8.6	1184	2386	1.097
430	229	1162	0	9.78	1.12	8.7	1367	3273	1.449
431	230	1182	0	4.63	1.09	8.2	1124	2153	0.992
432	230	499	0	2.83	1.07	9.1	1193	2423	1.127
433	230	645	0	2.60	1.09	17.3	1021	1828	1.036
434	230	659	0	1.86	1.08	17.8	1104	2111	1.184
435	230	678	0	0.85	1.08	17.1	1209	2528	1.370
436	230	368	0	0.85	1.14	26.4	1060	1986	1.240
437	230	369	0	0.85	1.14	26.7	1055	1969	1.234

TABLE B-I (continued)

Run No.	T_b °F	G lb/hr-ft^2	F_m	I.R.	Mass Balance Ratio	ΔT_{lm} °F	$\bar{U}_s$ Btu/hr-ft^2-°F	$\bar{h}_{c5}$ Btu/hr-ft^2-°F	CN5
438	231	371	0	0.86	1.13	26.8	1065	2005	1.254
439	231	362	0	0.86	1.13	26.8	1053	1962	1.230
440	229	521	0	2.81	-	8.5	1133	2190	1.016
441	229	538	0	1.65	-	9.3	1243	2645	1.224
442	229	541	0	0.65	1.02	8.3	1361	3234	1.413
443	229	1508	0	0.64	1.17	8.6	1398	3462	1.514
444	230	1276	0	0.71	1.19	7.0	1522	4293	1.721
445	229	809	0	0.78	1.17	7.0	1507	4184	1.689
446	249	500	0	1.02	0.93	8.1	1516	4007	1.660
447	249	256	0	-	-	7.2	1543	4192	1.675
448	249	277	0	0.81	1.14	7.7	1453	3586	1.492
449	349	277	0	0.80	1.14	7.7	1473	3714	1.536
450	349	278	0	0.80	1.15	7.5	1504	3913	1.599
451	249	277	0	0.81	1.14	7.6	1499	3885	1.592
452	230	268	0	0.73	1.24	7.9	1339	3107	1.349
453	229	256	0.001	0.75	1.21	7.7	1347	3149	1.357
454	229	246	0.002	0.76	1.19	7.9	1297	2894	1.271
455	229	241	0.004	0.77	1.18	8.0	1275	2788	1.234
456	229	222	0.012	0.79	1.14	8.2	1175	2351	1.070
457	230	258	0	0.75	1.21	7.9	1341	3118	1.353
458	230	153	0	0.79	1.15	8.0	1326	3033	1.325
459	230	147	0.002	0.82	1.11	8.2	1230	2578	1.158
460	230	148	0.004	0.79	1.16	8.2	1219	2529	1.141
461	230	148	0.007	0.79	1.15	8.4	1185	2389	1.091
462	229	138	0.019	0.81	1.12	8.6	1094	2048	0.959
463	230	152	0	0.80	1.14	7.8	1381	3332	1.429
464	230	72	0	0.76	1.20	7.9	1328	3046	1.327
465	230	52	0.005	0.9	1.00	8.0	1133	2188	0.999
466	229	57	0.009	0.82	1.11	8.4	1129	2177	1.008

TABLE B-I (continued)

Run No.	T_b °F	G lb/hr-ft^2	F_m	I.R.	Mass Balance Ratio	ΔT_{lm} °F	$\bar{U}_s$ Btu/hr-ft^2-°F	$\bar{h}_{c5}$ Btu/hr-ft^2-°F	CN5
467	228	52	0.020	0.85	1.07	8.4	1052	1909	0.897
469	230	70	0	0.81	1.13	7.8	1356	3197	1.377
470	229	21	0	0.78	1.17	6.8	1394	3416	1.412
472	230	27	0	0.75	1.2	6.5	1435	3663	1.479
473	230	30	0	0.72	1.25	6.9	1401	3450	1.428
474	229	21	0	0.78	1.15	6.6	1403	3474	1.420
475	228	3	0.065	0.94	0.96	6.5	1180	2370	1.02
477	229	20	0	0.79	1.14	6.9	1296	2886	1.227
478	229	344	0	0.87	1.09	15.5	1158	2315	1.241
479	229	338	0.001	0.89	1.06	15.6	1133	2218	1.198
480	229	336	0.002	0.88	1.07	15.8	1119	2168	1.177
481	229	346	0.003	0.81	1.16	16.3	1083	2037	1.123
482	229	331	0.008	0.89	1.06	16.6	1036	1879	1.050
483	229	341	0	0.83	1.13	14.9	1188	2435	1.284
484	229	242	0	0.83	1.15	16.1	1079	2025	1.114
485	228	227	0.001	0.90	1.05	15.9	1032	1866	1.034
486	228	242	0.002	0.80	1.17	16.9	1087	2055	1.144
487	228	227	0.005	0.86	1.08	17.1	972	1681	0.960
488	228	217	0.012	0.91	1.03	17.6	880	1425	0.835
489	229	240	0	0.86	1.10	16.3	1084	2042	1.126

TABLE B-II

SUMMARY OF RESULTS FOR NON-CONDENSABLE GAS RUNS

Run No.	CN5 (no gas)	CN5 (gas)	h_g Btu/hr-ft^2-°F	j_M	j_{MS}	Re_v
89	1.211	0.959	10,178	0.012	0.029	703
90	1.211	0.803	6,504	0.011	0.028	692
91	1.211	0.717	3,711	0.014	0.028	672
101	1.242	1.154	37,203	0.018	0.037	622
102	1.242	1.091	20,094	0.028	0.046	611
103	1.242	1.028	13,296	0.030	0.048	606
104	1.242	0.963	9,744	0.034	0.050	589
105	1.242	0.950	8,881	0.040	0.057	589
125	1.200	1.054	19,841	0.0373	0.0482	881
126	1.200	0.999	13,904	0.0383	0.0483	855
127	1.200	0.877	7,404	0.0333	0.433	831
131	1.292	1.086	15,410	0.0280	0.0395	925
132	1.292	0.985	9,145	0.0257	0.0368	930
133	1.292	0.790	4,439	0.0287	0.0385	875
134	1.292	0.739	3,630	0.0300	0.0402	886
137	1.284	0.848	5,433	0.0431	0.0663	417
138	1.284	0.818	4,819	0.0474	0.0706	419
139	1.284	0.730	3,622	0.0538	0.0755	394
140	1.284	0.617	2,601	0.0617	0.0804	358
150	1.160	1.045	23,109	0.0277	0.0550	453
151	1.160	1.063	28,127	0.0371	0.0616	469
152	1.160	1.085	37,769	0.0446	0.0681	467
155	1.150	1.012	19,017	0.0125	0.018	1822
247	1.273	0.958	7,181	0.0228	0.0484	510
248	1.273	0.916	5,962	0.0275	0.0528	501
249	1.273	0.885	5,197	0.0302	0.0550	517
252	1.273	0.881	5,231	0.0191	0.0602	348
253	1.273	0.899	5,548	0.0239	0.0618	370
254	1.273	0.859	4,692	0.0301	0.0802	312
255	1.273	0.746	3,224	0.0436	0.0808	300
256	1.273	0.691	2,655	0.0347	0.0625	389
260	1.277	1.213	47,209	0.0282	0.0440	816
261	1.277	1.115	16,806	0.0239	0.0405	781
279	1.272	1.118	17,742	0.0329	0.0478	813
280	1.272	1.054	11,757	0.0366	0.054	794
336	1.398	1.189	13,204	0.0161	0.0367	1357
337	1.398	1.121	9,196	0.0169	0.0373	1375
338	1.398	1.050	6,741	0.0196	0.0398	1342
339	1.398	1.015	5,836	0.0239	0.0431	1375
342	1.418	1.335	46,076	0.0270	0.0384	1309
343	1.418	1.204	15,750	0.0203	0.0322	1267
344	1.418	1.115	10,080	0.0212	0.0328	1272
345	1.418	0.894	4,519	0.0252	0.0365	1168

TABLE B-II (continued)

Run No.	CN5 (no gas)	CN5 (gas)	h_g Btu/hr-ft^2-°F	j_M	j_{MS}	Re_v
348	1.452	0.903	4,565	0.0312	0.0611	455
349	1.452	0.871	4,031	0.0309	0.0675	464
350	1.452	0.738	2,682	0.0429	0.0743	422
351	1.452	0.642	2,006	0.0473	0.0773	410
354	1.360	1.159	15,921	0.0238	0.0564	467
355	1.360	1.170	16,900	0.0288	0.0599	482
356	1.360	1.091	10,951	0.0366	0.0669	467
357	1.360	1.018	7,929	0.0426	0.0707	476
360[a]	1.011	0.677	3,230	0.0216	0.0825	359
361[a]	1.011	0.786	5,545	0.0277	0.0802	446
362[a]	1.011	0.726	3,987	0.0308	0.0822	428
363[a]	1.011	0.570	1,944	0.0402	0.0956	347
366[a]	1.144	1.080	71,427	0.0214	0.0278	1839
367[a]	1.144	1.058	42,173	0.0196	0.0260	1839
368[a]	1.144	0.995	18,545	0.0171	0.0236	1797
369[a]	1.144	0.805	7,543	0.0163	0.0224	1791
373[a]	1.060	0.935	13,025	0.00945	0.0204	2039
374[a]	1.060	0.898	9,612	0.0108	0.0212	2034
375[a]	1.060	0.823	5,993	0.0135	0.0228	2037
377[a]	0.769	0.609	4,754	0.0203	0.0672	365
378[a]	0.769	0.609	4,724	0.0257	0.0711	365
379[a]	0.769	0.523	2,579	0.0290	0.0733	341
380[a]	0.769	0.514	2,427	0.0369	0.0769	356
395[a]	1.080	0.880	7,922	0.0262	0.0819	398
396[a]	1.080	0.846	6,397	0.0305	0.0837	407
397[a]	1.080	0.800	4,999	0.0366	0.0873	401
398[a]	1.080	0.704	3,185	0.0455	0.0970	368
409	1.367	1.309	53,878	0.0210	0.0292	2713
414	1.363	1.313	68,395	0.0260	0.0439	1024
415	1.363	1.269	34,742	0.0206	0.0403	1039
416	1.363	1.246	27,271	0.0293	0.0471	1021
454	1.351	1.271	48,872	0.289	0.0474	683
455	1.351	1.234	32,193	0.0352	0.0536	669
456	1.351	1.070	11,303	0.0396	0.0584	617
459	1.395	1.158	15,174	0.0263	0.0604	408
460	1.395	1.141	13,889	0.0349	0.0662	411
461	1.395	1.091	10,963	0.0419	0.0726	411
462	1.395	0.959	6,552	0.0609	0.0909	383
465	1.352	0.999	8,380	0.0826	0.166	144
466	1.352	1.008	8,556	0.107	0.183	158
467	1.352	0.897	5,672	0.148	0.224	144
479	1.262	1.198	43,736	0.0184	0.0447	939
480	1.262	1.177	32,188	0.0219	0.0475	933

TABLE B-II (continued)

Run No.	CN5 (no gas)	CN5 (gas)	h_g Btu/hr-ft^2-°F	j_M	j_{MS}	Re_v
481	1.262	1.123	18,494	0.0203	0.0460	947
482	1.262	1.050	11,185	0.0264	0.0511	920
485	1.120	1.034	24,301	0.0196	0.0553	672
487	1.120	0.960	11,767	0.0320	0.0697	603
488	1.120	0.835	5,600	0.0305	0.0622	667

[a]Solids fouling present on tube inside surface.

APPENDIX C

THERMOCOUPLE CROSS-CALIBRATION CORRECTIONS

In order to check periodically the calibration of the thermocouples and provide a more accurate measurement of the temperatures used in calculating heat transfer coefficients, isothermal cross-calibration tests were carried out. At first these consisted of running the circulating water system with no heat input other than that provided by the circulating pump, and with no steam admitted to the condenser. Water temperatures were calculated for each tube outlet and the combined water inlet, using the individual thermocouple calibrations. However, because of the uncertainties in this method, and the fact that it could not provide a check of the steam temperatures, a special copper calibration block was designed and built as shown in Figure C-I. To calibrate the thermocouples, they were removed from their locations in the loop, and inserted at random in the drilled holes in the block. The block was brought to a steady state and the thermocouples read using their individual calibrations. A total of five to ten readings were obtained for each thermocouple during a calibration.

Cross calibrations consisted of averaging the measured individual temperatures and calculating the ΔT for each thermocouple required to bring its temperature to the group average. A total of nine such cross-calibrations was carried out using the copper block over a three month period, with the results shown in Table C-I. As noted, not all of the thermocouples were checked each time.

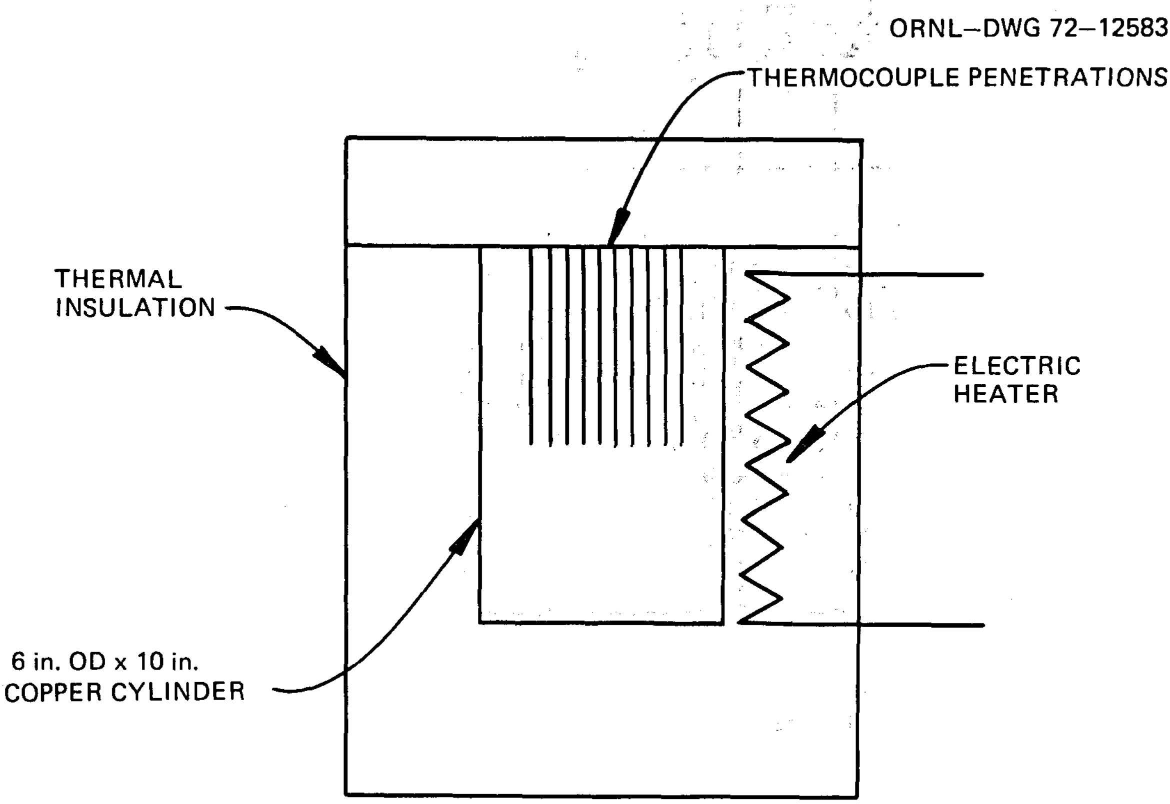

FIGURE C-I

SCHEMATIC DRAWING OF THERMOCOUPLE CROSS CALIBRATION BLOCK

TABLE C-I

CROSS CALIBRATION RESULTS

TC No.	Loop Location	7/29	7/30	7/31	9/10	9/11	9/16	11/14	12/13	12/16	Mean
		Correction Terms (°F)									
	Date	7/29	7/30	7/31	9/10	9/11	9/16	11/14	12/13	12/16	
	Temperature	212	200	205	160	160	107	205	219	206	Mean
6	Water Inlet	+0.08	-0.01								+0.04
7	Tube 1 Out	-0.20	-0.19	-0.18							-0.19
8	Tube 2 Out	-0.13	-0.04	-0.13	-0.19	-0.11	-0.17	-0.17	-0.14	-0.13	-0.14
9	Tube 3 Out	+0.03	+0.04	+0.04	+0.06	+0.06		+0.09	+0.07	+0.09	+0.05
10	Tube 4 Out	-0.11	-0.12	-0.05	+0.03	+0.02	0				-0.04
11	Tube 5 Out	+0.10	+0.17	+0.04	+0.03	+0.11	0	+0.09	-0.06		+0.06
12	Bundle Out	+0.23	+0.16	+0.14	-0.02	+0.02	+0.05		+0.07	+0.09	+0.09
23	Steam In					+0.02	+0.05				+0.04
24	Steam Out					+0.09	+0.14				+0.12
50	Water Inlet(1)			+0.11	+0.07	-0.04	+0.10	+0.26	+0.33	+0.22	+0.15
57	Tube 1 Out(1)				-0.06	-0.15	-0.17	-0.17	-0.23	-0.21	-0.16
58	Tube 4 Out(1)							-0.08	-0.06	-0.04	-0.06

(1) Thermocouples Nos. 50, 57 and 58 replaced Nos. 6, 7 and 10 respectively, following run 242.

The set of deviations obtained for each thermocouple for the nine calibrations were averaged and these mean values used in the computer program for correcting the temperatures measured in the condenser heat transfer tests. These are also given in Table C-I.

APPENDIX D

CALCULATION OF FLOW THROUGH THE CONDENSER BYPASS LINE

A flow of steam through the bypass line around the condenser runs resulted from failure sometime during the experimental program of the rupture disc (but not of its vacuum support plate). An estimate of the expected flow rates through the bypass line for each of the three operating temperatures was made by assuming critical (choking) flow through the passages in the support plate. These passages consisted of segments of six radial slots in the 0.01 in. plate with a combined flow area, as calculated from the dimensions shown in Figure D-I, of 0.208 in.^{2}

The critical mass flow rate for isentropic equilibrium expansion of saturated steam at 230°F is 1122 lb/hr-in.^{2} based on data in the ASME Steam Tables, which is equivalent to a mass flow rate of 232 lb/hr through the backup plate at 230°F. For 190°F and 160°F, the bypass flow rate was 107 and 55 lb/hr, respectively.

The result at 230°F agrees fairly well with the measured vent rate, which was found to be 315 lb/hr at that temperature with the condenser discharge valve completely closed off. Prior to the discovery of the bypass flow, it had been thought that this apparent vent rate represented leakage through the discharge valve.

The difference between the theoretical and the measured values reflect errors in the measurement of the vent rate itself, the error associated with assuming equilibrium choking flow, and the fact that the condenser discharge valve may have in fact had a leak. The latter assumption was subsequently found not to be valid. Tests after installation of

ORNL–DWG 72–12457

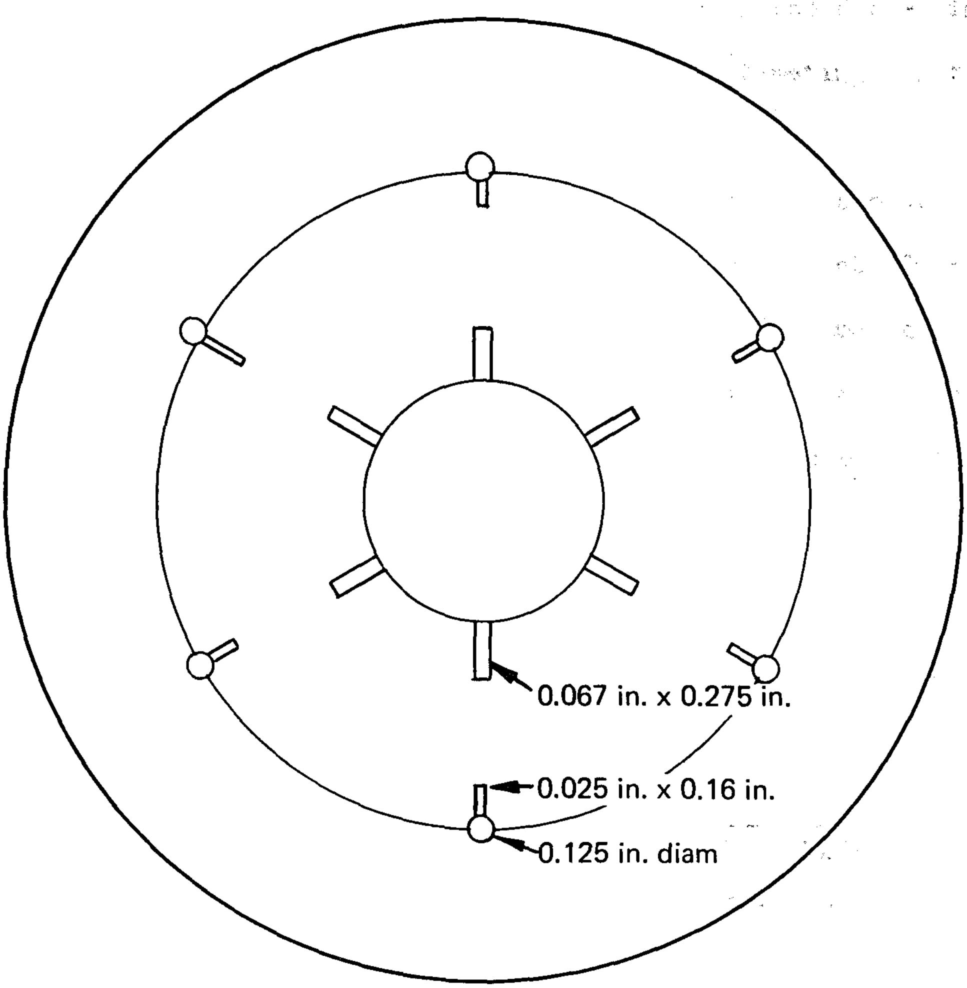

ESTIMATED TOTAL FLOW AREA = 0.208 in.^{2}

FIGURE D-I

AVERAGE SLOT DIMENSIONS IN RUPTURE DISC VACUUM SUPPORT PLATE a new rupture disc showed no vent steam flow with the discharge valve closed. The most likely reason for the difference is that a thin orifice does not have equilibrium flow. Although the magnitude of the expected deviation resulting from the nonequilibrium condition was not estimated, it is likely that it was in the direction of underestimating the flow through the orifice.

It was concluded that the best correction to use to account for the bypass flow is that based on the experimental measurement at 230°F. The corrections for 190°F and 160°F were taken to be in the same ratio as the theoretical prediction. The corrections, as shown in Table D-I, were subtracted from values of the vent rate for all runs following the bypass leak.

TABLE D-I

MASS FLOW CORRECTION TERMS

Steam Temperature °F	Flow Correction lb/hr
230	315
190	145
160	75

The time of occurrence of the leak is not known. Initially applying the correction to all of the data resulted in some runs prior to Run 157 giving low and occasionally negative values of the mass velocity. Following run 246, this condition did not occur. It was concluded that the correction should not apply prior to run 246.

VITA

David Martin Eissenberg was born in Brooklyn, New York, on August 5, 1929. He attended elementary schools in that city and was graduated from Brooklyn Technical High School in 1947.

He was graduated from the College of William and Mary in 1950 with a B. S. in Physics and from the Massachusetts Institute of Technology in 1952 with a B. S. in Chemical Engineering. He was graduated from the University of Tennessee with an M. S. in Chemical Engineering in 1963. He is a registered engineer in the state of Tennessee.

He has been employed by Union Carbide Corporation at the Oak Ridge National Laboratory since 1952, working in reactor development, heat transfer and fluid dynamics. From 1955 to 1958 he was on active duty with the United States Navy and holds the rank of Lieutenant in the Retired Reserve.

He is married to the former Ethel Mae Mikula, and has five children, Joel, Judith, Sara, Michael and Thomas.